Pt(II) and Pd(II) Complexes of Isocytosine and Guanine Ligands

Tautomerism, Linkage Isomerism and Hydrogen Bonding

Deepali Gupta

This work was carried out between March 2002 and July 2005 at the Lehrstuhl für Bioanorganische Chemie, Fachbereich Chemie, Universität Dortmund, Deutschland.

For my family

Table of Contents

Acknowledgments

> "I confess I am at somewhat a loss for words."
> *Spock, The Alternative Factor.*

This is perhaps the easiest and the hardest chapter that I have to write. It will be simple to name all the people who have supported me during the production of this thesis, but it will be difficult to thank them enough. Nevertheless, I will try.

First and foremost, I would like to thank my supervisor Professor Dr. Bernhard Lippert. He has guided me through my three and a half years with care and patience. He has been the best teacher and role model I could hope for and someone who I felt cared about my development as an academic. I will look back on my time as his student with great fondness and appreciation for many years to come. I am extremely grateful for the time and advice he has given me in relation to this thesis and also in relation to the broader dimensions of my academic life. It has been a rewarding and a valuable experience. Thanks for the kindness with which you have always treated me and for being available to answer a number of questions and resolve the doubts I always had.

I thank PD Dr. Andrea Erxleben and Dr. Jens Müller for numerous scientific discussions and suggestions and for being in my examination committee. I would like to express my gratitude to Prof. Dr. Martin Engelhard, Prof. Dr. Dr. h. c. Rolf Kinne, Dr. Jutta Roetter, Niklas Büdenbender and International Max Planck Research School for assistance and financial support. I am indebted to Ms. Michaela Markert and Ms. Birgit Thormann for their secretarial assistance and support in a number of ways.

I would like to thank Ms. Olga Karsten, my Auszubildende, and Mr. Volker Belting, my Wahl- Praktikant, for their contribution to the section 2.5. I thank Dr. Markus Huelsekopf and Prof. Dr. Ralf Ludwig for teaching me all what I know about the theoretical calculations and a lot more. I thank Mr. Matthias Rabiller for introducing me to 600 MHz NMR instrument and teaching me the ABC of protein purification. I would like to thank Prof. Dr. Burkhard Costisella, Ms. A. Danzmann, Ms. Nettelbeck, Dr. Jens Müller, Dr. Pablo Sanz Miguel and Ms. Marta Morell Cerdà for recording the ^{1}H NMR spectra; Mr. Markus Hüffner for doing the elemental analyses; Ms. Wilga Buß for recording the Raman spectra; Ms. Marta Morell Cerdà and Dr. Michael Roitzsch for carrying out some

List of Abbreviations

a	NH_3
A	general abbreviation for Adenine compounds or acceptor site
4,4'-bipy	4,4'-bipyridine
br	broad
C	general abbreviation for cytosine compounds
D	donor site
δ	NMR chemical shift in ppm
dien	diethylenetriamine
(dien)Pt^{II}	$[(dien)Pt(H_2O)]^{2+}$ or $[(dien)Pt(D_2O)]^{2+}$
(dien)Pd^{II}	$[(dien)Pd(H_2O)]^{2+}$ or $[(dien)Pd(D_2O)]^{2+}$
DMF	N,N'-dimethylformamide
DMSO	dimethylsulfoxide
DMSO-d_6	dimethylsulfoxide (deuterated)
DNA	deoxyribonucleic acid
en	ethylenediamine
EtOH	ethanol
9-EtGH	9-ethylguanine
G	general abbreviation for guanine compounds
IC	isocytosine anion
ICH	isocytosine
ICH$_2^+$	isocytosinium
ν	frequency
$\tilde{\nu}$	wavenumber
^3J	spin-spin coupling constant (here via three bonds)
m	medium
1-MeC	1-Methylcytosine
1-MeT	1-Methylthymine
1-MeU	1-Methyluracil
7-MeGH	7-methylguanine

9-MeGH	9-methylguanine
1-MeIC	1-Methylisocytosine
mRNA	messenger RNA
MeOH	methanol
NBO	Natural Bond Orbital
Nb	nucleobase or nucleobase complex
pH*	uncorrected pH meter reading in D_2O
PNA	Peptide Nucleic Acid
pu	purine
pym	pyrimidine
pyz	pyrazine
RNA	ribonucleic acid
s	strong
sh	shoulder
T	general abbreviation for thymine compounds
tRNA	transfer RNA
TSP	sodium-3-(trimethylsilyl)propanesulfonate
tmeda	*N, N, N', N'*-tetramethylethylenediamine
w	weak
W-C	Watson-Crick
X	any anion
Y	any cation

List of Compounds

1   [(dien)PdBr]Br

2   [(dien)Pd(ICH-$N3$)](NO$_3$)$_2$

3   [(dienPt)$_2$(IC-$N1,N3$)](ClO$_4$)$_3$ · 2H$_2$O

4   [(dienPd)$_2$(IC-$N1,N3$)](ClO$_4$)$_3$

5a   [(dien)Pt(ICH-$N1$)]$^{2+}$ #

5b   [(dien)PtCl]ClO$_4$

6   ICH · (1-MeC) · 2H$_2$O

7   [ICH · ICH$_2$]NO$_3$

8   1-MeIC

9   [1-MeICH](NO$_3$)$_3$(ClO$_4$)

10   [(dien)Pd(1-MeIC-$N3$)](ClO$_4$)$_2$

11   [(dien)Pt(1-MeIC-$N3$)](ClO$_4$)$_2$

12a [(dien)Pt(GH$_2$-$N9$)](Cl)ClO$_4$

12b 2{[(dien)Pt(GH$_2$-$N9$)](ClO$_4$)$_2$ · 2H$_2$O}

13   [(dienPt)$_2$(GH-$N7,N9$)](ClO$_4$)$_3$

14   *cis*-[(NH$_3$)$_2$Pt(9-EtGH-$N7$)Cl]Cl

15   *trans*-[(NH$_3$)Pt(9-EtGH-$N7$)I$_2$]

16   *trans*-[(NH$_3$)Pt(9-EtGH-$N7$)(pyrz)$_2$](NO$_3$)$_2$ · H$_2$O

17   *trans*-[(NH$_3$)Pt(9-EtGH-$N7$)(4,4'-bipyridine)$_2$](NO$_3$)$_2$

18   [(dien)Pt(7-MeGH-$N9$)](NO$_3$)(ClO$_4$)

19   *cis*-[(NH$_3$)$_2$Pt(9-EtGH-$N7$)$_2$](NO$_3$)$_2$

20a *cis*-[(NH$_3$)$_2$Pt(7-MeGH-$N9$)$_2$]Cl$_2$·3H$_2$O

20b *cis*-[(NH$_3$)$_2$Pt(7-MeGH-$N9$)$_2$]Cl$_2$·2H$_2$O

21   *cis, cis*-[{(NH$_3$)$_2$Pt}$_2$(7-MeGH-$N3,N9$)Cl$_2$]Cl$_2$·3H$_2$O

22   *cis*-[(NH$_3$)$_2$Pt(9-EtGH-$N7$)(pyrz)]$^{2+}$ #

23   *cis*-[(NH$_3$)$_2$Pt(9-EtGH-$N7$)(bipy)]$^{2+}$ #

24   [{*cis*-(NH$_3$)$_2$Pt(9-EtGH-$N7$)}$_2$-(μ-bipy)]$^{2+}$ #

     # in solution

Parts of the results reported in this thesis have already been published or are in press:

1. <u>D. Gupta</u>, M. Huelsekopf, M. Morell Cerdà, R. Ludwig, B. Lippert, "Complex Formation of Isocytosine Tautomers with Pd (II) and Pt (II)", *Inorg. Chem.* **2004**, *42*, 5117-5125.

2. <u>D. Gupta</u>, M. Roitzsch, B. Lippert, "Isocytosine as a Hydrogen Bonding Partner and as a Ligand in Metal Complexes", *Chem. Eur. J.*, in press.

Science never solves a problem without creating ten more.

George Bernard Shaw

1. Introduction

The human genome consists of three billion base pairs along forty-six DNA molecules contained in twenty-three pairs of chromosomes.[1] DNA is a linear polymer that is composed of four different building blocks, the nucleotides. It is in the sequence of the nucleotides in the polymers where the genetic information carried by chromosomes is located. Each nucleotide is composed of three parts: (1) a nitrogenous base known as purine (adenine (A) and guanine (G)) or pyrimidine (cytosine (C) and thymine (T)); (2) a sugar, deoxyribose; and (3) a phosphate group. The order of bases along the DNA molecules is known as the DNA sequence.[1]

Adenine (A)   Guanine (G)   Cytosine (C)   Thymine (T)
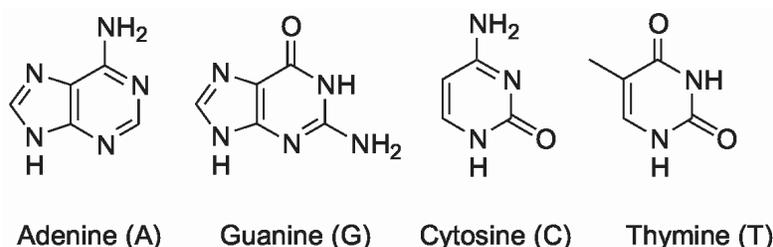
Chart 1 Schematic representation of Adenine, Guanine, Cytosine and Thymine.

The structure, stability and reactivity of the double-helix DNA is affected by the binding to divalent metal cations.[2] These interactions have been investigated by a variety of spectroscopic techniques. These studies indicated that alkaline earth metal ions interact mainly with the DNA phosphates, stabilizing the double helix by reducing the overall electrostatic repulsion, while a destabilization of the DNA duplex can be induced by transition metal ions that preferentially bind to the bases.[2] Metal ions, in the form of appended complexes, have been used to introduce site-specific redox- and photo-active centers in DNA and address questions regarding charge transport.

Depending on the type of metal ion (main group or transition metal; charge; d-electron configuration; hardness or softness), its binding preference (phosphate oxygens; heterocyclic part; site of heterocycle; mono or multi-functional), and

other ligands already bound to the metal ion, the net effect on the nucleic acid (duplex) at higher metallation levels may lead to strong thermal stabilization or pronounced destabilization due to the disruption of an ordered structure.[3]

The best understood metal-ion interactions with DNA are those involving the platinum drugs *e.g.*, *Cisplatin. Cisplatin* is one of a number of platinum coordination complexes with antitumour activity. The potential of this compound as an antitumour agent was recognized through an observation made by Barnett Rosenberg and co-workers. This accidental discovery initiated a series of investigations and studies into the effects of platinum compounds and cell division.[4]

In 1970, further studies performed by Rosenberg and his colleagues revealed that these compounds displayed significant antitumour activity and demonstrated that diamminedichloroplatinum(II), specifically the *cis* isomer, was extremely effective against sarcoma 180 and L1210 leukemia in mice.[4]

The efficacy of the platinum complex as an anticancer agent has now been established in a variety of animal tumor models and in human cancer. The anticancer properties of *cisplatin* stem from the relative ease of substitution of the chlorine ligands with the nucleophilic species like nucleic acid bases of a DNA strand. Before *cisplatin* binds to such nucleophiles, it is usually converted to the active form by aquation. The conversion occurs intracellularly as the lower chloride concentrations permit it. The resulting electrophile can bind to a variety of macromolecules having nucleophilic groups, which include DNA. It is now widely accepted that DNA is the primary target of *cisplatin*. This function is believed to be the largest contribution to its cytotoxicity.[4]

Cisplatin forms covalent bonds with nucleophilic sites on guanine present in all DNA. As *cisplatin* is a bifunctional agent, it is able to bind to two sites in a DNA strand. This results in the formation of inter- and intra- chain cross-linkings which interferes with cellular transcription and replication. Regulatory mechanisms

detect the abnormal DNA and so activate a chain of responses to try and correct it. This, ultimately, causes cell death (apoptosis).[4]

Multiple hydrogen bonding has been found to be the driving force in the molecular recognition process in metal nucleobase complexes.[5] The interaction of nucleic acid bases with metal cations has a strong effect on the structures and properties of nucleic acids. The replacement of the protons involved in hydrogen bonding between the nucleobases by the metal entities has led to the synthesis of the compounds which are relevant in biology and medicine.[6-12] Novel molecular architectures for nucleobases and metal entities that include triplets,[13-15] tetrads,[11,12,16-19] hexagons,[20,21] molecular boxes[18,22] and self-assembled nucleobase aggregates,[23-25] have been synthesized that exploit the right angles formed by the metal-N(1) and metal-N(7) purine bases. Theoretical studies have been carried out at different levels to explore the effect of metals on the formation of nucleobase pairs and trimers.[14,26-36]

The dimerization of Pt(II)-coordinated Guanine-Cytosine base pairs yields a metalated GCGC base tetrad.[11,12] The crystal structure of this platinum-modified base tetrad reveals a unique multicenter hydrogen bonding pattern around guanine O(6) that is strongly affected by the presence of the platinum.[12] The influence of the metals on the neighboring hydrogen bonds is crucial in building a stable molecular assembly from metal coordinated nucleobases. This compound contains an unprecedented hydrogen bonding pattern between deprotonated guanine and neutral cytosine that involves cytosine H(5) and guanine N(1). Such a hydrogen bonding pattern could be very important in DNA chemistry as it expands the possible hydrogen bonding patterns in DNA base pairing interactions.

The tautomeric form of nucleobases determines their interactions with other nucleobases,[37-40] and their ability to be incorporated into stable nucleic acid structures.[37-41] Thus, the occurrence of spontaneous mutations in the DNA has been related to the presence of minor tautomers of the nucleobases. Minor

tautomeric forms have been found experimentally in DNAs containing modified nucleobases, such as isoguanosine,[42] which exists in both enol and keto tautomeric forms, and N^4-methoxycytosine, which is found in the mutagenic imino form in different DNA structures.[43-46] Mutagenicity induced by the occurrence of minor tautomeric forms has also been investigated in halo derivatives of uracil.[47-49]

Metal binding to a certain site of the heterocyclic nucleobase may cause a shift of a weakly acidic proton to another site, thereby generating a metal complex of a nucleobase tautomer structure normally present in a concentration too low to be detected experimentally. A series of such complexes with Pt^{II} and Pt^{IV} have been prepared, isolated and in some cases characterized by X-ray crystallography. The imino tautomers of cytosine and adenine have been found in model nucleobases in the presence of metals.[3,50]

The existence of tautomeric equilibria in nucleobases under physiological conditions has many biotechnological applications. These molecules might display multiple recognition patterns depending on the complementary base. A direct biotechnological application of the relationship between tautomerism and recognition patterns is in the design of compounds which are able to stabilize anomalous forms of DNAs.

The base-pair formation is neither prevented nor diminished when metal coordinates to a nucleobase donor atom remote from its hydrogen bonding site.[51] On the contrary, the base-pair formation is reinforced. Studies have established that G/C Watson-Crick pairing is strengthened due to the metallation either at N7 of the guanine or N(1) of the cytosine.[51]

These findings led to the pursuit of the idea of synthesizing the artificial oligonucleotide analogs that consist of a backbone of metal ions Pt^{2+} and bridging ligands.[51] These cationic complexes are expected to show a high affinity towards

the polyanions DNA and RNA. Therefore, they might be useful as antigene[52,53] and antisense[54,55] reagents.

1.1   Antigene and Antisense Technology

The majority of genes are expressed as the proteins they encode. The process occurs in two steps:

- Transcription = DNA → RNA
- Translation = RNA → protein

The concept of antisense-mediated gene inhibition, first introduced by Stephenson and Zamecnik in 1978,[54] has now emerged as a potentially powerful alternative to conventional cancer chemotherapy. The term "antisense" refers to the fact that the nucleic acid synthesized is complementary to the coding (*i.e.*, "sense") genetic sequence of the target gene.

The gene expression may be interrupted at either of the two stages. The first is transcription, the stage at which a gene's code is transferred to a messenger RNA (mRNA) that leaves the cell nucleus. One idea is to engineer an antisense strand which is capable of interacting with a specific strand of the DNA double helix, thereby creating a triplex (a triple-strand helix) within a gene or in one of its control elements. This in turn may prevent the gene's code from being read. Hence, this is known as antigene technology.[52,53]

The other interruptible stage is translation, where the unpaired nucleotides of the mRNA are read by transfer RNA (tRNA) anticodons as the ribosome proceeds to encode the protein. If an antisense strand can hybridize with a specific mRNA, the resulting duplex may prevent translation. This is known as antisense technology.[54,55] Antisense constructs hybridize in an antiparallel orientation to the sense mRNA through Watson-Crick base-pairing. This may occur because

- the ribosome cannot gain access to the nucleotides in the mRNA or
- duplex RNA is quickly degraded by ribonucleases in the cell

1.2 Aim of the Project

Synthetic oligonucleotides have shown an immense promise and have been extremely useful in gene activation and repression strategies over the past 20 years. However, several factors have limited their potential, namely the susceptibility to nuclease digestion. A modified oligonucleotide, peptide nucleic acid or PNA,[56] was developed which displayed high affinity and specificity of binding to DNA and RNA and showed great resistance to both nucleases and proteases.[57]

PNAs are nucleic acid analogs in which the phosphodiester backbone has been replaced with a polyamide backbone.[56] The backbone contains no phosphate groups and hence, is not charged. Consequently, there is very little repulsion when the PNA hybridizes to its target nucleic acid sequence, leading to a more stable complex.[57] A further increase in the affinity can be achieved by modifying the backbone in such a way that it is positively charged.[58] It was indeed the case when the phosphodiester backbone was replaced with a guanidine residue.[59-62]

Our ongoing research[51,63,64] in this area is focused on the synthesis of artificial oligonucleotide analogs (Chart 2) that consist of a backbone of metal ions and
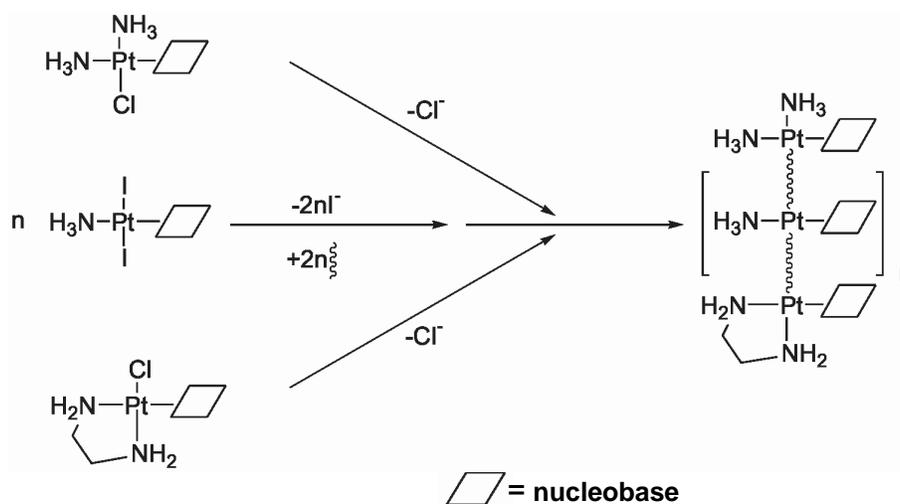
Chart 2 Schematic view of the strategy for the synthesis of cationic di- (n = 0), tri- (n = 1), and oligonucleotides (n $\geq$ 2) with a Pt^{2+} backbone. (Adopted from ref. 62)

bridging ligands, with the nucleobases bound to the metal centers either through N1 (unsubstituted pyrimidine bases), via N9 (unsubstituted purine bases) or N7 (N9-substituted purine bases) sites. These cationic oligonucleotides are expected to be kinetically robust. Moreover, the nucleobases attached to the metal centers are forced in a more or less coplanar orientation and the hydrogen bonding properties are usually maintained. The cationic oligonucleotides can function as antisense[54,55] and antigene[52,53] reagents due to their ability to bind both DNA and RNA targets with high specificity and affinity.

The ligands of choice for the present work were common and rare nucleobases such as isocytosine, guanine, 9-ethylguanine and 7-methylguanine. These ligands were studied with regard to the effects of metallation on hydrogen bonding properties and tautomerism.

As it turned out, the planned fixation of a suitable metal entity to a particular site of a nucleobase or to a particular tautomer of a nucleobase in most cases is anything but trivial. Understanding factors which determine the reactivity of individual nucleobase tautomers toward metal species eventually proved to be essential.

2. Results and Discussions

2.1 Complex Formation of Isocytosine Tautomers with Pd[II] and Pt[II]

2.1.1 Introduction

Isocytosine (ICH, 2-aminopyrimidin-4-(3*H*)-one) is a structural isomer of cytosine (C) and exists as two major tautomers (Chart 3), **1a** and **1b**. A third, minor tautomer (not shown) adopts an enol structure.
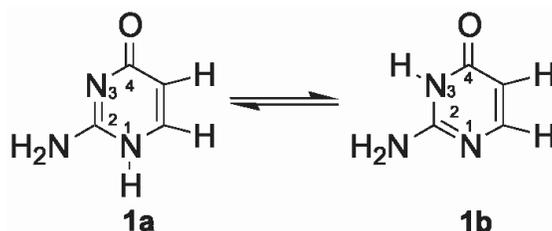
Chart 3 Two tautomeric forms of ICH.

Although not a natural nucleobase like cytosine, nucleosides of isocytosine have been reported to exhibit interesting pharmaceutical properties,[65,66] and the C(5)-glycosidic derivative pseudoisocytidine (ΨIC) has proven a valuable tool for molecular biology studies (Chart 4), *e.g.* for DNA triplex formation[67] and mechanistic studies of RNA catalysis.[68]
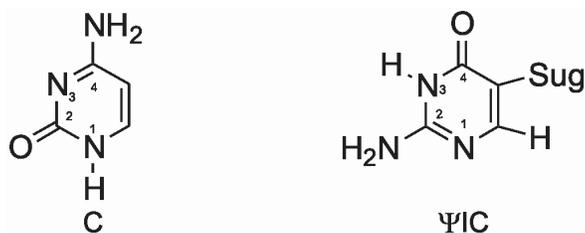
Chart 4 Cytosine and C(5)-glycosidic derivative pseudoisocytidine ΨIC.

Moreover, the potential usefulness of isocytosine as a hydrogen bonding partner of the likewise non-natural isoguanine in oligonucleotides has been a point of interest.[67,69-76] Our focus on isocytosine originates from its potential metal binding

properties and our general interest in metal complexes of ligands existing as different tautomers.[77-81] Metal complex formation with isocytosine has previously been studied by other groups,[82-85] and there are examples of X-ray structurally characterized metal compounds with O(4)[84] or N(3)[85] coordination. Various substituted isocytosine derivatives (substituents at N(1), N(2), C(5) positions) have likewise been studied.[86]

2.1.2 Aim of the Project

At the outset of our work, we were intrigued by the potential of isocytosine to form inert metal complexes of tautomer **1b**, hence metal compounds with N(1) coordination. Brüning et al. have previously observed that with cytosine the minor tautomer could be complexed by metal ions to an extent that exceeded its occurrence in solution by far.[77,78] Moreover, examples of both linkage isomers (metal at N(1) or N(3)) were isolated on a preparative scale and characterized by X-ray crystal structure analysis. In its deprotonated form, the isocytosine tautomer **1a** provides, in principle, the ability of recognizing guanine nucleobases in a way different from that of cytosine (Chart 5), namely in a reversed Watson-Crick manner.
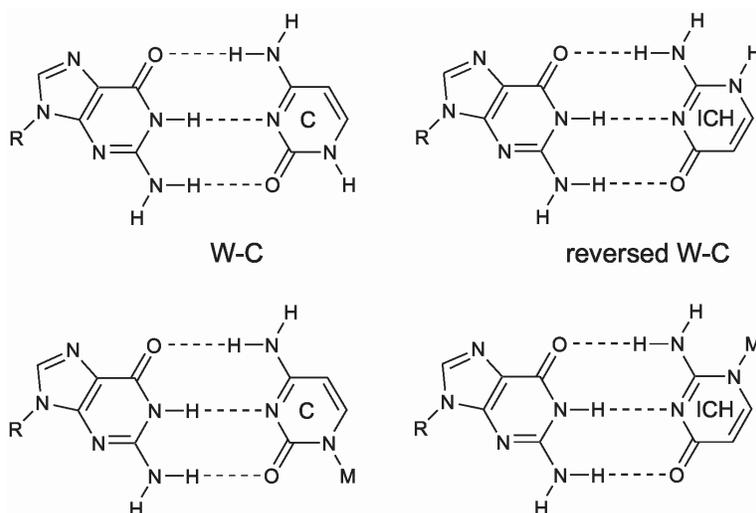
Chart 5 Pairing patterns between guanine, cytosine, isocytosine, metalated cytosine and metalated isocytosine.

Similarly, a N(1) metalated isocytosine anion can interact with guanine in this fashion, unlike N(1) metalated cytosinate, which pairs according to

Watson-Crick.[51] These considerations can be extended to pairing motifs between cytosine and neutral, protonated, or metalated isocytosine (Chart 6) and contrasted with the situation in hemiprotonated cytosine pairs ("i-motif").[87]

hemiprotonated C
i-motif
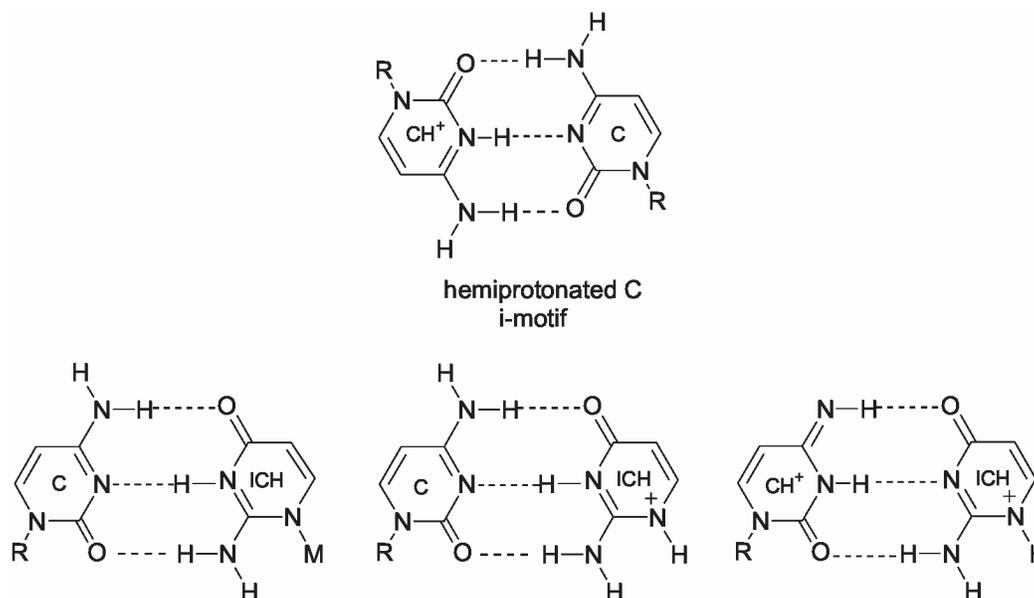
Chart 6 Pairing motifs between cytosine and neutral, protonated or hemiprotonated cytosine pairs.

Our particular interest in this ligand was the metal binding behavior of tautomer **1b** and specifically the attachment of a Pt^{II} entity to the N(1) position. This way we wanted to generate platinated nucleobase analogs (Chart 7) which, when incorporated into a suitable backbone,[51,88] might give rise to artificial, cationic oligonucleotide analogs with the ability to recognize natural nucleobases via hydrogen bond formation.
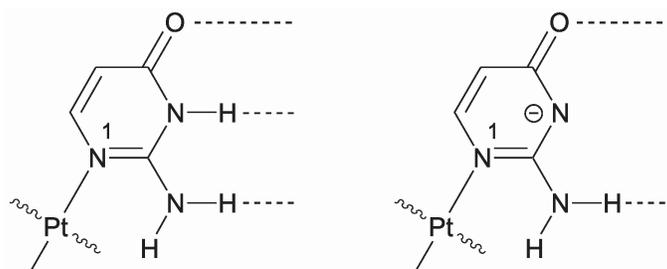
Chart 7 N(1)-platinated forms of isocytosine (neutral ligand left; anionic ligand right).

2.1.3 Tautomerism of Isocytosine

Isocytosine crystallizes in two tautomeric forms: 1,4-dihydro-2-amino-4-oxo-pyrimidine (keto-N(1)H, **1a**) and 3,4-dihydro-2-amino-4-oxo-pyrimidine (keto-N(3)H, **1b**), in an exact 1:1 ratio.[89,90] The tautomers are hydrogen bonded to each other in a manner similar to that of the guanine and cytosine pair in DNA.[91] A number of electronic spectroscopic studies[92-97] have been carried out to study the tautomerism of isocytosine. These studies reveal that the ratio of the two tautomers present in solution is solvent and temperature dependent. In ethanol and diethyl ether, keto-N(3)H form **1b** predominates over keto-N(1)H form **1a**, while in aqueous solution the two forms are present (Chart 8) in almost 1:1 ratio.[93,94,96]
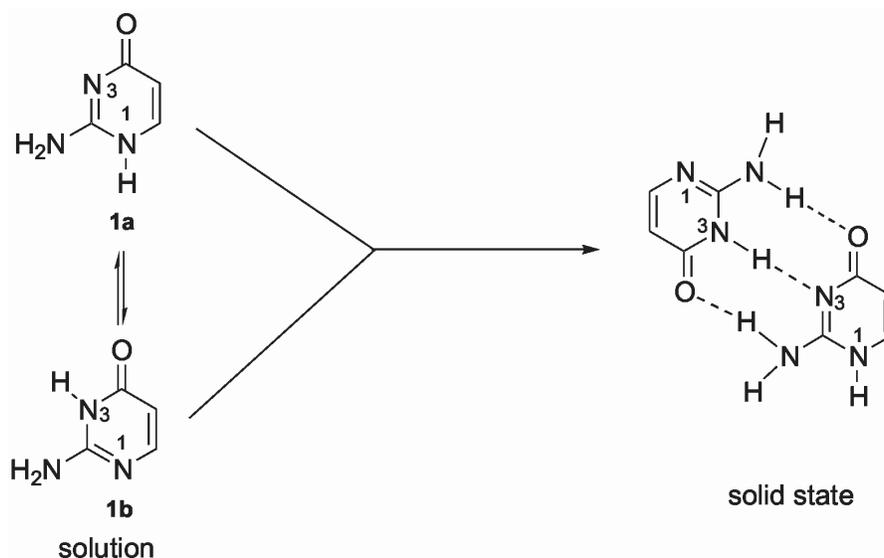
Chart 8 Tautomerism of ICH in solution (1a, 1b) and hydrogen bonded adduct 1a – 1b in the solid state.

Temperature-dependent solution studies[94] indicate that in aqueous solution, with the rise in temperature, keto-N(1)H tautomer **1a** becomes more stable as compared to keto-N(3)H tautomer **1b**. Morita and Nagakura[93] have also determined the energy differences and entropy changes between the two (keto-N(1)H *vs.* keto-N(3)H) forms to be 1.3 kcal/mol and 4.7 cal/mol K, respectively, on the basis of the temperature-dependence of the absorption spectra of the molecules.

Several quantum-mechanical computational studies[98-100] have been carried out on different tautomers of isocytosine. In the gas phase, the keto-N(3)H tautomer **1b** is more stable than the keto-N(1)H tautomer **1a.** From the calculated and experimental data, it was found that in a solid argon matrix[98] isocytosine is present as a mixture of both enol and keto-N(3)H **1b** tautomeric forms with the enol form being dominant.

Our calculations on two tautomers (keto-N(1)H and keto-N(3)H) in gas phase are in agreement with the calculations carried out earlier.[98,99] The energy difference between keto-N(3)H form **1b** and the keto-N(1)H form **1a** using Lanl2dz and 6-31+G* basis sets[101-103] is -8.4 and -11.0 kcal/mol, respectively.

2.1.4 Solution Studies of Isocytosine

Brown and Teitei[96] reported pK_a values of 4.0 and 9.59, which were obtained by means of ultraviolet spectroscopy. In the course of the present work, pK_a values of isocytosine were determined using pH dependent (Figure 1) ^{1}H NMR spectroscopic measurements. The pK_a for the protonated ICH_2^+ was found to be 4.07 ± 0.01, and for the neutral ICH 9.47 ± 0.03. Chart 9 depicts the two acid-base equilibria.
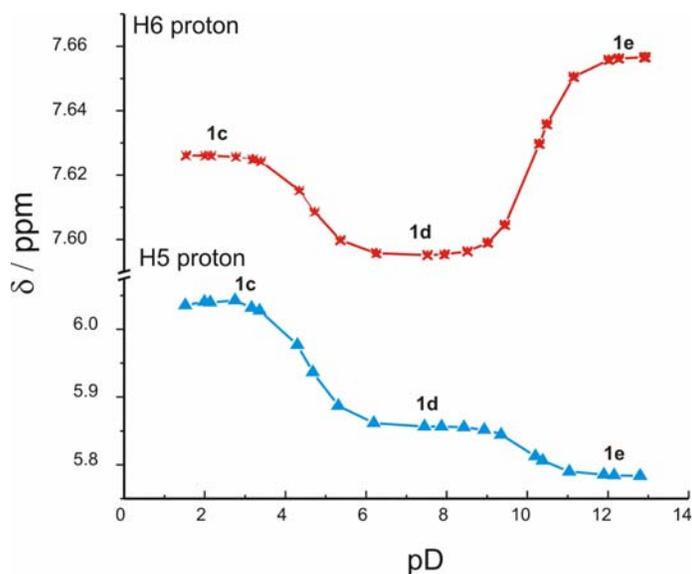
Figure 1 pD dependence (δ, ppm) of H5 and H6 resonances of ICH in D_2O.
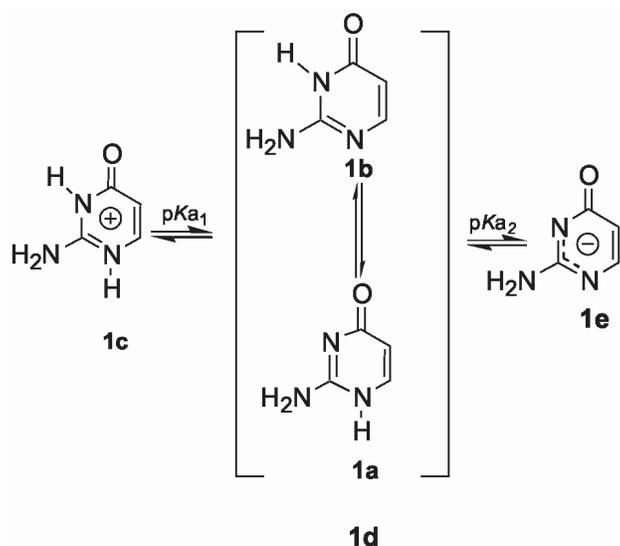
Chart 9 Acid-base equilibria

Raman spectra of isocytosine were recorded in the solid state as well as in different solvent mixtures of DMF and H_2O. For the solid isocytosine (Figure 2), in the spectral range $400 - 1700$ cm^{-1}, there was a series of characteristic twin bands[104] due to complex ring bending (798 cm^{-1}, 785 cm^{-1}) and stretching modes of the ring (1232 cm^{-1}, 1210 cm^{-1}) for the two tautomers. The band at 798 cm^{-1} for the deformation mode can be assigned to the keto-N(1)H tautomer **1a** of isocytosine [ref. section 2.2]. The band at 785 cm^{-1} is subsequently assigned to the keto-N(3)H tautomer **1b** of isocytosine.
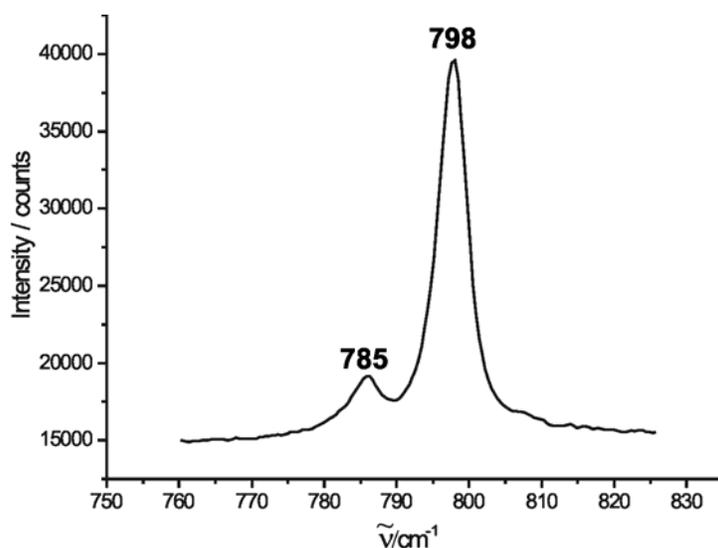
Figure 2 A section of a solid state Raman spectrum of ICH.

Similarly, the band at 1232 cm^{-1} is assigned to the stretching mode of the keto-N(1)H tautomer **1a** of isocytosine and correspondingly, the other band at 1210 cm^{-1} to the keto-N(3)H tautomer **1b**. There are also twin bands at 791 cm^{-1} and 787 cm^{-1} for isocytosine in pure DMF but there is only one band observed at 1214 cm^{-1}, which is strongly asymmetric, however. In water, there is a broad band at 791 cm^{-1} and another one at 1232 cm^{-1}, which possibly is due to two species present, although there is no clear separation of individual peaks. As DMF is successively diluted with water, there is a shift to higher wavenumbers, *i.e.* from 789 cm^{-1} to 791 cm^{-1} and from 1214 cm^{-1} to 1232 cm^{-1}, yet there is no separation of individual peaks as is the case for isocytosine in the solid state and in pure DMF.

2.1.5 Reactions of (dien)Pd^{II} with Isocytosine

In order to study the metal binding to isocytosine and to identify the various binding sites, the reactions were carried out on the NMR scale. 1:1, 1:3 and 3:1 mixtures of isocytosine and [(dien)Pd(D$_2$O)](NO$_3$)$_2$ were prepared and reactions were carried out without pH* adjustment at the start of the reaction. The samples were kept at 40 °C for few hours until no further changes were detected in the ^{1}H NMR spectra. A typical spectrum (Figure 3) consists of four sets of aromatic H5 and H6 resonances (doublets each, $^3J \sim 6.7 - 7.3$ Hz) sets.
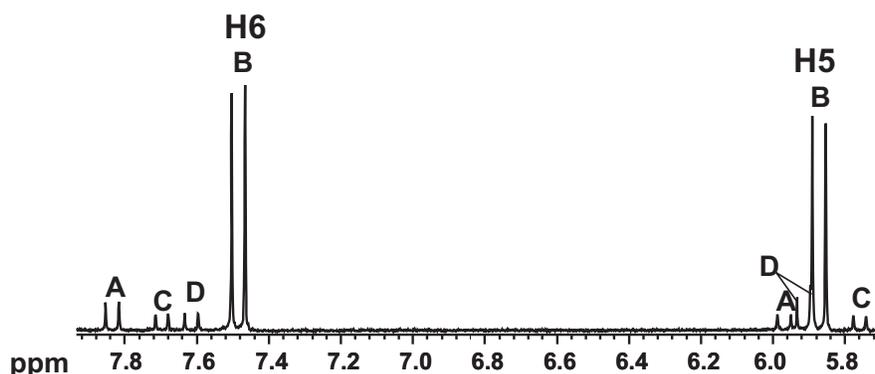
Figure 3 ^{1}H NMR spectrum (D$_2$O, pH* 4.0, isocytosine resonances only) of reaction mixture (1:1) of [(dien)Pd(D$_2$O)]$^{2+}$ and isocytosine after few hours at 40 °C. Assignment of resonances (A)–(D) was made on the basis of their pD dependence. A, B, C, D are assigned to N(1), N(3), N(1)N(3) and free ICH, respectively.

Typically, 1:1 reaction mixtures were treated with acid and/or base over a wide pH* range and ^{1}H NMR spectra were recorded. The four sets of resonances (A) - (D) were assigned based on pD dependent (Figures 4 and 5) ^{1}H NMR spectroscopic measurements.

Resonances (C) are due to the dinuclear species, $[(dienPd)_2(IC-N1,N3)]^{3+}$ as this set of resonances is insensitive to pD. An intense set of resonances (B) is assigned to the N(3) linkage isomer, $[(dien)Pd(ICH-N3)]^{2+}/[(dien)Pd(IC-N3)]^+$, pK_a 6.50 ± 0.01, by comparison with the spectrum of the isolated compound, the structure of which has been established through X-ray crystallography (see below). The set of resonances furthest downfield (A) is assigned to the N(1) linkage isomer, $[(dien)Pd(ICH-N1)]^{2+}/[(dien)Pd(IC-N1)]^+$, pK_a 6.20 ± 0.01. Finally, the set of resonances (D) belongs to free isocytosine, ICH_2^+/ICH, pK_a 4.07 ± 0.01.
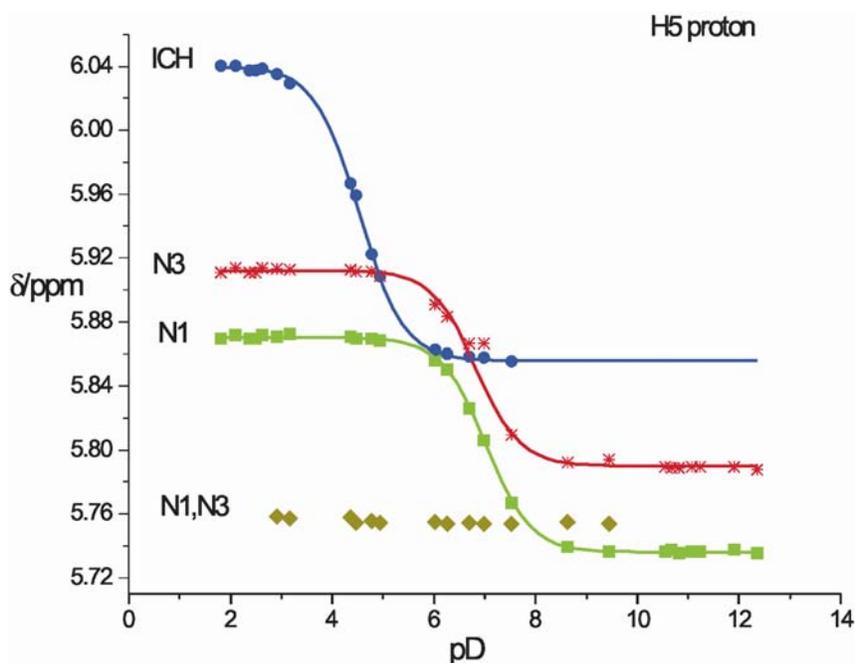
Figure 4 pD dependence (δ, ppm) of H5 proton for $[(dien)Pd(ICH-N1)]^{2+}$ (N1), $[(dien)Pd(ICH-N3)]^{2+}$ (N3), $[(dienPd)_2(IC-N1,N3)]^{3+}$ (N1,N3) and free isocytosine (ICH) in D_2O.
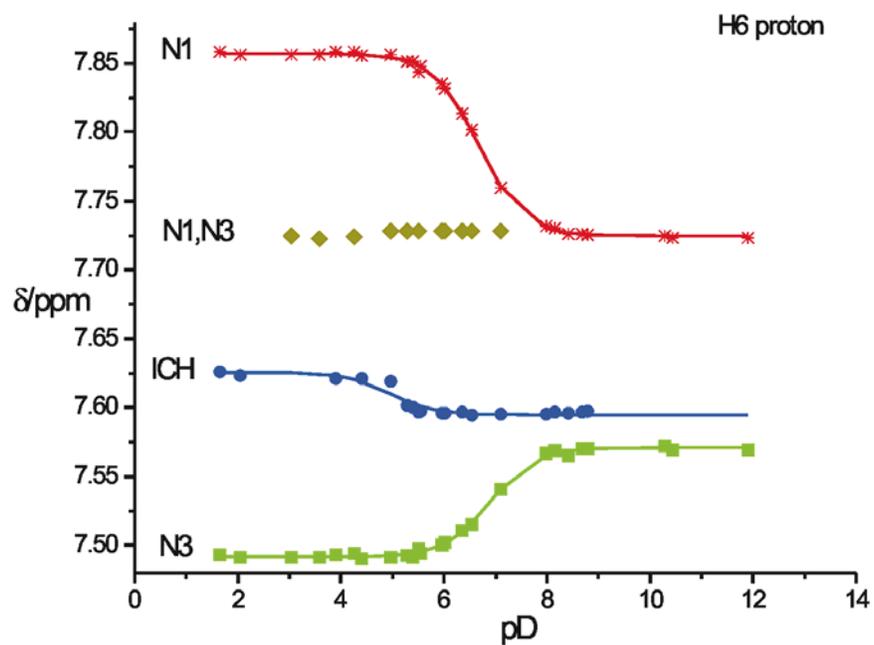
Figure 5 pD dependence (δ, ppm) of H6 proton for [(dien)Pd(ICH-*N1*)]$^{2+}$ (N1), [(dien)Pd(ICH-*N3*)]$^{2+}$ (N3), [(dienPd)$_2$(IC-*N1,N3*)]$^{3+}$ (N1,N3) and free isocytosine (ICH) in D$_2$O.

2.1.6 Characterization of [(dien)PdBr]Br (1)

In order to study (dien)Pd^{II} binding to isocytosine, (**1**) was prepared analogously to [(dien)PtI]I.[105] Yellow crystals were isolated and characterized by X-ray crystallography. A view of [(dien)PdBr]Br is given in Figure 6.
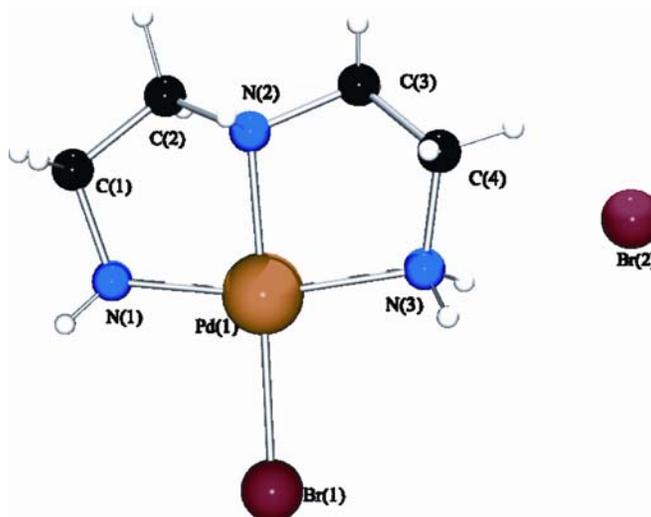
Figure 6 View of [(dien)PdBr]Br (1) with atom numbering scheme.

Table 1 Selected distances (Å) and angles (º) for [(dien)PdBr]Br (1)

[(dien)PdBr]Br (1)			
Pd(1)-Br(1)	2.4303(7)	Pd(1)-N(2)	2.013(4)
Pd(1)-N(1)	2.036(4)	Pd(1)-N(3)	2.049(4)
N(2)-Pd(1)-Br(1)	173.7(2)	C(1)-N(1)-Pd(1)	108.1(4)
N(1)-Pd(1)-Br(1)	96.37(2)	C(3)-N(2)-Pd(1)	108.3(4)
N(3)-Pd(1)-Br(1)	96.4(2)	C(2)-N(2)-Pd(1)	108.2(3)
N(2)-Pd(1)-N(3)	83.9(2)	C(4)-N(3)-Pd(1)	108.5(3)
N(1)-Pd(1)-N(3)	165.8(2)		

Selected bond lengths and angles for [(dien)PdBr]Br are given in Table 1. Bond distances and bond angles within the diethylenetriamine are normal and agree with the previously reported values. The Pd-N distances range from 2.013(4) - 2.049(4) Å and are likewise normal. The dien ligand has a characteristic sting-ray geometry[106] with the central methylene groups C(2) and C(3) of the dien ligand above the PdN_3Br plane. Deviations of carbon atoms of the dien ligand from the least-squares planes formed by the PdN_3Br plane are 0.15(1) Å (C1), -0.40(1) Å (C2), -0.40(1) Å (C3) and 0.16(1) Å (C4). The bromide anion is involved in numerous hydrogen bonding interactions with the NH_2 and NH groups of dien, N(1)-H···Br(2), 3.584(5) Å, N(1)-H···Br(2), 3.512(5) Å, N(3)-H···Br(2), 3.509(4) Å, N(3)-H···Br(2), 3.482(4) Å and N(2)-H···Br(2), 3.373(4) Å.

2.1.7 Characterization of [(dien)Pd(ICH-*N3*)](NO₃)₂ (2)

The reaction of (dien)Pd[II] with isocytosine was carried out on a preparative scale and the solution was kept for crystallization at room temperature. The yellow crystals were isolated and the characterization of the compound was achieved by X-ray analysis as well as IR, Raman and NMR spectroscopy. ^{1}H NMR spectra were recorded in D_2O and it was found that there was an immediate equilibration of the compound in solution to give four sets of resonances (A) – (D), (refer Figure 3) with set (B) dominating.

A view of the molecular cation of [(dien)Pd(ICH-*N3*)](NO$_3$)$_2$ (**2**) is given in Figure 7. Pd is bonded through the N(3) position of the isocytosine (Pd-N(3), 2.029(3) Å). Distances and angles within the ICH ligand are not unusual.
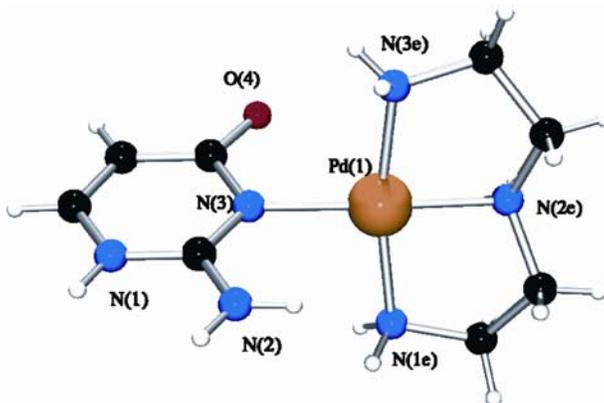
Figure 7 View of cation of [(dien)Pd(ICH-*N3*)](NO$_3$)$_2$ (2) with atom numbering scheme.

Angles about the Pd deviate markedly from ideal square-planar (*e.g.* N(1e)-Pd-N(2e), 84.8(2)°; N(1e)-Pd-N(3e), 167.8(2)°), as expected. The dien chelate adopts the characteristic sting-ray geometry[106] with the methylene groups C(2e) and C(3e) above the PdN$_4$ plane. The ICH plane forms an angle of 73.2(1)° with the Pd coordination plane. A comparison of the external angles at N(3) (Pd-N(3)-C(4), 114.5(3)°; Pd-N(3)-C(2), 125.2(3)°) shows these to be unequal. Consequently, O(4) is closer to Pd as compared to N(2). N(1)H, N(2)H$_2$, and O(4) of the ICH ligand are involved in numerous hydrogen bonding interactions. For example, the proton at N(1) is "chelated" by two oxygen atoms of a nitrate anion, whereas the two protons of N(2) form hydrogen bonds to oxygens of two different nitrate anions. O(4), on the other hand, is bonded to a proton of the amino group N(3e) of the dien ligand. None of these contacts (2.9 – 3.1 Å) between heavy atoms is particularly short.

2.1.8 Reactions of (dien)Pt^{II} with Isocytosine

Analogous NMR scale reactions (Figure 8) were also performed with [(dien)Pt(D$_2$O)](NO$_3$)$_2$ and isocytosine. The reaction conditions were similar except that the completion of the reactions took two days in the case of Pt.
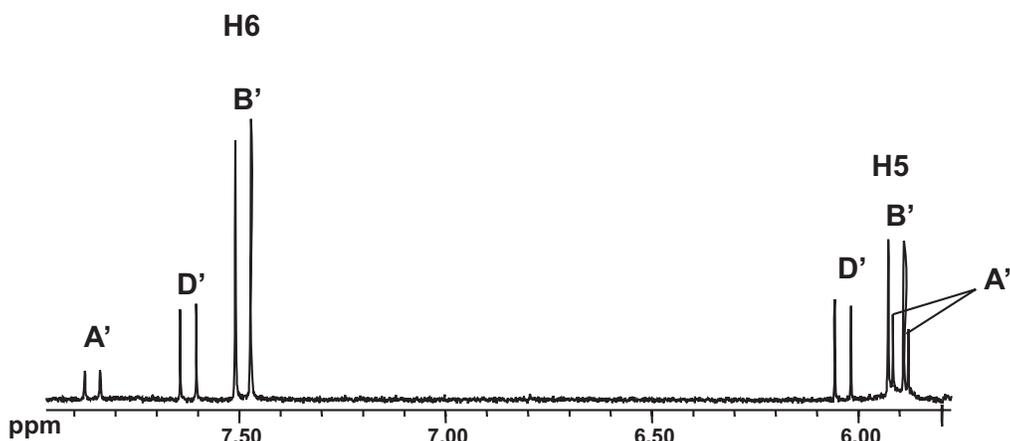
Figure 8 ^{1}**H NMR spectrum (D$_2$O, pH* 1.3, isocytosine resonances only) of reaction mixture (1:1) of [(dien)Pt(D$_2$O)]$^{2+}$ and isocytosine after 2 days at 40 ˚C. Assignment of resonances (A'), (B'), (D') was made on the basis of their pD dependence. A', B' and D' are due to the N(1), N(3) and free ICH, respectively.**

Later, pD dependent ^{1}H NMR spectroscopic measurements (Figures 9 and 10) were carried out. Depending on the pD of the solution, there were three or four sets of resonances observed. As explained above, resonances (A') – (D') were assigned on the basis of their pD dependence. The species distribution was similar to that in the (dien)Pd^{II}/ICH system. Relevant pK_a values are 6.39 ± 0.03 for [(dien)Pt(ICH-*N3*)]$^{2+}$ and 5.97 ± 0.03 for [(dien)Pt(ICH-*N1*)]$^{2+}$.
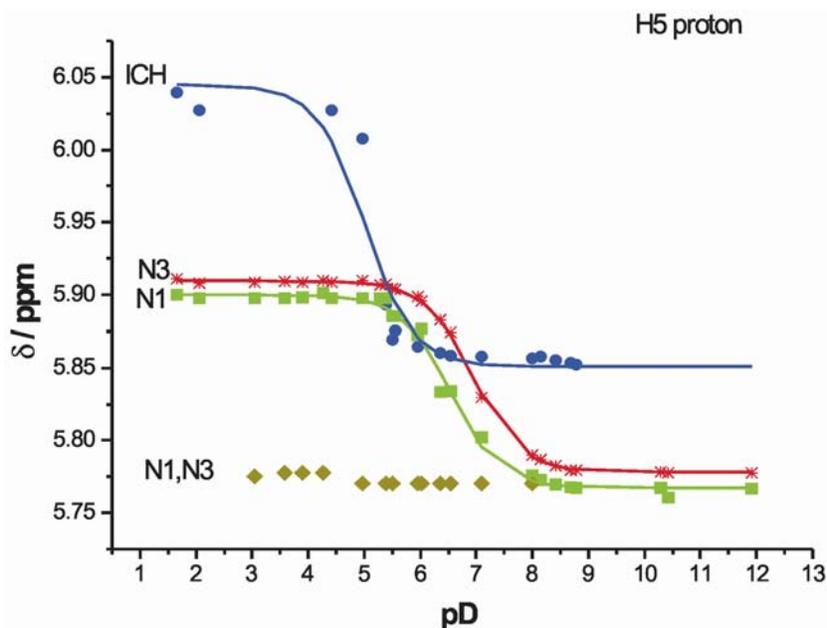
Figure 9 pD dependence (δ, ppm) of H5 proton for [(dien)Pt(ICH-*N1*)]$^{2+}$ (N1), [(dien)Pt(ICH-*N3*)]$^{2+}$ (N3), [(dienPt)$_2$(IC-*N1,N3*)]$^{3+}$ (N1,N3) and free isocytosine (ICH) in D$_2$O.
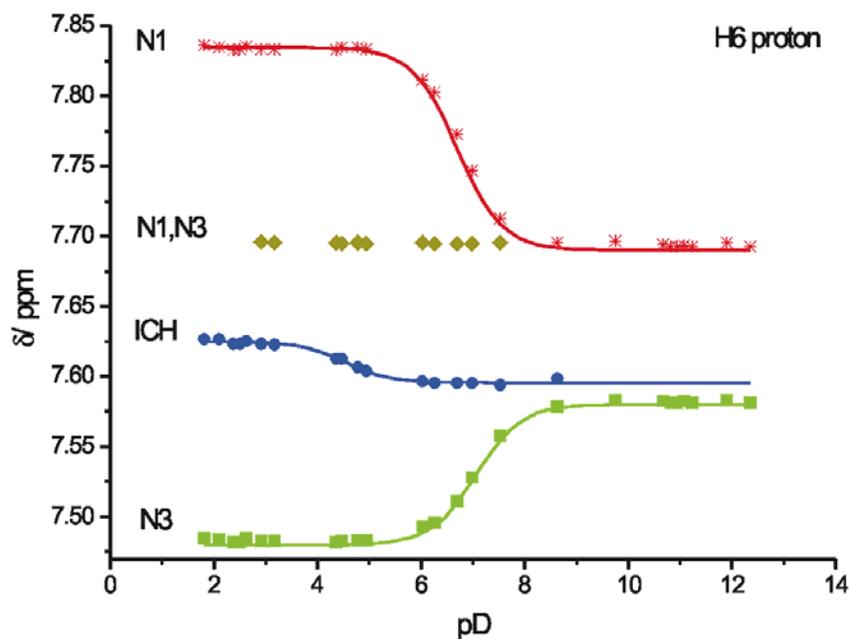
Figure 10 pD dependence (δ, ppm) of H6 proton for [(dien)Pt(ICH-*N1*)]$^{2+}$ (N1), [(dien)Pt(ICH-*N3*)]$^{2+}$ (N3), [(dienPt)$_2$(IC-*N1,N3*)]$^{3+}$ (N1,N3) and free isocytosine (ICH) in D$_2$O.

2.1.9 Characterization of [(dienM)$_2$(IC-*N1,N3*)](ClO$_4$)$_3$ (M = Pt^{II}, 3 or Pd^{II}, 4)

1:3 mixtures of isocytosine and [(dien)M(D$_2$O)]$^{2+}$ were kept at 40 °C for a few hours. Initially, a typical spectrum at pD 4.6 consisted of four sets of aromatic H(5) and H(6) isocytosine resonances (doublets each, ^3J ~ 6.7 – 7.3 Hz). The most intense set of resonances was due to the N(3) linkage isomer and correspondingly, the other sets of resonances belonged to the free ligand, N(1) linkage isomer and N(1),N(3) dinuclear species. pD's of the samples were subsequently adjusted to 7.6 and [(dien)M(D$_2$O)]$^{2+}$ solutions were successively added to the reaction mixtures. This was repeated until only a single set of resonances due to **3** or **4** was observed.

Both **3** and **4** display ^{1}H NMR resonances, which are insensitive to pD over a wide range. However, at pD 1.2, **4** decomposes in the solution to give ICH and (dien)Pd^{II}, whereas **3** is converted into [(dien)Pt(ICH-*N1*)]$^{2+}$ (**5a**) (ref. section 2.1.10).

Views of the molecular cations **3** and **4** are shown in Figures 11 and 12. Selected bond lengths and angles for **3** and **4** are given in Table 2. Pd and Pt have the expected square-planar coordination geometries.
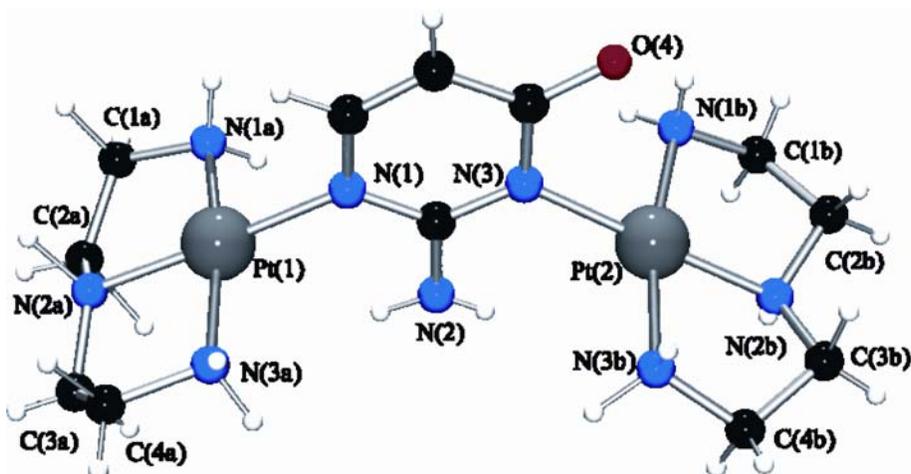
Figure 11 View of cation of [(dienPt)$_2$(IC-*N1,N3*)](ClO$_4$)$_3$ (3) with atom numbering scheme.
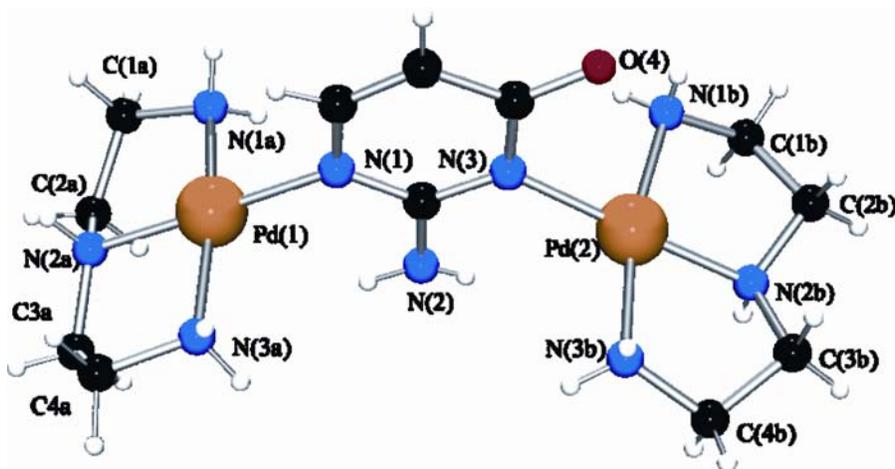
Figure 12 View of cation of [(dienPd)$_2$(IC-*N1,N3*)](ClO$_4$)$_3$ (4) with atom numbering scheme.

As can be seen, metals are bonded through N(1) and N(3) positions of the IC; M(1)-N(1) has the distances ranging from 2.026(6) to 2.034(3) Å and M(2)-N(3) from 2.037(3) to 2.039(6) Å for Pd and Pt, respectively. Distances and angles within the IC ligand are not unusual.

Angles about Pd and Pt deviate markedly from ideal square-planar (*e.g.* N(1a)-M(1)-N(2a), 84.6(2) to 84.9(2)°; N(1a)-M(1)-N(3a), 167.8(2) to 176.6(2)°; N(1b)-

M(2)-N(2b), 84.9(2) to 85.2(2)°; N(1b)-M(2)-N(3b), 168.4(2) to 169.1(3)° for Pd and Pt, respectively). The M-N(dien) distances range from 1.999(4) Å in M(1)-N(2a) or M(2)-N(2b) to 2.039(4) Å in M(1)-N(3a) or M(2)-N(3b), and are likewise normal. The dien ligands, "a" and "b", adopt the characteristic sting-ray geometries[106] with the central methylene groups C(2) and C(3) of the two dien ligands pointing in the same direction, yet in opposite directions for "a" and "b".

Deviations of carbon atoms of the two dien ligands from the least-squares planes formed by the PtN_4 plane are -0.52(1) Å (C2a), -0.36(1) Å (C3a), -0.02(1) Å (C1a) and 0.29(1) Å (C4a) as well as 0.50(1) Å (C2b), 0.62(1) Å (C3b), -0.003(1) Å (C4b), and -0.15(1) Å (C1b). Thus, the two halves of the dien ligands undergo marked distortions from the case of a symmetrical distribution of the two carbon atoms of an ethylenediamine ring.[106]

For the corresponding Pd compound, these values are rather similar. IC planes form angles of approximately 86° and 74° with the respective Pd(1)/Pt(1) and Pd(2)/Pt(2) coordination planes. The external angles at N(1) and N(3) (M(1)-N(1)-C(6), 120-121°; M(1)-N(1)-C(2), 120-122°; M(2)-N(3)-C(4), 118-119°; M(2)-N(3)-C(2), 120-121°) are quite similar.

The water molecules, dien ligands, perchlorate anions, $N(2)H_2$ and O(4) of the IC ligand are involved in numerous intramolecular and intermolecular short contacts. For example, the protons at N1(a/b), N2(a/b) and N3(a/b) of dien ligands are hydrogen bonded to various oxygen atoms of different perchlorate anions, water molecules and O(4) of the IC ligand, whereas the two protons of N(2) in IC form hydrogen bonds to oxygen of a perchlorate anion and a water molecule.

A motif is also present in the solid structure, where O(4) of the IC ligand forms hydrogen bonds to protons at N(1) of dien ligands of two different molecules. None of these contacts (2.9 – 3.1 Å) between heavy atoms is particularly short.

Table 2 Selected distances (Å) and angles (º) for 3, 4

	3	**4**
M(1)···M(2)	5.90(2)	5.89(2)
M(1)-N(1)	2.034(3)	2.026(6)
M(1)-N(1a)	2.042(3)	2.039(5)
M(1)-N(2a)	1.999(3)	2.006(8)
M(1)-N(3a)	2.034(3)	2.033(5)
M(2)-N(3)	2.037(3)	2.039(6)
M(2)-N(1b)	2.032(3)	2.037(5)
M(2)-N(2b)	1.999(4)	2.009(8)
M(2)-N(3b)	2.048(3)	2.049(5)
M(1)N$_4$/ICH[a]	86.9(1)	86.2(2)
M(2)N$_4$/ICH[a]	74.6(1)	74.8(2)
C(2)-N(1)-C(6)	116.6(4)	116.1(6)
C(2)-N(3)-C(4)	120.3(4)	120.6(6)
N(1)-C(2)-N(3)	123.9(3)	124.0(4)

[a]Dihedral angle between M coordination plane (M-N$_4$) and IC

2.1.10 Characterization of [(dien)Pt(ICH-*N1*)]$^{2+}$ (**5a**) and [(dien)PtCl]$^+$ (**5b**)

In the course of these studies, it was noticed that in acidic medium the dinuclear complex **3** could be converted into the mononuclear complex [(dien)Pt(ICH-*N1*)]$^{2+}$ (**5a**), which contains the desired tautomer **1b** bonded to Pt via the N(1) position.

The time course of the reaction was followed by ^{1}H NMR spectroscopy. The stacked plot of the downfield regions in the ^{1}H NMR spectra is shown in Figure 13. A small proton-deuterium coupling was also observed for the H5 proton of isocytosine which undergoes a partial exchange with the ^{2}D.
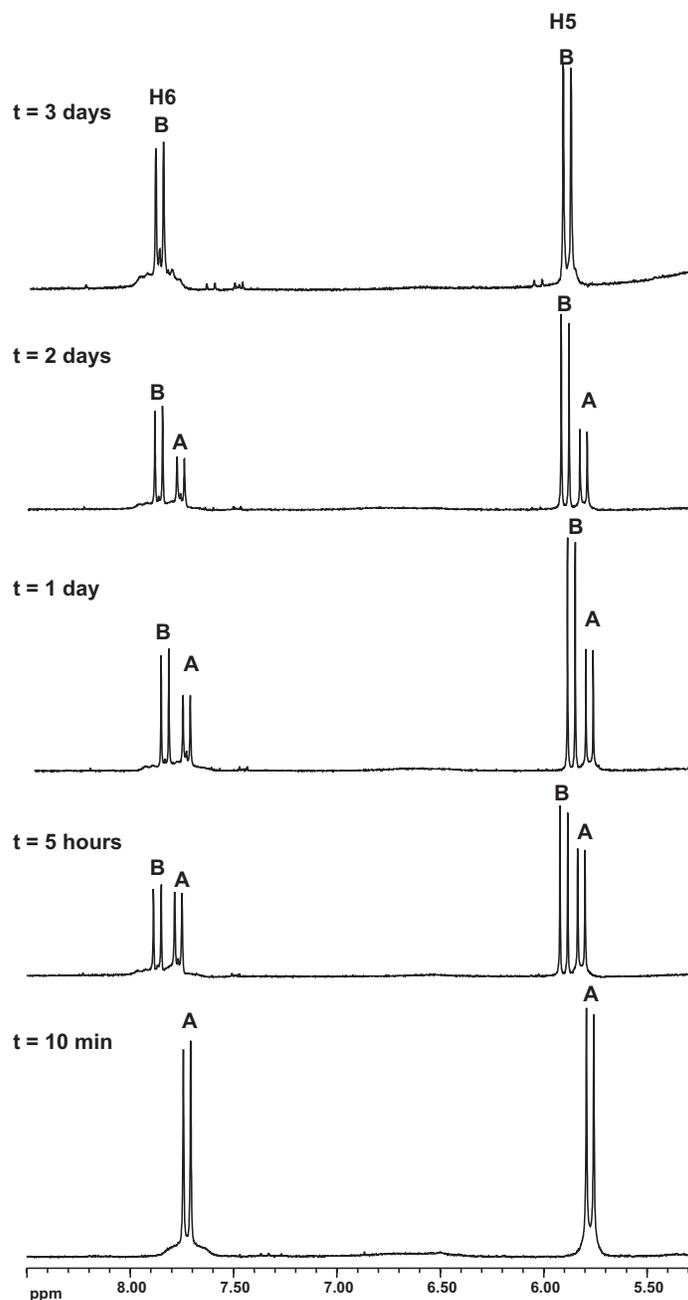
Figure 13 Stacked plot of the downfield regions in the ^{1}H NMR spectra (200 MHz, D$_2$O, pH* 1.0, isocytosine resonances only). The set of resonances A is due to [(dienPt)$_2$(IC-*N1,N3*)]$^{3+}$ and set B is assigned to the [(dien)Pt(ICH-*N1*)]$^{2+}$ on the basis of their pD-dependent shifts.

Unfortunately, our attempts to isolate **5a** have failed so far. We propose that removal of the (dien)Pt^{II} entity from N(3) of **3** follows a way which Lippert et al. have shown to take place with N(3) platinated 1-methyluracil and 1-methylthymine model nucleobases.[107-109] According to it (Chart 10), protonation

of the exocyclic O(4) oxygen atom labilizes the Pt-N(3) bond to such an extent that it breaks. The enol tautomer formed initially converts then quickly into the oxo tautomer **5a.**
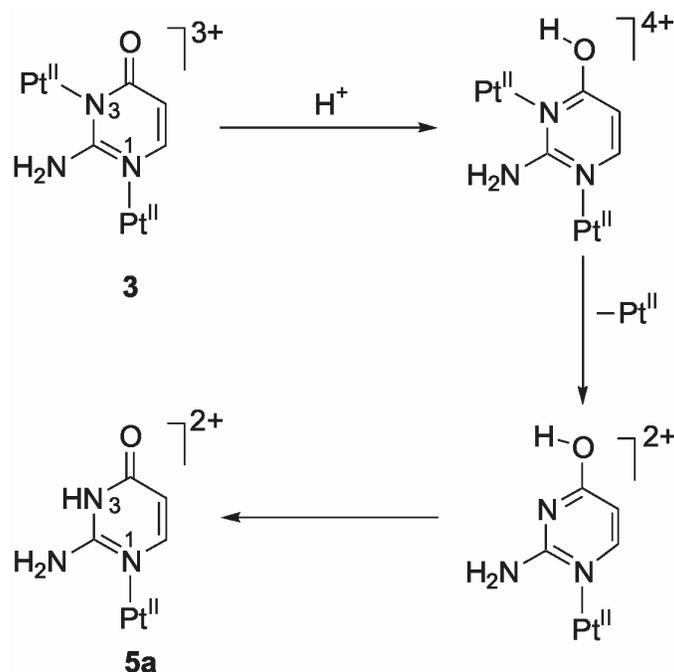
Chart 10 Proposed removal of the (dien)Pt^{II} entity from N(3) of 3.

Crystallization during the course of the work described above yielded a sample suitable for X-ray analysis. Unfortunately, the analysis revealed the structure **5b** (Figure 14) instead of **5a.** Table 3 provides a few selected structural details of the compound **5b.**
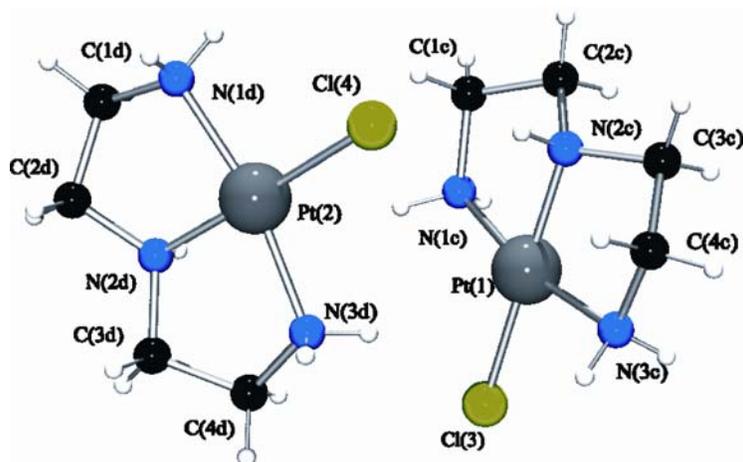
Figure 14 View of cations of [(dien)PtCl]ClO$_4$ (5b) with atom numbering scheme.

The geometry of the (dien)Pt^{II} entity is not unusual and compares well with the published data,[106] including the deviations of angles at the Pt from 90°. Out of the eight CH$_2$ groups, the four central methylene groups C(2c) and C(3c), C(2d) and C(3d) are on the same side of the Pt(1)N$_4$ and Pt(2)N$_4$ planes, respectively.

Bond distances and bond angles within the diethylenetriamine are normal and agree with the previously reported values. The molecular ions, [(dien)PtCl]$^+$, are arranged in a *head-tail* orientation in the crystal such that the Cl groups can participate in various intermolecular and intramolecular hydrogen bonding interactions, viz. N(2c)-H···Cl(4), 3.27(2) Å, N(1c)-H···Cl(3), 3.35(2) Å and N(3d)-H···Cl(4), 3.39(2) Å. The perchlorate anions form several hydrogen bonds to the dien-NH$_2$ and dien-NH groups. None of these contacts (3.1 – 3.4 Å) between heavy atoms are particularly short.

Table 3 Selected distances (Å) and angles (°) for [(dien)PtCl]ClO$_4$ (5b)

[(dien)PtCl]ClO$_4$ (5b)			
Pt(1)-Cl(3)	2.301(4)	Pt(2)-Cl(4)	2.307(4)
Pt(1)-N(1c)	2.04(2)	Pt(2)-N(1d)	2.03(2)
Pt(1)-N(2c)	2.00(2)	Pt(2)-N(2d)	2.01(2)
Pt(1)-N(3c)	2.05(2)	Pt(2)-N(3d)	2.05(2)
Cl(3)-Pt(1)-N(1c)	95.5(3)	Cl(4)-Pt(2)-N(1d)	95.4(4)
Cl(3)-Pt(1)-N(2c)	179.4(4)	Cl(4)-Pt(2)-N(2d)	177.4(4)
Cl(3)-Pt(1)-N(3c)	95.3(3)	Cl(4)-Pt(2)-N(3d)	96.0(3)
N(1c)-Pt(1)-N(2c)	85.0(4)	N(1d)-Pt(2)-N(2d)	83.3(5)
N(1c)-Pt(1)-N(3c)	168.4(4)	N(1d)-Pt(2)-N(3d)	167.6(5)
N(2c)-Pt(1)-N(3c)	84.2(5)	N(2d)-Pt(2)-N(3d)	84.2(5)

2.1.11 Reactions of *trans*-(NH$_3$)$_2$Pt^{II} with Isocytosine

In an attempt to obtain metal complexes containing the N(1) linkage isomers of isocytosine, several reactions at different ratios Pt:ICH (1:1; 1:3; 3:1 etc.) were

performed with *trans*-[(NH$_3$)$_2$Pt(D$_2$O)$_2$]$^{2+}$ and isocytosine and followed by ^{1}H NMR spectroscopy.

Unfortunately, due to the large number of resonances (ca. 12 sets of doublets) it was not possible to interpret the complicated spectra (Figure 15) obtained after the reaction. However, it was clearly evident that there was always a predominance of N(3) linkage isomers (H5 resonances in the range 5.6 - 6.2 ppm) over N(1) linkage isomers (H6 resonances, 7.4 – 8.2 ppm), if chemical shifts of the (dien)Pt^{II} linkage isomers were taken as a reference.
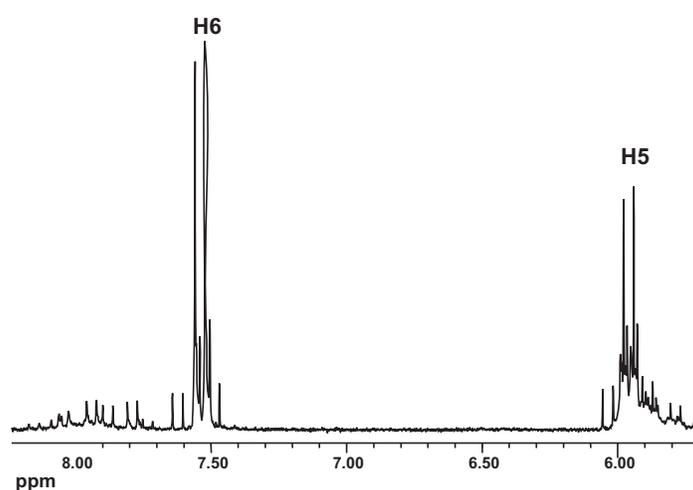
Figure 15 ^{1}**H NMR spectrum (D$_2$O, pH* 2.3, isocytosine resonances only) of reaction mixture (1:1) of *trans*-[(NH$_3$)$_2$Pt(D$_2$O)$_2$]$^{2+}$ and isocytosine after two days at 40 ˚C.**

2.1.12 Reactions of *cis*-(NH$_3$)$_2$Pt^{II} with Isocytosine

Several reactions at different ratios Pt:ICH (1:1; 1:3; 3:1 etc.) were carried out with *cis*-[(NH$_3$)$_2$PtCl$_2$] and isocytosine at room temperature and at 40 ˚C. The reactions were followed by ^{1}H NMR spectroscopy.

For the reactions performed at 40 ˚C, complicated spectra were obtained (ca. 10 sets of doublets) which were difficult to interpret. In contrast, the ^{1}H NMR spectra (Figure 16) for the reaction at room temperature, exhibited three sets of doublets. A set of resonances (C) was assigned to free isocytosine on the basis of the pD-dependence carried out earlier. The most intense set of resonances (B) was

assigned to N(3) linkage isomer (H5 resonances at 5.90 ppm; H6 resonances at 7.49 ppm), if chemical shifts of the (dien)Pt^{II} linkage isomer were taken as a reference. Correspondingly, the set of resonances (A) might be due to N(1) linkage isomer (H5 resonances at 5.87 ppm; H6 resonances at 7.87 ppm). However, it was not possible to isolate and separate the different products.
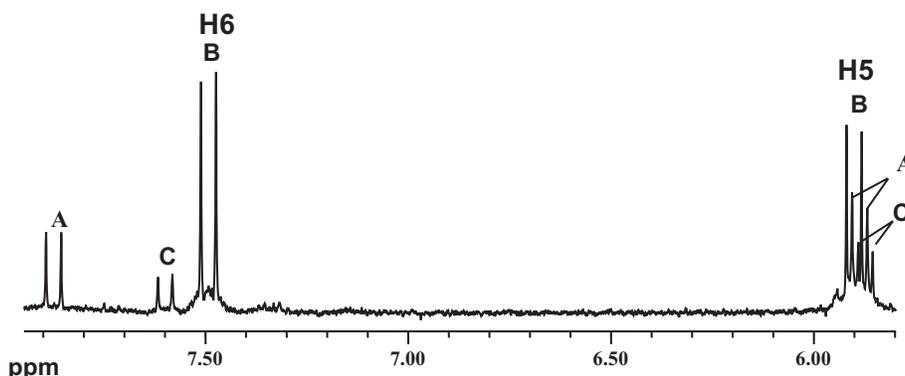
Figure 16 ^{1}H NMR spectrum (D$_2$O, pH* 5.3, isocytosine resonances only) of reaction mixture (3:1) of *cis*-[(NH$_3$)$_2$PtCl$_2$] and isocytosine after five days at room temperature. The set of resonances A is assigned to N(1) linkage isomer, B is due to the N(3) linkage isomer and finally, C is the free ligand.

2.1.13 Other Attempts to obtain N(1) Linkage Isomers

Attempts to prepare and isolate N(1) linkage isomers of isocytosine using different metal species, such as K$_2$PdCl$_4$, K$_2$PtCl$_4$, *cis*-[(NH$_3$)$_2$Pt(1-MeC)Cl]Cl, *trans*-[(NH$_3$)$_2$Pt(1-MeC)Cl]Cl, *trans*-[(NH$_3$)$_2$Pt(9-RGH-*N7*)Cl]Cl and *trans*-[(NH$_3$)$_2$Pt(1-MeT)Cl] (with 1-MeC = 1-methylcytosine, 9-RGH = 9-methyl- or 9-ethylguanine, 1-MeT = 1-methylthymine), or different solvents (ethanol, DMF, acetone) were likewise unsuccessful. It was found that there was always a predominance of N(3) linkage isomers over N(1) isomers. N(1) linkage isomers were formed only in small amounts.

2.1.14 Theoretical Calculations

Molecular geometries of a variety of compounds have been computed in an attempt to better understand the apparent preference of Pt^{II} and Pd^{II} electrophiles for the N(3) site of ICH. Figure 17 provides views of optimized structures of the

N(1) and N(3) linkage isomers of $[(NH_3)_3Pt(ICH)]^{2+}$, *trans*-$[(NH_3)_2PtCl(ICH)]^+$, and *cis*-$[(NH_3)_2PtCl(ICH)]^+$.

$[(NH_3)_3Pt(ICH-N1)]^{2+}$ $[(NH_3)_3Pt(ICH-N3)]^{2+}$

trans-$[(NH_3)_2PtCl(ICH-N1)]^+$ *trans*-$[(NH_3)_2PtCl(ICH-N3)]^+$

cis-$[(NH_3)_2PtCl(ICH-N1)]^+$ *cis*-$[(NH_3)_2PtCl(ICH-N3)]^+$
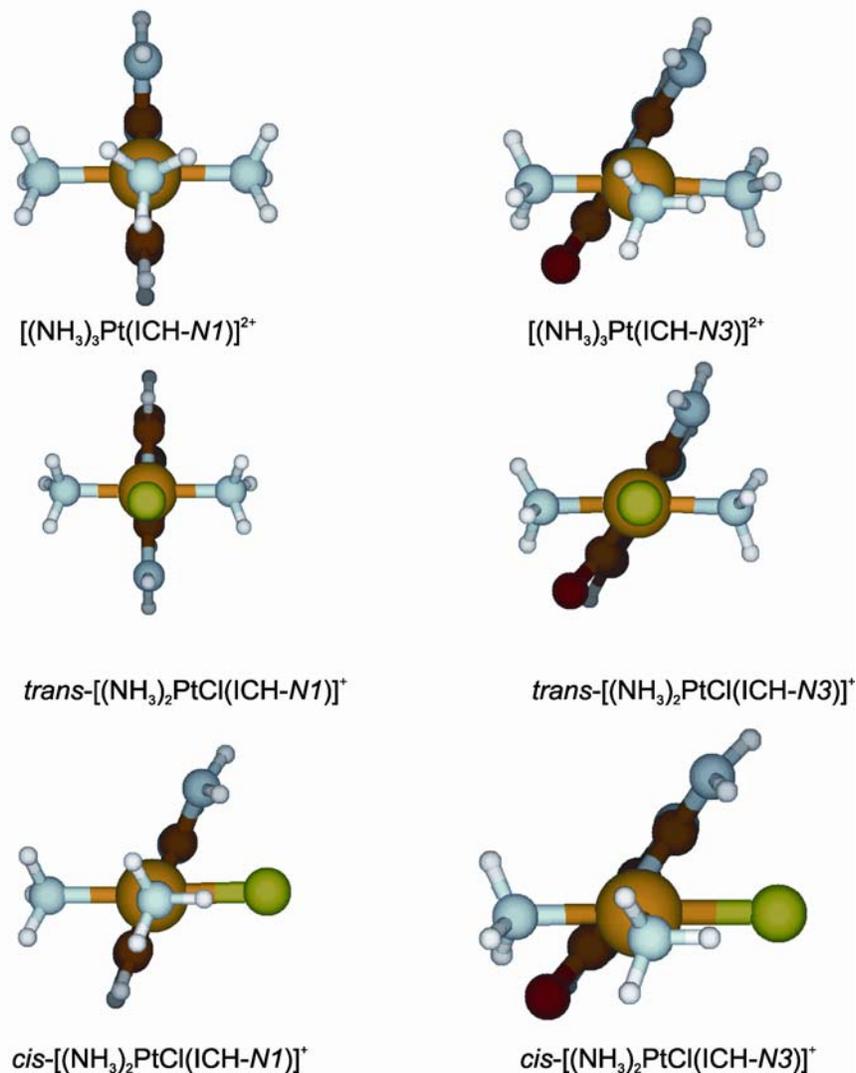
Figure 17 Optimized computed structures of N(1) and N(3) linkage isomers of $[(NH_3)_3Pt(ICH)]^{2+}$, *trans*-$[(NH_3)_2PtCl(ICH)]^+$ and *cis*-$[(NH_3)_2PtCl(ICH)]^+$.

Calculations of relative energies of N(1) and N(3) linkage isomers in the case of $(NH_3)_3Pt^{II}$ reveal a preference of the Pt^{II} entity for N(3) (ΔE = 12.2 kcal/mol). The comparison between the two geometries shows that in the N(1) linkage isomer the heterocycle is perpendicular to the PtN_4 plane. The lack of any hydrogen bonding between the two trans-positioned NH_3 groups at the Pt and the exocyclic amino group of ICH and the inability of O(4) to interact with any of the other

ligands of Pt is consistent with this finding. On the other hand, in the N(3) linkage isomer the isocytosine ring forms an angle of ca. 55° with the PtN_4 plane due to the possibility of intramolecular hydrogen bonding between O(4) of ICH and one of the NH_3 ligands of Pt (O···N, 2.79 Å).

The computations furthermore suggest weak hydrogen bonding between a second NH_3 and the exocyclic amino group $N(2)H_2$ (N···N, 3.27 Å), which has undergone some pyramidalization. This finding is consistent with results of recent *ab initio* calculations which suggest that contrary to long-time beliefs that nucleobase-NH_2 groups are perfectly planar, exocyclic amino groups can be partially sp^3 hybridized[110] with the ability to function as a hydrogen bonding acceptor in nucleic acid structures.[111]

The situation with the two linkage isomers of *trans*-$[(NH_3)_2PtCl(ICH)]^+$ closely parallels that of $[(NH_3)_3Pt(ICH)]^{2+}$. In the N(1) linkage isomer, the ICH ring is perpendicular to the PtN_3Cl plane, while it is tilted (56.9°) in the case of the N(3) isomer. The energy difference is 4.2 kcal/mol, again with the N(3) linkage isomer being the more stable one.

For the two isomers of *cis*-$[(NH_3)_2PtCl(ICH)]^+$, the energy difference is 6.9 kcal/mol, with the N(3) linkage isomer being again the more stable one. In both isomers, the ICH plane is tilted with respect to the PtN_3Cl plane by 63.8° (N(1) isomer) and 55.7° (N(3) isomer). It appears that, at least with the N(1) isomer, weak hydrogen bonding between $N(2)H_2$ of ICH and the Cl ligand is responsible for this feature.

With the N(3) linkage isomer, in addition to such a possibility also hydrogen bonding between O(4) of ICH and one NH_3 ligand (O···N, 2.75 Å) as well as the Cl and one NH_3 ligand (Cl···N, 3.01 Å) is possible. It is to be noted that none of the intramolecular hydrogen bonds is to be considered particularly strong, simply because the angles at the acceptor (*e.g.* Cl) are not very favorable, *e.g.* Pt-Cl···H, 62.8°, in *cis*-$[(NH_3)_2PtCl(ICH-N3)]^+$ (see, however, below). An interesting detail of

both isomers of *cis*-[(NH$_3$)$_2$PtCl(ICH-*N3*)]$^+$ is the pyramidalization of the amino group of ICH, in that it is opposite to that seen in the *trans*-[(NH$_3$)$_2$PtCl(ICH-*N3*)]$^+$ and [(NH$_3$)$_3$Pt(ICH-*N3*)]$^{2+}$. It indeed strongly suggests that there is hydrogen bonding between N(2)H$_2$ and Cl.

Calculations were performed (Figure 18) on a series of bis(isocytosine) complexes of *trans*-(NH$_3$)$_2$Pt^{II}, which differed in their combinations of binding sites (linkage isomers) and their rotameric forms.

Figure 18   Optimized computed structures of the three types of bis(isocytosine) complexes of *trans*-(NH$_3$)$_2$Pt^{II} with different rotamers.

As far as relative energies are concerned, the following picture emerged (Figure 19): (i) The *head-head* form of *trans*-[(NH$_3$)$_2$Pt(ICH-*N1*)$_2$]$^{2+}$ (Ia) is the least stable form, and the *head-tail* rotamer of *trans*-[(NH$_3$)$_2$Pt(ICH-*N3*)$_2$]$^{2+}$ (IIb) is the most stable one (ΔE = -35.9 kcal/mol). (ii) The *head-tail* rotamer (Ib) of *trans*-[(NH$_3$)$_2$Pt(ICH-*N1*)$_2$]$^{2+}$ is only slightly more stable than its *head-head* rotamer (-1 kcal/mol), while the second rotamer IIa (*head-head*) of *trans*-[(NH$_3$)$_2$Pt(ICH-*N3*)$_2$]$^{2+}$ is considerably less stable than its *head-tail* rotamer, albeit still the second most stable species (-17.7 kcal/mol).
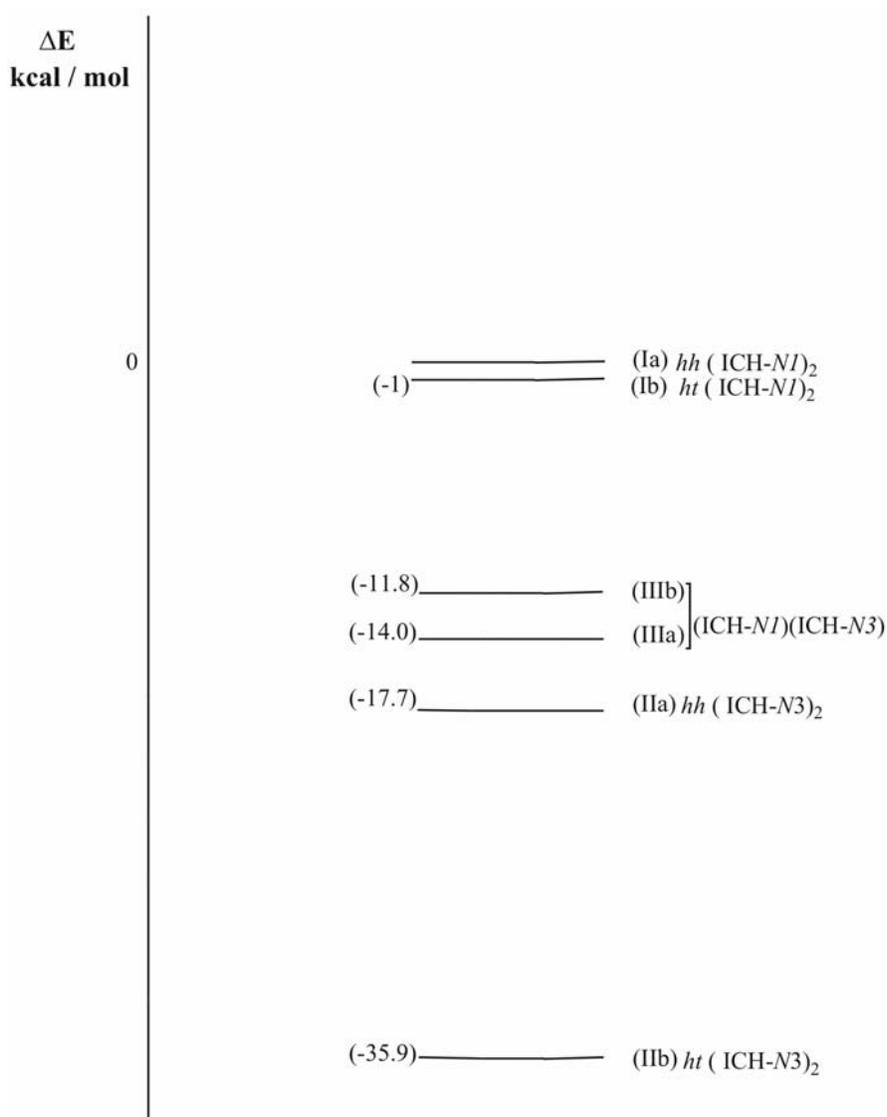
Figure 19   Relative energies of the six bis(isocytosine) complexes of *trans*-(NH$_3$)$_2$Pt^{II} shown in Figure 18.

There are two rotameric forms of the mixed complex *trans*-[(NH$_3$)$_2$Pt(ICH-*N3*)(ICH-*N1*)]$^{2+}$ with O(4) of (ICH-*N3*) either opposite to N(2)H$_2$ of (ICH-*N1*) (IIIa) or with O(4) of (ICH-*N3*) opposite to H6 of (ICH-*N1*) (IIIb). The former is stabilized by 14 kcal/mol relative to the least stable form (Ia), and (IIIb) is more stable by 11.8 kcal/mol.

Taken together, these results again confirm the preference of *trans*-(NH$_3$)$_2$Pt^{II} for N(3) binding to ICH. With regard to the most stable compound, the *head-tail* rotamer IIb, it is reminiscent of the *head-tail* rotamer of *trans*-[(NH$_3$)$_2$Pt(cytosine-*N3*)]$^{2+}$ which is likewise more stable than its *head-head* form.[27] Although internucleobase hydrogen bonding is not possible because of the large separation between opposite exocyclic O(4) and N(2)H$_2$ groups, there is a possibility for hydrogen bonding between NH$_3$ ligands and the O(4) groups (2.84 Å), leading to a tilting of the bases with respect to the Pt coordination plane (56.9°), very much as in the minimum energy structure of the bis(cytosine) compound (60°).[27] With N(1)-Pt coordination, no such hydrogen bonding is possible.

As to the reasons for the preference of the N(3) site of ICH for Pt and Pd am(m)ine complexes, we considered a favorable orientation of the dipole moment of one of the two tautomers (**1a**, Chart 3) as a possible explanation, very much as previously considered for the preferential binding of metal ions to N(7) of guanine nucleobases.[112,113] However, the results of these calculations (not shown) were inconsistent with the experimental findings and the energy calculations.

NBO (Natural Bond Orbital)[114-116] calculations were subsequently carried out which showed that in the N(3) linkage isomer of [(NH$_3$)$_3$Pt(ICH-*N3*)]$^{2+}$ not only hydrogen bonds between the NH$_3$ ligand and O(4) of ICH were formed but that in addition hydrogen bonding took place between a second NH$_3$ ligand and the substantially pyramidalized exocyclic amino group of ICH. In fact, both hydrogen bonds stabilize the minimum structure in the same order of magnitude.

Table 4 **Calculated energies (E), energy differences (ΔE), NBO delocalization energies (ΔE_{deloc}) for the complex [(NH$_3$)$_3$Pt(ICH-*N3*)]$^{2+}$ as a function of angle between 64° to 89°. The total delocalization energies ($\Delta E^{(2)}$) in column 6 are obtained by summing up the single contributions $\Delta E^{(2)}$ n$_O$ → o*$_{NH}$ and $\Delta E^{(2)}$ n$_N$ → o*$_{NH}$ in columns 4 and 5.**

			ΔE_{deloc}/kJmol^{-1}		
Angle/°	E/Hartrees	ΔE/kJmol^{-1}	$\Delta E^{(2)}$ n$_O$ → o*$_{NH}$	$\Delta E^{(2)}$ n$_N$ → o*$_{NH}$	$\Delta E^{(2)}$$_{tot}$
116	683.318595	0.0	15.19	16.90	32.09
111	683.318436	0.4177	11.00	12.47	23.47
106	683.317965	1.6549	7.45	8.91	16.36
101	683.317352	3.2651	4.06	5.31	9.37
96	683.316605	5.2272	-	2.34	2.34

NBO delocalization energies $\Delta E^{(2)}$ n$_O$ → o*$_{NH}$ and $\Delta E^{(2)}$ n$_N$ → o*$_{NH}$ were obtained (Table 4) by starting out from the minimum structure and by varying the dihedral angle between the ICH plane and the PtN$_4$ plane between 64° and 89°. The decreasing delocalization energies (Figure 20) can be readily correlated to decreasing hydrogen bond strengths and decreasing total energies of the structures.
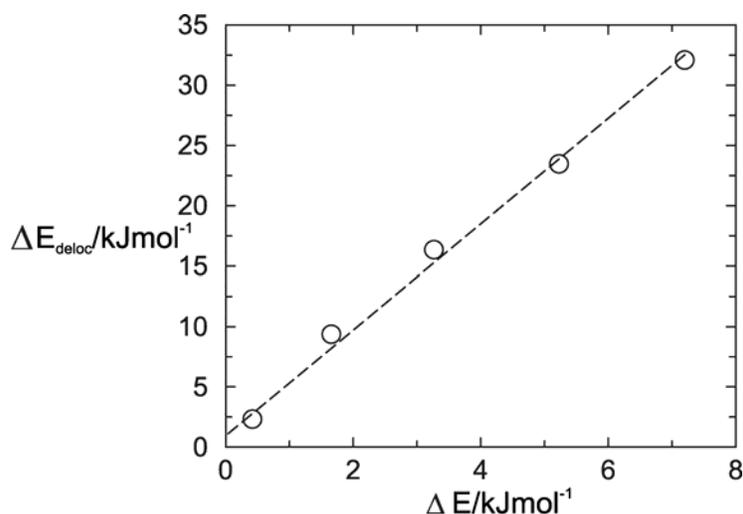
Figure 20 **Correlation between the total NBO delocalisation energies (ΔE_{deloc}) and the energy differences for the complex [(NH$_3$)$_3$Pt(ICH-*N3*)]$^{2+}$ as a function of angle between 64° to 89°. The linear relation suggests that the complex [(NH$_3$)$_3$Pt(ICH-*N3*)]$^{2+}$ is clearly stabilized by hydrogen bonding.**

This suggests that the observed preference of the $(NH_3)_3Pt^{II}$ entity for N(3) of ICH is primarily caused by favorable intramolecular hydrogen bonding. We assume that similar reasons apply to the other complexes. Interestingly, the degree of pyramidalization of the exocyclic amino group is largest when the ICH plane is substantially tilted with respect to the Pt plane, and lost once the heterocycle approaches a perpendicular orientation. We are aware that the inclusion of solvent molecules and the consideration of anions may modify the picture, yet the experimental findings in aqueous solution are consistent with the picture drawn on the basis of the NBO calculations.

The molecular geometries of [(dien)Pd(ICH-*N1*)]$^{2+}$, [(dien)Pd(ICH-*N3*)]$^{2+}$, [(dien)Pt(ICH-*N1*)]$^{2+}$, [(dien)Pt(ICH-*N3*)]$^{2+}$, [(tmeda)Pt(ICH-*N1*)]$^{2+}$ and [(tmeda)Pt(ICH-*N3*)]$^{2+}$ have also been computed. The N(1) linkage isomers (Figure 21) of (dien)M^{II} (M = Pd^{II}, Pt^{II}) are similar.
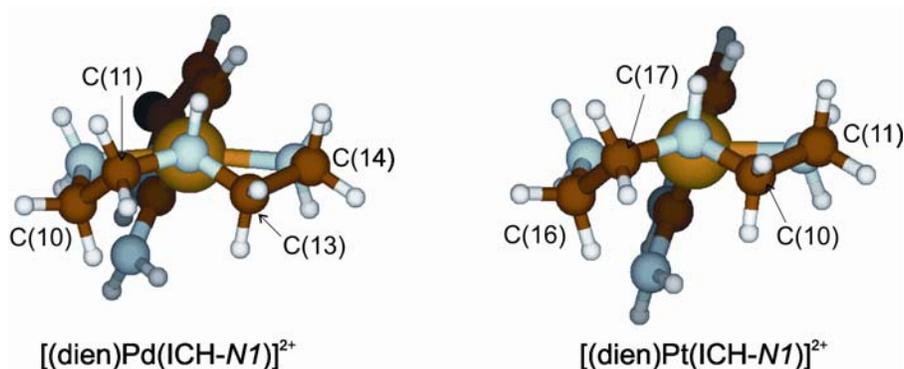
Figure 21 **Optimized computed structures of [(dien)Pd(ICH-*N1*)]$^{2+}$ and [(dien)Pt(ICH-*N1*)]$^{2+}$.**

The angle between the MN$_4$ plane and the ICH plane is 64.2° (M = Pd) and 69.0° (M = Pt). It is possible only as a result of the intramolecular hydrogen bond, which is between the exocyclic amino group N(2)H$_2$ of ICH and one of the two amino groups of the dien ligand. As can be seen, the ICH amino group has undergone some pyramidalization to be able to act as a H bond acceptor, but the hydrogen bond (N(2)H$_2$···NH$_2$(dien) 3.287 Å for Pd and 3.425 Å for Pt compound) is not to be considered particularly strong due to a somewhat unfavorable angle between the dien-NH$_2$ donor and the acceptor. Nevertheless, this hydrogen bond

appears to be responsible for the differences in distortions of the two en halves of the dien ligands. Deviations of carbon atoms from the mean-squares planes in the Pd complex are -0.89 Å (C10) and -0.25 Å (C11), as opposed to -0.69 Å (C13) and -0.15 Å (C14). For the corresponding Pt compound, these values are rather similar.

The N(3) linkage isomers (Figure 22) of (dien)M^{II} are likewise very similar. The ICH plane is tilted by 58.5° (Pd) and 56.0° (Pt), respectively, relative to the MN$_4$ coordination plane.

$[(dien)Pd(ICH-N3)]^{2+}$ $[(dien)Pt(ICH-N3)]^{2+}$
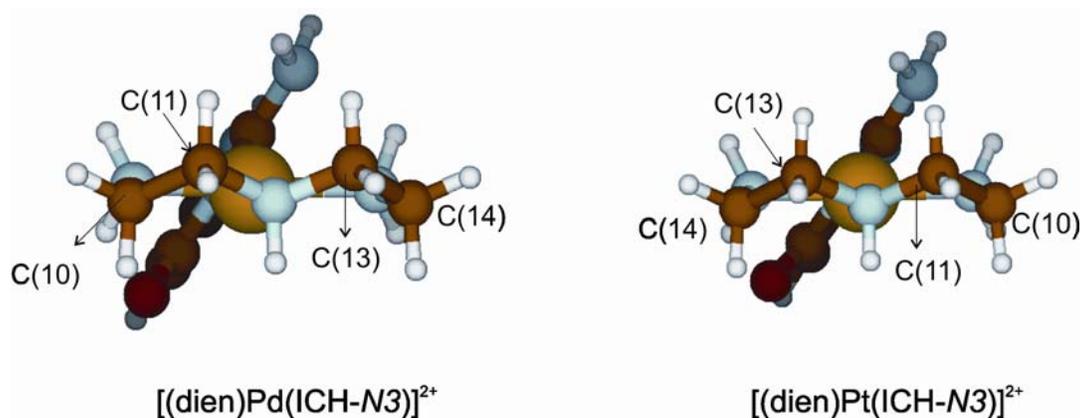
Figure 22 Optimized computed structures of $[(dien)Pd(ICH-N3)]^{2+}$ and $[(dien)Pt(ICH-N3)]^{2+}$.

Both NH$_2$ groups of the dien ligands are involved in hydrogen bond formation with O(4) as well as N(2)H$_2$ of ICH. Hydrogen bond lengths are for O(4)-NH$_2$(dien) 2.843 Å (Pd) and 2.826 Å (Pt), whereas those involving the N(2)H$_2$ of ICH and dien-NH$_2$ are 3.435 Å (Pd) and 3.336 Å (Pt). Again, the exocyclic NH$_2$ group of ICH has undergone a marked pyramidalization. The dien puckers have the characteristic sting-ray geometries[106] with the central methylene groups C(2) and C(3) above the MN$_4$ plane. Deviations of carbon atoms from the mean-squares planes for the Pd complex are -0.11 Å (C10) and 0.52 Å (C11), as opposed to 0.53 Å (C13) and -0.06 Å (C14). These deviations are comparable to those for the Pt complex.

A comparison of the total energies of the ICH linkage isomers of (dien)M^{II} reveals that both for Pd and Pt the N(3) isomers are lower in energy, by 15.97 kcal/mol

(Pd) and 15.87 kcal/mol (Pt). These energy differences are larger than those found for the linkage isomer complexes of $(NH_3)_3Pt^{II}$, where the N(3) site was preferred by ΔE = 12.2 kcal/mol. The N(3) isomer of $(NH_3)_3Pt^{II}$ adopts a similar orientation (dihedral angle 55°) as seen in $[(dien)Pt(ICH\text{-}N3)]^{2+}$, with a normal hydrogen bond of 2.79 Å between NH_3 of Pt and O(4) of ICH, and a long contact (3.27 Å) between NH_3 of Pt and $N(2)H_2$ of ICH. In contrast, in $[(NH_3)_3Pt(ICH\text{-}N1)]^{2+}$ the ICH is perpendicular to the PtN_4 plane with no hydrogen bonding interactions between ICH and the two *trans*-positioned NH_3 ligands at all, unlike in $[(dien)Pt(ICH\text{-}N1)]^{2+}$ (see above). We conclude from this difference that the hydrogen bond between $ICH\text{-}N(2)H_2$ and the $dien\text{-}NH_2$ group must be very weak and that the preference for N(3) is aided by formation of the hydrogen bond involving O(4) of the N(3) linkage isomer.

The calculated structures of the ICH linkage isomers (Figure 23) of *N, N, N', N'*-tetramethylethylenediamineplatinum(II), $(tmeda)Pt^{II}$, reveal that, in neither isomer is there an involvement of any of the exocyclic groups of the ICH in intramolecular hydrogen bonding.

$[(tmeda)Pt(ICH\text{-}N1)]^{2+}$ $[(tmeda)Pt(ICH\text{-}N3)]^{2+}$
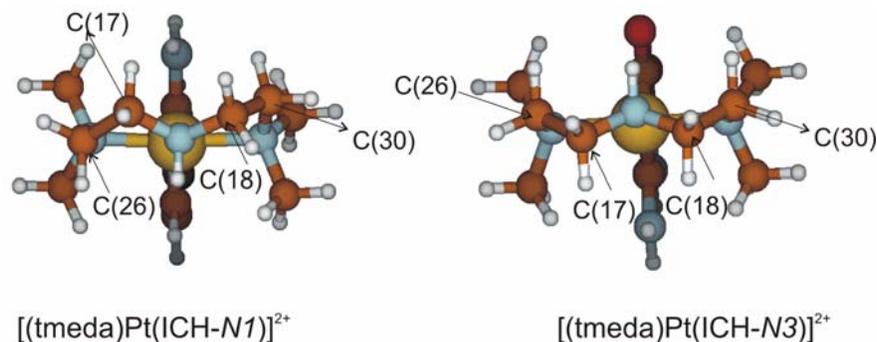
Figure 23 Optimized computed structures of $[(tmeda)Pt(ICH\text{-}N1)]^{2+}$ and $[(tmeda)Pt(ICH\text{-}N3)]^{2+}$.

The dihedral angles between the ICH and the PtN_4 planes are 89.6° and 90.0° for N(1) and N(3) linkage isomers, respectively. Moreover, and consistent with this view, is the planarity of $N(2)H_2$ group. The puckers of the two halves of the tmeda ligand are nevertheless somewhat distorted. Deviations of carbon atoms from the mean-squares plane for the N(1) linkage isomer are -0.92 Å (C26) and -0.46 Å

(C17), as opposed to -0.58 Å (C18) and 0.07 Å (C30) whereas, deviations of carbon atoms from the mean-squares plane for the N(3) linkage isomer are 0.15 Å (C26) and -0.50 Å (C17), as opposed to -0.50 Å (C18) and 0.07 Å (C30). The energy difference between the two isomers is 11.56 kcal/mol in favor of the N(3) isomer.

A comparison of all the three systems, hence of $(NH_3)_3Pt^{II}$, $(dien)Pt^{II}$, and $(tmeda)Pt^{II}$ therefore suggests that the higher strength of the Pt-(ICH-*N3*) bond is the major determinating factor in the preference for binding, and that intramolecular hydrogen bonding involving O(4) in the N(3) isomer adds to the stability, while the contribution of $N(2)H_2$ group to hydrogen bonding is small.

Finally, calculations were also performed on dinuclear complexes (Figure 24 and 25) of $(dien)M^{II}$, namely, $[(dienPd)_2(IC-N1,N3)]^{3+}$ and $[(dienPt)_2(IC-N1,N3)]^{3+}$. The structures of the two complexes were found to be very similar.
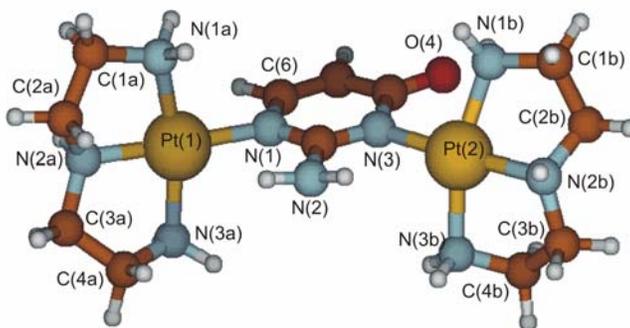
Figure 24 Optimized structure of $[(dienPt)_2(IC-N1,N3)]^{3+}$ with atom numbering scheme.
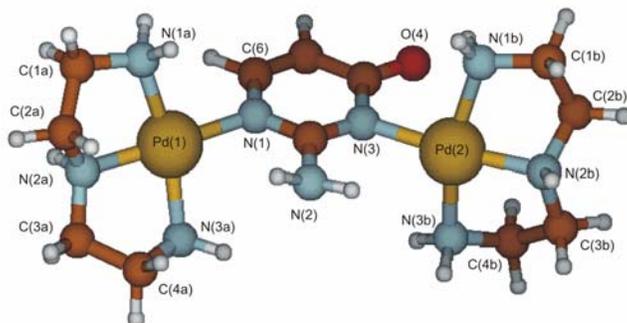
Figure 25 Optimized structure of [(dienPd)$_2$(IC-*N1,N3*)]$^{3+}$ with atom numbering scheme.

There is generally good agreement between the dinuclear compounds of (dien)Pd^{II}, (dien)Pt^{II} and the X-ray structures of **3** and **4**, respectively. Discrepancies are probably a consequence of crystal packing forces and the presence of the counter anions in the solid state structures.

For instance, in the calculated complex, the angle between the Pd(1)N$_4$ plane and the isocytosine plane is 62.3°, yet this angle is 86.9° in the solid state structure (see Table 2). Similarly, the angle between the Pt(2)N$_4$ plane and the isocytosine plane is 63.3°, which is much smaller than in the X-ray structure. The angle between the Pt(1)N$_4$ plane and the isocytosine plane is 82.7° and the angle between the Pd(2)N$_4$ plane and the isocytosine plane is 70.6° which are in the same range as in the X-ray characterized complexes **3** and **4**, respectively.

The M-N(dien) distances range from 2.07 Å in M(1)-N(2a) or M(2)-N(2b) to 2.122 Å in M(2)-N(3a) or M(2)-N(3b), and are likewise normal. For Pd and Pt complexes, the dien ligands ("a" and "b") bonded to N(1) and N(3) positions of isocytosine have different geometries.

Deviations of carbon atoms of the dien ligand from the mean-squares plane formed by the M(1)N$_4$ plane range from -0.11 to -0.30 Å (C1a), -0.65 to -1.04 Å (C2a), -0.24 to -0.80 Å (C3a) and -0.89 to -1.41 Å (C4a) and for M(2)N$_4$ plane range from 0.30 Å (C1b), 0.81 to 0.87 Å (C2b), 0.34 to 0.39 Å (C3b), and 0.95 to 1.0 Å (C4b). The angles and bond lengths of the isocytosine ring are normal.

The NH_2 groups of the dien ligands are involved in hydrogen bond formation with O(4). Hydrogen bond lengths are for O(4)-NH_2(dien) 2.871 Å (Pd) and 2.806 Å (Pt). Only in the case of the Pd complex is there a short contact between N(2)H_2 of isocytosine and (dien)-NH_2 (3.341 Å). Again, the exocyclic NH_2 group of isocytosine has undergone a slight pyramidalization.

2.1.15 Summary

Isocytosine (ICH) exists in solution as two major tautomers, the keto form with N(1) carrying a proton (**1a**) and the keto form with N(3) being protonated (**1b**). In water, **1a** and **1b** exist in equilibrium with almost equal amounts of both forms present. Reactions with a series of Pd^{II} and Pt^{II} am(m)ine species such as (dien)Pd^{II}, (dien)Pt^{II}, *cis*-$(NH_3)_2Pt^{II}$ and *trans*-$(NH_3)_2Pt^{II}$ reveal, however, a distinct preference of these metals for the N(3) site, as determined by ^{1}H NMR spectroscopy. Individual species have been identified by the pD dependence of the ICH resonances. The pK_a values (calculated for H_2O) for deprotonation of the individual tautomer complexes are 6.5 and 6.4 for the N(3) linkage isomers of (dien)Pd^{II} and (dien)Pt^{II}, respectively, as well as 6.2 and 6.0 for the N(1) linkage isomers. With (dien)M^{II} (M = Pt, Pd) preferential coordination of tautomer **1a**, hence via the N(3) position, is observed.

The crystal structure analysis of [(dien)Pd(ICH-*N3*)]$(NO_3)_2$ **2** is reported. With an excess of (dien)M^{II} also dinuclear species [(dienM)$_2$(IC-*N1,N3*)]$^{3+}$ (M = Pd^{II}, and Pt^{II}) form, which were isolated as their ClO_4^- salts (**3**, **4**) and structurally characterized. In strongly acidic medium [(dienPt)$_2$(IC-*N1,N3*)]$^{3+}$ is converted to [(dien)Pt(ICH-*N1*)]$^{2+}$, hence to the Pt^{II} complex of tautomer **1b**.

Ab initio calculations have been performed for tautomer compounds of composition [$(NH_3)_3$Pt(ICH)]$^{2+}$, *cis*- and *trans*-[$(NH_3)_2$PtCl(ICH)]$^+$, as well as *trans*-[$(NH_3)_2$Pt(ICH)$_2$]$^{2+}$. Without exception, N(3) linkage isomers are more stable, in agreement with experimental findings. As to the reasons of this binding preference, a NBO (Natural Bond Orbital) analysis for [$(NH_3)_3$Pt(ICH-*N3*)]$^{2+}$

strongly suggests that intramolecular hydrogen bonding between trans-positioned NH_3 ligands and the two exocyclic groups of the ICH is of prime importance.

DFT calculations, which were also extended to (tmeda)Pt[II] linkage isomers suggest that intramolecular hydrogen bonding between the ICH tautomers and the co-ligands at M, while adding to the preference for N(3) coordination, is not the major determining factor. Rather it is the inherently stronger Pt-N(3) bond which favors complexation of **1a**. The calculations furthermore show a marked pyramidalization of the NH_2 group of ICH in the complex once the heterocyclic ligand forms a dihedral angle < 90˚ with the Pt coordination plane.

2.1.16 Discussion

Applying in particular late transition elements, Lippert et al. have demonstrated in a number of cases, that it is possible to isolate and study different metalated forms of tautomers. For example, of the unsubstituted nucleobase cytosine, both N(3) and N(1) linkage isomers of Pt[II] have been isolated,[77,78] very much as in the case of uracil anions,[18] and with 1-methylcytosine both metal complexes of the dominant 4-aminooxo tautomer and the rare 4-iminooxo tautomer[50,117] have been crystallized. In one case, even both forms coexist in a single Pt[II] complex.[118] Similar examples exist for guanine[119] and adenine nucleobases[82,120-122] and the rare 4-hydroxo-2-oxo tautomer of 1-methyluracil has likewise been isolated as a metal-stabilized form.[108] The topic of metal tautomer complex formation has recently also attracted the interest of theoretical and computational chemists,[123-125] who clearly confirm the enormous influence metal coordination can have. Thus in the case of unsubstituted cytosine, Brüning et al. have detected a remarkable promotion of N(1) binding of am(m)ine containing Pt[II] and Pd[II] species in relationship to the tautomer distribution disfavoring the N(3)H tautomer by far.[77,78] The low abundance of Pt[II] and Pd[II] complexes of isocytosine with N(1) coordination in solution and our failure to isolate such compounds, reflect the same principle; unfortunately to our disadvantage. Our efforts to accomplish N(1) coordination of ICH by changing the co-ligands at Pt[II] to some

extent[126] were likewise not successful. These findings are in qualitative agreement with the results of our computational studies which suggest an inherently stronger binding of ICH through N(3) for both Pt^{II} and Pd^{II}.

2.2   Isocytosine as a Hydrogen Bonding Partner

2.2.1 Introduction

ICH exists as two major tautomers, **1a** and **1b** which crystallize in a 1:1 ratio[89] (Chart 11) and form a hydrogen bonded adduct[90] in the solid state.
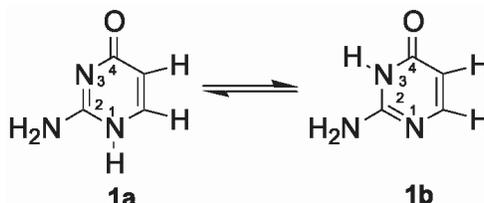
Chart 11 Two tautomeric forms of ICH in the solid state.

Our particular interest in this ligand was the metal binding behavior of tautomer **1b** and specifically the attachment of a Pt[II] entity to the N(1) position. As it turned out, tautomer **1a** is more reactive toward metal ions, leading to preferential binding of Pt[II] and Pd[II] electrophiles via the N(3) position.

We have examined the possibility of shifting the equilibrium between **1a** and **1b** by adding a co-hydrogen bonding partner, which exclusively interacts with one of the two tautomers. This aspect relates to the more general and in particular biologically relevant question of nucleobase tautomerism and mispairing leading to mutagenesis.

2.2.2 Aim of the Project

A number of temperature dependent solution studies[94] have been carried out, which suggest that ICH exists in solution as a mixture of the two forms **1a** and **1b**. However, these studies were not able to distinguish which tautomer predominates. It has also been observed that the electronic absorption spectra[92-97] of ICH change on going from aqueous to nonaqueous solution. Therefore, it was postulated that this behavior of ICH might be dependent on the change of tautomeric ratio caused by the nature of solvent, the temperature and that ICH exists predominately as keto-N(3)H form **1b** in ethanol and diethyl ether,

while in aqueous solution the two tautomers **1a** and **1b** coexist in comparable amounts. Certain bands in the Raman spectra of ICH also shift to higher wavenumbers, *i.e.* from 789 cm^{-1} to 791 cm^{-1} and from 1214 cm^{-1} to 1232 cm^{-1}, as DMF is successively diluted with water, though there was no separation into individual peaks as is the case for isocytosine in the solid state and in pure DMF.

In a similar way it has been demonstrated that 2'-deoxy-N(6)-methoxyadenosine (mo^{6}A) can undergo amino-imino tautomerism, depending on the hydrogen bonding partner added,[127,128] and detection of createnine by a designed receptor is accompanied by a change in tautomer structure of the receptor.[129]

In more general terms, it is evident that tautomer equilibria are subject to changes in the presence of components capable of interacting with one of the two tautomers preferentially.[130] Therefore, we were intrigued by the possibility of shifting the equilibrium between **1a** and **1b** by adding a co-hydrogen bonding partner, which exclusively interacts with one of the two tautomers.

2.2.3 Characterization of 1b · (1-MeC) · 2H$_2$O (6)

As pointed out in the introduction (Chart 11), crystallization of ICH from water yields a 1:1 distribution of the two tautomers **1a** and **1b**, which is favorable as a consequence of complementary hydrogen bonding between the two tautomers. Cocrystallization of ICH with 1-methylcytosine (1-MeC) from H$_2$O solution gave crystals of **1b** · (1-MeC) · 2H$_2$O (**6**). A view of the hydrogen-bonded pair is given in Figure 26.

The two different heterocycles are readily distinguished due to the presence of a methyl group in 1-MeC. In the solid, the 1:1 triply hydrogen-bonded complex consists of neutral 1-MeC and ICH bases, bonded in a Watson-Crick fashion. ICH is present exclusively as its keto-N(3)H tautomer **1b**. In addition to the unambiguous location and refinement of the proton at N(3) of ICH, the heavy atom geometrical parameters are in accord with this interpretation.
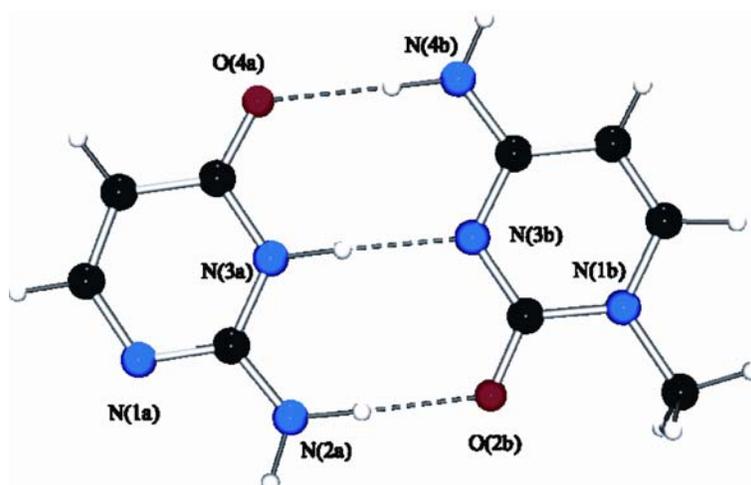
Figure 26 View of the hydrogen bonded pair ICH · (1-MeC) · 2H₂O (6). ICH is present as tautomer 1b. The water molecules are omitted for clarity.

The exclusive presence of **1b**, among others, also firmly established by the large value of the endocyclic bond angle at N(3), C(2a)-N(3a)-C(4a), 122.1(2)°. The bond length changes are minimal for 1-MeC[131] and ICH.[89] Structural details of the two heterocycles are listed in Table 5.

Table 5 Selected distances (Å) and angles (⁰) for 1b · (1-MeC) · 2H₂O (6)

	ICH	1-MeC
O(4)-C(4)	1.255(3)	-
O(2)-C(2)	-	1.248(3)
N(1)-C(2)	1.345(2)	1.395(3)
N(1)-C(6)	1.355(3)	1.365(3)
N(3)-C(2)	1.369(3)	1.352(3)
N(3)-C(4)	1.379(3)	1.340(2)
N(4)-C(4)	-	1.332(3)
C(5)-C(6)	1.351(3)	1.416(3)
N(1)-C(2)-N(3)	122.8(2)	119.2(2)
N(1)-C(6)-C(5)	126.3(2)	121.3(2)
C(2)-N(1)-C(6)	120.9(2)	120.4(2)

C(2)-N(3)-C(4)	122.1(2)	119.6(2)
N(2)-C(2)-N(3)	116.7(2)	-
O(2)-C(2)-N(3)	-	122.3(2)
N(3)-C(4)-C(5)	115.5(2)	116.7(2)

The isocytosine moiety and 1-MeC are nearly coplanar (deviation 3.6°). The interbase hydrogen bonding is strong and nearly linear, viz. N(4b)-H···O(4a), 1.94(2) Å, N(3a)-H···N(3b), 1.861(2) Å and N(2a)-H···O(2b), 1.85(2) Å, corresponding to distances of 2.882(3) Å, 2.894(3) Å, and 2.874(3) Å between the heavy atoms. In addition to this principal hydrogen bonding pattern, pairs of **1b** and 1-MeC are further linked by hydrogen bonds between N(4B)···O(2BA), 2.893(3) Å and N(2A)···O(4AB), 2.904(3) Å to produce a tape structure (Figure 27). These hydrogen bonds are between identical molecules, hence, contacts are between 1-MeC molecules on one hand, and **1b** molecules on the other. Tapes of **6** extend along the b-axis, with mean stacking distances of 3.50 Å and opposite directions between stacked tapes. Additional hydrogen bonding involving the water of crystallization also contributes to the overall crystal stability: O(2W)-H···O(4A), 2.996(3) Å and O(1W)-H···N(1A), 2.909(3) Å. In addition, there is a weak contact between C(6B)-H and O(1W) 3.623(3) Å.
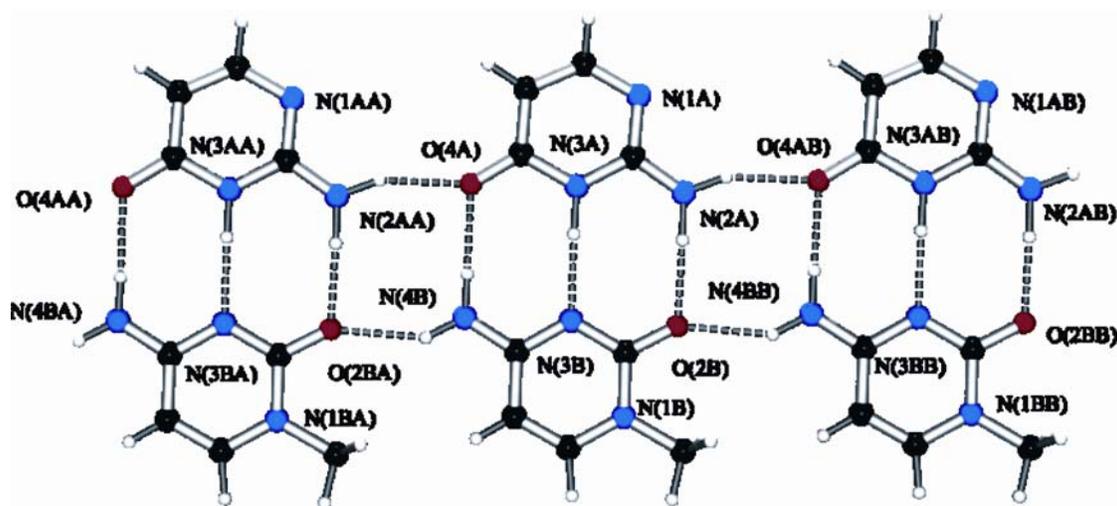
Figure 27 Pairs within 1b · (1-MeC) · H$_2$O associate via additional hydrogen bonds to give an infinite tape structure. The water molecules are omitted for clarity.

A Raman spectrum of ICH · (1-MeC) · 2H$_2$O was recorded in the solid state in the spectral range 400 – 1700 cm^{-1}. There are characteristic bands present at 774 cm^{-1} and 782 cm^{-1} as well as at 1264 cm^{-1} and 1217 cm^{-1} due to complex ring bending and stretching modes of 1-MeC and ICH. A comparison of Raman spectra of 1-MeC,[132] ICH[126] and compound ICH · (1-MeC) · 2H$_2$O suggests that the band at 774 cm^{-1} is due to the ring deformation mode of 1-MeC, while the band at 782 cm^{-1} is assigned to a similar mode of the keto-N(3)H tautomer **1b** of isocytosine. Similarly, the band at 1264 cm^{-1} is assigned to the stretching mode of 1-MeC and, correspondingly, the other band at 1217 cm^{-1} to the keto-N(3)H tautomer **1b**.

2.2.4 Complementary Hydrogen Bond Formation of 1a

Although it is possible to postulate complementary hydrogen bond formation between the ICH tautomer **1a** and a guanine nucleobase (Chart 12), we were unable to prove such a possibility.
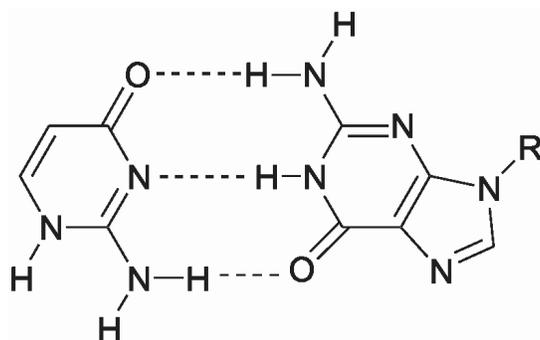
Chart 12 Feasible hydrogen bond formation between the Watson-Crick face of guanine and the O(4)N(3)N(2) face of tautomer 1a of ICH.

Attempts to cocrystallize ICH and 9-methylguanine or guanosine did not yield 1:1 adducts, possibly due to the low solubilities of the guanine components relative to ICH in water. However, even ^{1}H NMR spectroscopy in DMSO-d_6 did not provide any compelling evidence in favor of such a hydrogen bonding pattern. Although a concentration-dependence of 1:1 mixtures of ICH and guanosine could be obtained, albeit in a narrow concentration range only (10 – 70 mMol/L), the downfield shift of NH and NH$_2$ resonances with increasing concentrations were

within the range found for self-association of the individual components guanosine[133] and ICH (data not shown), hence in the order of 0.03 ppm for the concentration range mentioned. These ^{1}H NMR studies were hampered by the fact that the DMSO-d_6 samples were not free of water and contained between 2.5 and 5 equiv of H_2O per guanosine and ICH, with more diluted samples having a higher water content. Addition of molecular sieves, while reducing the water content and increasing the downfield shifts of the NH_2 resonances clearly beyond those of self-pairing, at the same time led to coalescence of the two NH protons (broad resonance at 10.82 ppm, halfwidth ca. 180 Hz) due to exchange. Lippert et al. have observed this phenomenon before and believe that it is due to the partial hydrolysis of the zeolite and generation of OH$^-$.

2.2.5 Characterization of [1a · ICH$_2$]NO$_3$ (7)

Eventually, the goal of selectively crystallizing the keto-N(1)H tautomer **1a** was achieved in the presence of protonated isocytosine. [**1a** · ICH$_2$]NO$_3$ (**7**) was isolated as single crystals and studied by X-ray analysis. The structure of **7** consists of two crystallographically independent entities (I, II) and two nitrate anions. Both heterocycles form pairs (Figure 28) with their own, symmetry related moieties.
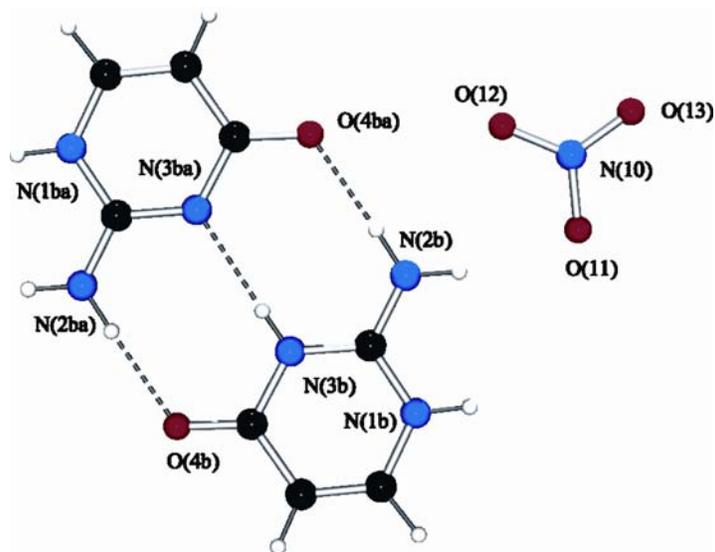
Figure 28 View of one (II) of the two crystallographically independent hydrogen bonded pairs present in [1a · ICH$_2$]NO$_3$ (7). Only one position of the disordered proton in the central hydrogen bond is shown.

This feature is reminiscent of that of $[C \cdot CH]_2 \cdot [ZnCl_4]$ (C = unsubstituted cytosine, CH = cytosinium), where likewise two independent hydrogen bonded base pairs between cytosinium and cytosine are formed.[134] Each pair is held together by three hydrogen bonds (Figure 28) between the respective O(4), N(3), and N(2) sites.

The central proton, that between the two N(3) sites, is disordered over two positions, both of which have been detected in the electron density map. The large values of the endocyclic bond angles at N3(a/b), C2(a/b)-N3(a/b)-C4(a/b), ca. 122°, and N1(a/b), C2(a/b)-N1(a/b)-C6(a/b), ca. 121°, also indicate that the proton is disordered over the central hydrogen bond. Within the two pairs, the two isocytosine rings (Table 6) therefore cannot be differentiated into neutral and protonated form, and the geometries of the two rings are identical within standard deviations.

Table 6 Selected distances (Å) and angles (º) for [1a · ICH$_2$]NO$_3$ and ICH (7)

	$[1a \cdot ICH_2]NO_3$		ICH[89]	
	a*	b*	1a	1b
O(4)-C(4)	1.237(2)	1.250(2)	1.248(3)	1.246(3)
N(1)-C(6)	1.363(3)	1.358(3)	1.358(3)	1.350(3)
N(1)-C(2)	1.345(2)	1.354(3)	1.357(3)	1.330(3)
N(2)-C(2)	1.314(3)	1.310(3)	1.323(3)	1.324(3)
N(3)-C(2)	1.342(3)	1.338(2)	1.333(3)	1.369(3)
N(3)-C(4)	1.381(2)	1.374(3)	1.363(3)	1.375(3)
C(4)-C(5)	1.437(3)	1.433(3)	1.438(3)	1.422(3)
C(5)-C(6)	1.330(3)	1.333(3)	1.331(3)	1.356(3)
N(1)-C(2)-N(3)	119.7(2)	119.5(2)	121.8(1)	121.9(1)
N(1)-C(2)-N(2)	120.7(2)	119.9(2)	118.9(1)	120.3(1)
N(1)-C(6)-C(5)	121.2(2)	120.9(2)	120.5(1)	125.9(1)
C(2)-N(1)-C(6)	120.9(2)	121.1(2)	120.2(1)	115.9(1)

C(2)-N(3)-C(4)	122.1(2)	121.9(2)	119.4(1)	123.3(1)
N(2)-C(2)-N(3)	119.6(2)	120.6(2)	119.3(1)	117.8(1)
O(4)-C(4)-C(5)	123.5(2)	123.1(2)	122.0(1)	126.4(1)
O(4)-C(4)-N(3)	119.8(2)	119.6(2)	119.3(1)	118.8(1)
N(3)-C(4)-C(5)	116.7(2)	117.3(2)	118.7(1)	114.8(1)
C(4)-C(5)-C(6)	119.3(2)	119.3(2)	119.1(1)	118.2(1)

*Molecules a and b in hemiprotonated ICH.

Thus, the situation is different from that for neutral isocytosine,[89] where the two tautomers **1a** and **1b** are clearly identified on the basis of significant differences in a number of bond lengths and internal ring angles. Despite this disorder, there can be no doubt, however, that **7** represents the adduct between tautomer **1a** and the isocytosinium cation (ICH_2^+). Regardless where the central proton is located, it will always generate a pair of **1a** and ICH_2^+ (Chart 13).
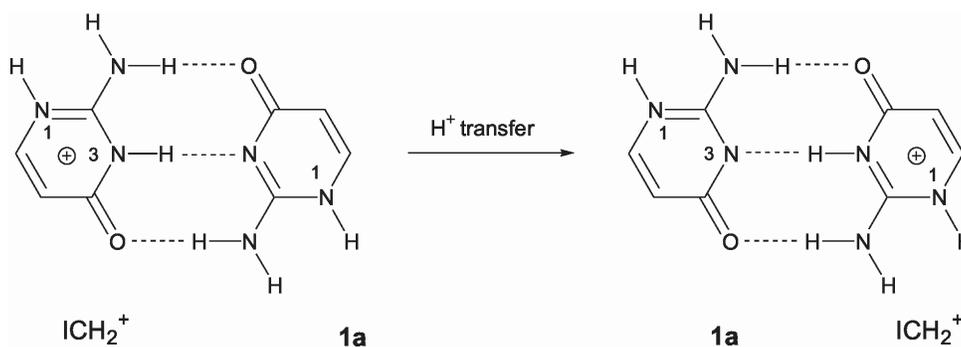
Chart 13 Hydrogen bonded adduct of 1a and ICH_2^+ as present in compound [1a · ICH_2]NO_3. H^+ transfer does not alter the composition.

Hydrogen bonding distances within the two crystallographically different pairs are (I) [N(3a)···N(3ab)], 2.842(2) Å and (II) [N(3b)···N(3ba)], 2.835(2) Å, (I) [N(2a)···O(4ab)], 2.834(2) Å, and (II) [N(2b)···O(4ba)], 3.022(3) Å. In hemiprotonated 1-methylcytosine compounds ([(1-MeC)$_2$H]$^+$X$^-$),[135-137] the central hydrogen bond compares well with that found in [**1a** · ICH_2]NO_3, but the outer hydrogen bonds (ca. 2.75 Å vs. 2.90 Å) differ markedly, as expected. The same should be expected for [**1a** · ICH_2]NO_3 in the absence of disorder.

Pairs I and II of **1a** · ICH_2^+ are part of a ribbon structure (Figure 29) which forms as a consequence of additional hydrogen bonds between pairs I and II. Of pair I, C(5)H sites act as donors and O(4) sites as acceptors, whereas of pair II, N(2)H$_2$ groups act as donors and O(4) sites as acceptors. The four intermolecular hydrogen bonds between pairs I and II are then between C(5bb)H (I) and (O4ab) (II), 3.196(3) Å as well as O(4bb) (I) and N(2ac)H$_2$ (II), 3.022(3) Å. The hydrogen bond between C(5)H and O(4) is reminiscent of similar hydrogen bonds found in recent years between nucleobases.[138-140]
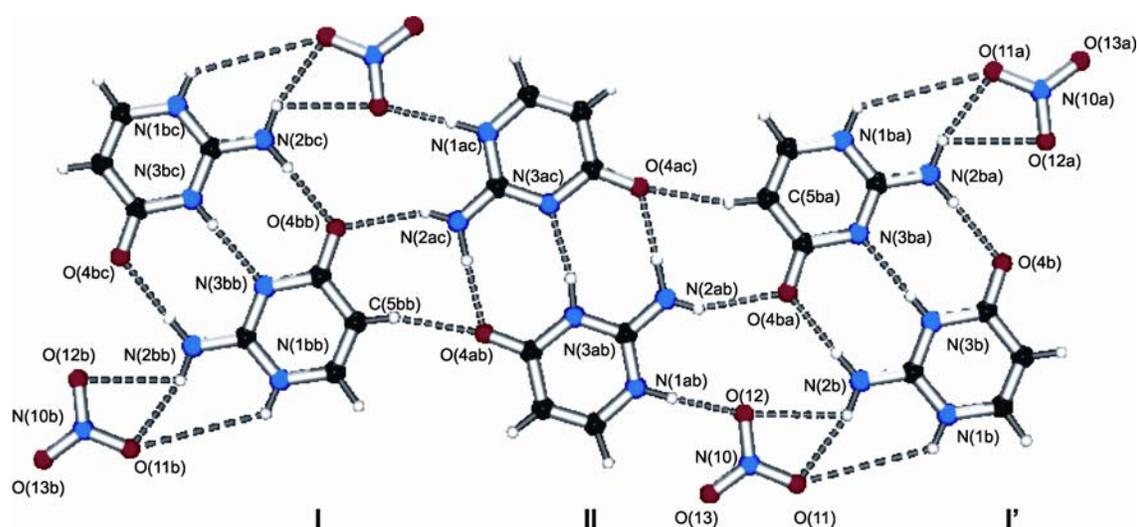
Figure 29 Association of the crystallographically independent pairs of I and II and the nitrate anions in [1a · ICH$_2$]NO$_3$. In both pairs of 1a and ICH$_2^+$ disordered protons have been fixed in the idealized positions in the central hydrogen bonds.

As can be also seen from Figure 29, the nitrate anions of [**1a** · ICH_2]NO$_3$ are involved in hydrogen bonding as well. The shortest ones are those which involve N(1)H (N···O, 2.77(3) to 2.80(2) Å) or NH$_2$ (N···O, 2.99(3) Å) sites. I and II as well NO$_3^-$ form a tape structure with individual tapes forming stacks with ca. 3.3 Å stacking distances. There are additional weak short contacts between the nitrate oxygen atoms and aromatic hydrogen atoms, i.e. C(5)H···O, 3.507(3) Å and C(6)H···O, 3.507(3) Å.

2.2.6 Summary

Isocytosine (ICH) **1** exists in solution in an equilibrium of tautomers **1a** and **1b** with the N(1) position and the N(3) position carrying the acidic proton, respectively. In the solid state, both tautomers coexist in a 1:1 ratio. As we show, the N(3)H tautomer **1b** can selectively be crystallized in the presence of the model nucleobase 1-methylcytosine (1-MeC). In **1b** · (1-MeC) · $2H_2O$ **6** pairs with three hydrogen bonds between the components as well as H bonds between identical molecules are formed, leading to an infinite tape structure. On the other hand, the N(1)H tautomer **1a** cocrystallizes with protonated ICH to give [**1a** · ICH_2]NO_3 **7**, again with three hydrogen bonds between the partners, yet the acidic proton disordered over the two entities.

2.2.7 Discussion

External factors are known to affect tautomer equilibria. Apart from factors such as aggregation state, solvent and temperature, the presence of hydrogen bonding partners or metal coordination can shift tautomer equilibria.[127-130] Here, we have demonstrated that the two dominant tautomers of isocytosine, the N(1)H tautomer **1a** and the N(3)H tautomer **1b** can be individually crystallized in the presence of the isocytosinium cation and neutral 1-methylcytosine, respectively. In both compounds, the two partners are involved in triple hydrogen bond formation.

2.3   1-Methylisocytosine as a Ligand for (dien)M^{II} (M = Pt^{II}, Pd^{II})

2.3.1 Introduction

Isocytosine bears a structural relationship to the canonic bases (Chart 14) cytosine and guanine. Even though ICH is not involved directly as a carrier of the genetic code, it is of biological significance, and its medical applications are numerous.[141] A variety of 2-aminopyrimidin-4-ones display anticancer, antiviral or antibacterial properties[142-146] or are valuable agrochemicals.[147] Platinum complexes of isocytosine and its derivatives have attracted considerable attention because of their antitumour activity.[148]

There are a few examples of spectroscopically[82-85,126] or crystallographically characterized metal complexes of isocytosine derivatives.[84,85,126] In the course of our studies on isocytosine, we have also synthesized a methyl derivative of isocytosine. In the present work, we report the preparation and structural characterization of Pt(II) and Pd(II) complexes of 1-MeIC.
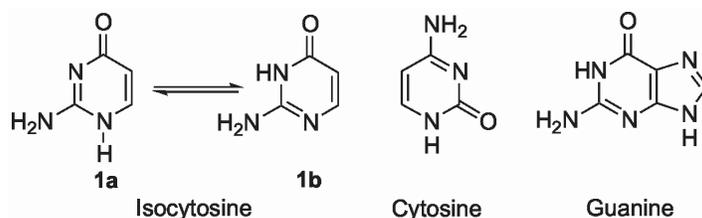
Chart 14 Ilustration of a structural relationship between isocytosine, cytosine and guanine.

2.3.2 Aim of the Project

We were particularly interested in synthesizing the metal complexes of 1-MeIC and to observe whether these cationic complexes undergo a significant amount of deamination to the corresponding complexes of 1-methyluracilate (1-MeU) under alkaline conditions or not. Šponer et al. have previously reported[149] facile deamination of cytosine for the cationic complexes of 1-methylcytosine and 1,5-dimethylcytosine (1,5-DiMeC).

2.3.3 Synthesis of 1-MeIC (8)

The methylation of isocytosine (2-aminopyrimidin-4-(3*H*)-one) was carried out in an analogous manner as 1-MeC.[150] The trimethylsilyl-protected isocytosine was treated with methyl iodide which resulted in methylation at N(1) and N(3). Cleavage of the protecting group (O–SiMe$_3$) with 6M acetic acid (Chart 15) yielded two isomeric monomethyl derivatives, 1-MeIC and 3-MeIC. The crude product was washed with a large amount of water and redissolved in ethanol, kept at 4 °C for a day. White crystalline product precipitated out of the solution which was later purified over the sephadex G25 column with a yield of 60%. The product (1-MeIC) was identified by elemental analysis and single-crystal X-ray diffraction analysis of fully protonated 1-MeIC. The experimental procedure employed here was found to be suitable for preparation of larger quantities than those described in literature.[151,152]
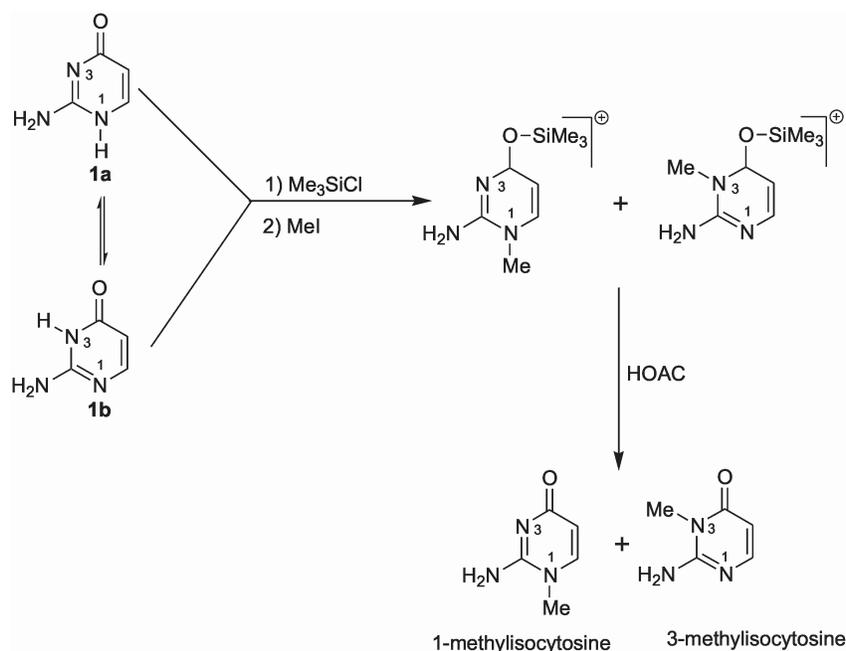
Chart 15 Strategy for the synthesis of 1-methylisocytosine.

2.3.4 Solution Equilibrium of 1-MeIC

The nucleobases predominantly exist in amino-oxo tautomeric forms. However, in the gas phase and in low-temperature matrices 9-methylguanine and 1-MeC also exist in the rare amino-hydroxy tautomeric forms.[153] In earlier studies of the

IR spectrum of matrix-isolated 1-MeIC some weak bands were observed that could not be assigned to the amino-oxo tautomer.[154] These bands have been assigned (Chart 16) to the imino-oxo tautomeric form of 1-MeIC.
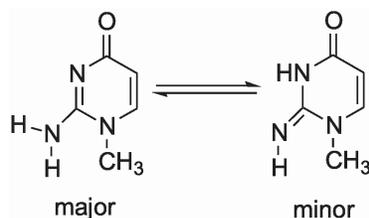
Chart 16 Amino-oxo (left) and imino-oxo (right) tautomeric forms of 1-MeIC.

Brown and Teitei[96] have reported pK_a values for isocytosine and its derivatives by means of ultraviolet spectroscopy, though not for 1-MeIC. Neutral 1-MeIC can be protonated (pK_a of the protonated 1-MeICH was found to be 4.02 ± 0.04). A second deprotonation step for the exocyclic amino group occurs only in strongly basic medium (p$K_a > 14$). In the course of the present work, the pK_a value of 1-MeIC was also determined using pH dependent (Figure 30) ^{1}H NMR spectroscopic measurements. The samples were treated with acid and/or base over a wide pD range and ^{1}H NMR spectra were recorded.
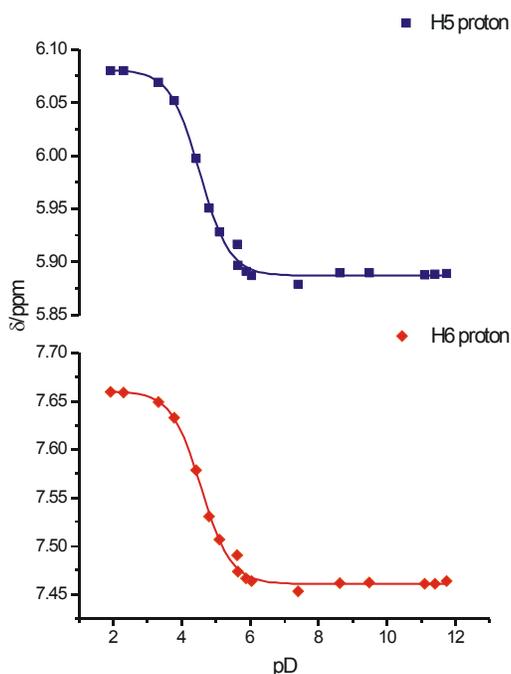
Figure 30 pD dependence (δ, ppm) of H5 and H6 resonances of 1-MeIC in D$_2$O.

2.3.5 Characterization of [1-MeICH]$_4$(NO$_3$)$_3$(ClO$_4$) (9)

In order to study the tautomeric equilibria of isocytosine, an attempt was also made to isolate hemiprotonated 1-MeIC (ref. section 2.2). However, crystallization of 1-MeIC from H$_2$O solution at pH* equal to its pK_a value (4.0) gave crystals of fully protonated, [1-MeICH]$_4$(NO$_3$)$_3$(ClO$_4$) **9**. A view of the hydrogen-bonded cations is given in Figure 31.
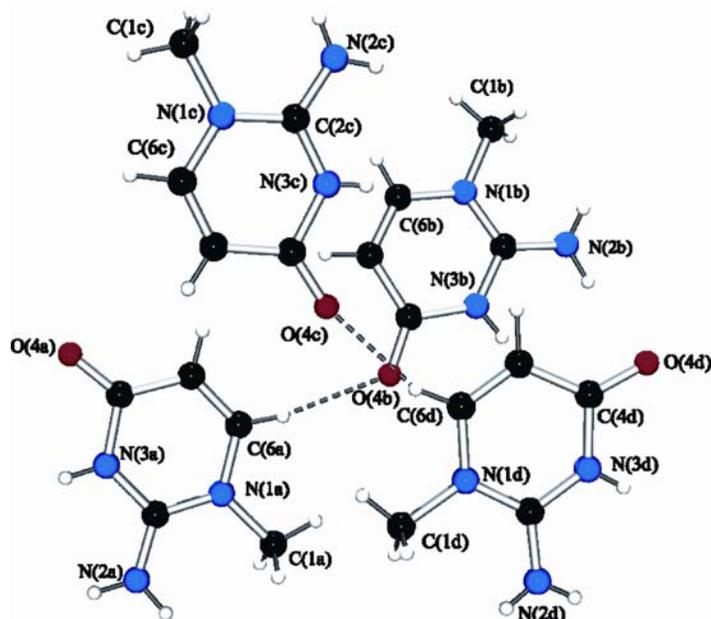
Figure 31 View of the cations of [1-MeICH]$_4$(NO$_3$)$_3$(ClO$_4$) (9). A perchlorate and three nitrate anions have been omitted for clarity.

The structure consists of four crystallographically independent bases ("a", "b", "c", "d"), a disordered perchlorate and three nitrate anions. Within the four heterocycles, each of the two bases are linked via C(6)H and O(4) bond, viz. C(6a)···O(4b), 3.141(4) Å and C(6d)···O(4c) 3.107(5) Å between the rings "a" and "b" and "c" and "d", respectively. In recent years, these C-H···O bonds have been well documented for the nucleobases.[138-140]

The bases are further linked by additional hydrogen bonding interactions. In rings "a" and "b", hydrogen bonding occurs between N(3b)-H···O(4a), 2.831(4) Å and N(2b)-H···O(4a), 2.796(4) Å. The rings "c" and "d" are associated by a C(5)-H···O(4) bond, C(5c)···O(4d), 3.034(4) Å. From ring "b", the mean stacking

distances for the rings "c" and "d" are ca. 2.83 Å and 3.28 Å, respectively. The endocyclic bond angles at N(3), C(2a)-N(3a)-C(4a), 125.1(3)º, C(2b)-N(3b)-C(4b), 126.4(3)º, C(2c)-N(3c)-C(4c), 126.1(3)º and C(2d)-N(3d)-C(4d) 125.4(3)º, have large values due to the protonation. The protons at N(3) sites have been unambiguously located and refined. Structural details are listed in Table 7.

Table 7 Selected distances (Å) and angles (º) for [1-MeICH]$_4$(NO$_3$)$_3$(ClO$_4$) (9)

| | [1-MeICH]$_4$(NO$_3$)$_3$(ClO$_4$) (9) | | | |
	A	**B**	**C**	**D**
O(4)-C(4)	1.230(4)	1.216(4)	1.213(4)	1.219(4)
N(1)-C(6)	1.379(4)	1.386(5)	1.386(4)	1.379(5)
N(1)-C(2)	1.350(4)	1.340(4)	1.352(4)	1.350(4)
N(1)-C(1)	1.471(5)	1.471(5)	1.469(5)	1.470(5)
N(2)-C(2)	1.308(4)	1.311(4)	1.307(4)	1.304(5)
N(3)-C(2)	1.352(4)	1.350(4)	1.339(4)	1.350(4)
N(3)-C(4)	1.383(4)	1.402(4)	1.401(4)	1.398(4)
C(4)-C(5)	1.428(4)	1.444(5)	1.440(5)	1.438(6)
C(5)-C(6)	1.333(5)	1.330(5)	1.330(5)	1.335(5)
N(1)-C(2)-N(3)	118.2(3)	118.4(3)	118.2(3)	119.7(3)
N(1)-C(2)-N(2)	122.4(3)	122.3(3)	121.5(3)	122.2(3)
N(1)-C(6)-C(5)	122.4(3)	123.2(4)	122.6(3)	122.7(4)
C(2)-N(1)-C(6)	119.6(3)	119.1(3)	119.5(3)	119.7(3)
C(2)-N(3)-C(4)	125.1(3)	126.4(3)	126.1(3)	125.4(3)
N(2)-C(2)-N(3)	119.4(3)	119.3(3)	120.3(3)	119.7(3)
O(4)-C(4)-C(5)	126.5(3)	128.0(3)	127.0(3)	127.1(3)
O(4)-C(4)-N(3)	118.9(3)	119.5(3)	119.7(3)	119.3(3)
N(3)-C(4)-C(5)	114.6(3)	112.5(3)	113.3(3)	113.6(3)
C(4)-C(5)-C(6)	120.0(3)	120.3(3)	120.3(3)	120.1(3)

Within the crystal, the bases are packed in a ladder like form (Figure 32) where the bases resemble the rungs of the ladder. Hydrogen bonding by the anions also contributes to the crystal stability. The nitrate anions form a number of hydrogen bonds, N(2a)-H···O, 2.867(3) Å, N(2d)-H···O, 2.881(5) Å, N(2d)-H···O, 2.916(4) Å, N(2d)-H···O, 2.943(4) Å, N(2c)-H···O, 2.998(4) Å and N(3a)-H···O, 2.737(3) Å. The perchlorate anion is hydrogen bonded to N(3c)-H···O, 2.860(4) Å and N(2c)-H···O, 2.998(4) Å.
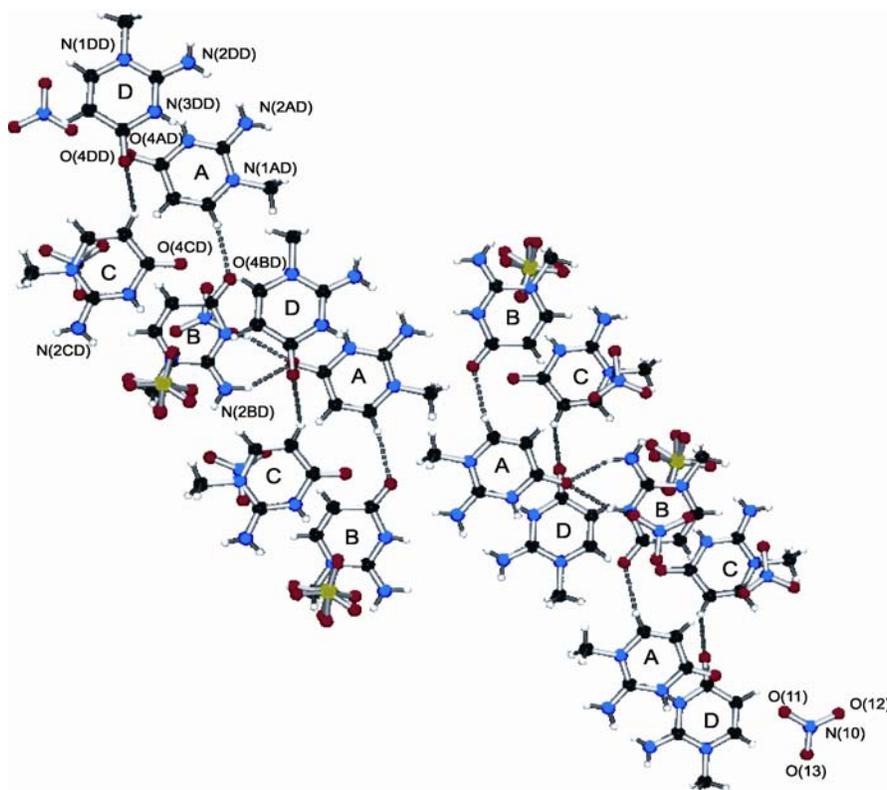
Figure 32 View of the hydrogen bonded bases in [1-MeICH]$_4$(NO$_3$)$_3$(ClO$_4$) (9). The anions are also involved in hydrogen bonding (not shown for clarity).

2.3.6 (dien)Pt^{2+} and 1-MeIC

1:1 mixtures of 1-MeIC and [(dien)Pt(D$_2$O)]$^{2+}$ were kept at 40 °C for two days. The reaction was carried out without adjustment of pD. Initially, a typical spectrum (Figure 33) at pD 3.0 consisted of two sets of aromatic H(5) and H(6) 1-MeIC resonances (doublets each, ^3J ~ 7.6 – 7.9 Hz). The set of resonances was assigned to the N(3) linkage isomer, by comparison with the spectra of the

isolated compound (H5 resonances at 5.9 ppm; H6 resonances at 7.5 ppm). Furthermore, poorly resolved [195]Pt satellites were also present for the H5 proton. The coupling constant is $^3J_{Pt-H} \sim 18.4$ Hz.
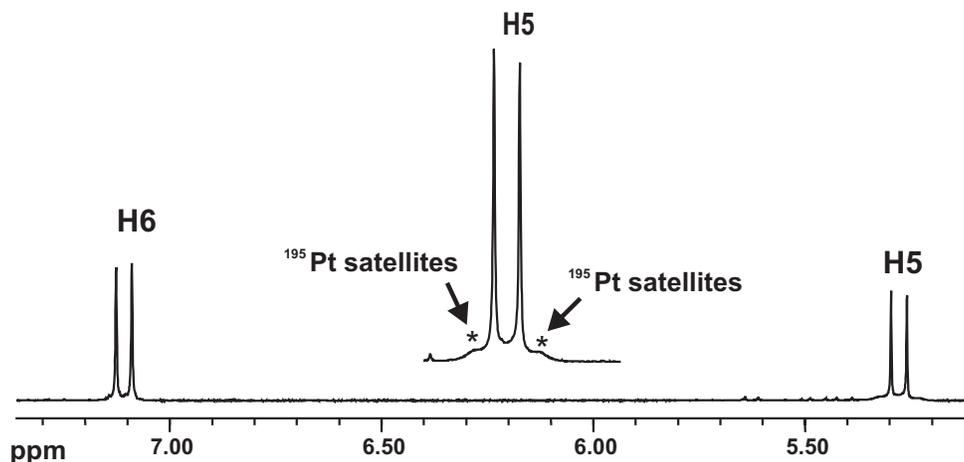
Figure 33 **Section of ^{1}H NMR spectrum (D$_2$O, pH* 3.0, 1-MeIC resonances only) of reaction mixture (1:1) [(dien)Pt(D$_2$O)]$^{2+}$ and 1-MeIC after 2 days at 40 °C. The set of resonances has been assigned to the N(3) linkage isomer. An enlarged view of H5 proton is also shown and the ^{195}Pt satellites are indicated.**

2.3.7 (dien)Pd^{2+} and 1-MeIC

Similar reactions (Figure 34) were also performed with [(dien)Pd(D$_2$O)]$^{2+}$. For Pd(II) reaction kinetics were faster[155,156] than the corresponding Pt(II) species. Consequently, the reaction was complete in a few hours as compared to two days for the Pt(II) species.
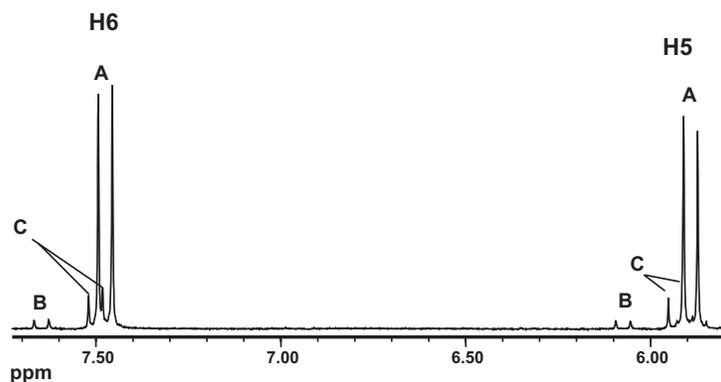
Figure 34 1-MeIC resonances of the sample obtained by reacting (1:1; pH* 1.8) mixtures of [(dien)Pd(D$_2$O)]$^{2+}$ and 1-MeIC in D$_2$O after a few hours at 40 °C. The set of resonances A is due to the N(3) linkage isomer, B is assigned to the free ligand and C might be due to the migration of Pd^{II} entity from N(3) to N(4) position.

The set of resonances (A) was assigned to N(3) linkage isomer by comparison with the spectra of the isolated compound. The chemical shifts of doublets (B) were those of free 1-MeIC. The species distribution (Table 8) was similar to that in (dien)Pt^{II}/1-MeIC system. However, a major difference with the (dien)Pt^{II} species discussed above is that even at low pD (*e.g.* pD 2.2) a low intensity set of resonances (C) is present.

Table 8 ^{1}**H NMR chemical shifts (ppm) and** ^3J **values (Hz) of 1-MeIC H5 and H6 doublets (D$_2$O, pH* 2.0) of [(dien)Pd(1-MeIC-*N3*)]$^{2+}$ (A), (1-MeIC)/(1-MeICH)$^+$ (B), and [(dien)Pd(1-MeIC-*N4*)]$^{2+}$ (C).**

	H5	H6	^3J (H5, H6)
A	5.89	7.49	7.6
B	6.07	7.65	7.9
C	5.93	7.50	7.6

The set of resonances (C) might be due to the migration of (dien)Pd^{II} from N(3) to N(4). The migration of (dien)Pt^{II} has been observed for the 1-MeC system.[157] The major difference between the two systems is that the signals for the migration product are significantly downfield in the 1-MeC. In the 1-MeC system, the migration brings the (dien)Pt^{II} in the vicinity of H5 proton which results in a significant downfield shift. However, in the 1-MeIC system, the metal is far-away from the H5 proton to cause any significant downfield shift. This observation is in accordance with an earlier report on the kinetics of the (dien)Pd^{II} for the cytidine system.[158]

2.3.8 X-ray Crystallographic Studies of 1-MeIC Complexes with (dien)Pd^{2+} (**10**) and (dien)Pt^{2+} (**11**)

Preparative work with (dien)M^{2+} (M = Pd or Pt) has yielded complexes of 1-MeIC, all of which contain the 1-MeIC base bonded to the metal via N(3). X-ray crystal structures (Figures 35 and 36) were obtained for [(dien)Pd(1-MeIC-*N3*)](ClO$_4$)$_2$ (**10**) and [(dien)Pt(1-MeIC-*N3*)](ClO$_4$)$_2$ (**11**). The cations of **10** and **11** are rather

similar. Selected bond distances and angles of these compounds are listed in Table 9.
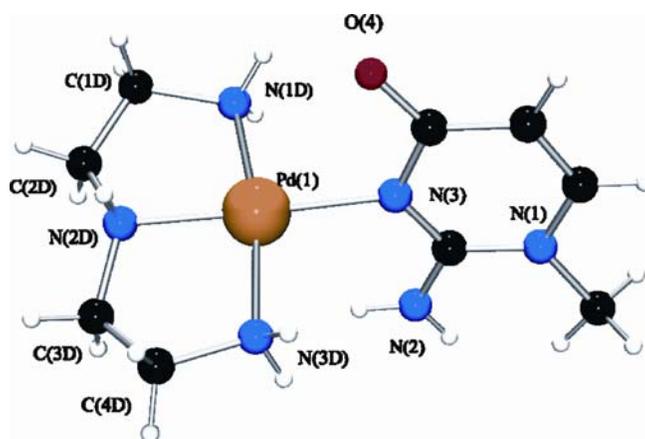
Figure 35 View of the cation of [(dien)Pd(1-MeIC-*N3*)](ClO$_4$)$_2$ (10) with atom numbering scheme.
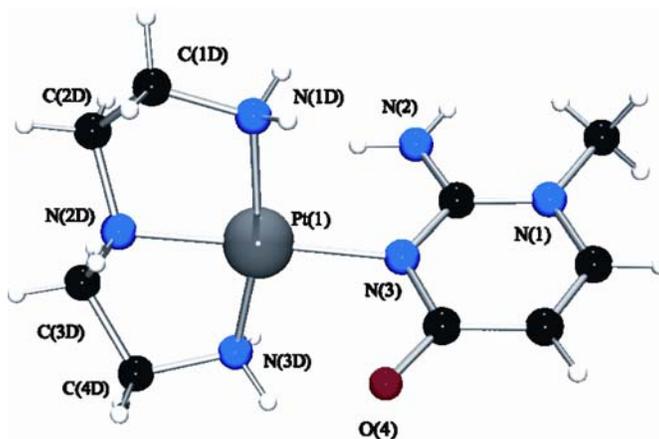
Figure 36 View of the cation of [(dien)Pt(1-MeIC-*N3*)](ClO$_4$)$_2$ (11) with atom numbering scheme.

The 1-MeIC plane forms an angle of 73.9˚ and 75.7˚ with Pd and Pt coordination planes, respectively. The geometry of the (dien)M^{2+} (M = Pd or Pt) is not unusual and compares well with the published data,[106,159,160] including the deviation of angles at the metal from 90˚. The distances from the metal (M = Pd or Pt) to the central nitrogen atom for the dien ligand are shorter than the distances to the peripheral nitrogen atoms. This might be an effect of the 1-MeIC ligand and/or the size of the metal atom being incompatible with the linear N(1D)-M-N(3D) arrays. Of the four CH$_2$ groups of the dien ligand, the two central ones C(2D) and

C(3D) are pointing on the same side of the PdN$_4$ plane, deviations from the PdN$_4$ plane being 0.20(1) Å C(2D) and 0.35(1) Å C(3D).

Table 9 Selected distances (Å) and angles (⁰) for [(dien)M(1-MeIC-*N3*)](ClO$_4$)$_2$ (M = Pd (10) and Pt (11))

	10		**11**
Pd(1)-N(3)	2.036(5)	Pt(1)-N(3)	2.045(9)
Pd(1)-N(1D)	2.026(7)	Pt(1)-N(1D)	2.03(2)
Pd(1)-N(2D)	1.991(8)	Pt(1)-N(2D)	1.98(2)
Pd(1)-N(3D)	2.055(7)	Pt(1)-N(3D)	2.05(2)
N(1D)-Pd(1)-N(2D)	85.7(3)	N(1D)-Pt(1)-N(2D)	82.6(5)
N(1D)-Pd(1)-N(3D)	169.1(3)	N(1D)-Pt(1)-N(3D)	166.7(4)
N(2D)-Pd(1)-N(3D)	84.4(3)	N(2D)-Pt(1)-N(3D)	85.9(5)
N(1D)-Pd(1)-N(3)	95.1(2)	N(1D)-Pt(1)-N(3)	96.1(4)
N(2D)-Pd(1)-N(3)	175.8(3)	N(2D)-Pt(1)-N(3)	176.0(4)
N(3)-Pd(1)-N(3D)	95.1(3)	N(3)-Pt(1)-N(3D)	95.8(4)
Pd(1)-N(3)-C(4)	114.8(5)	Pt(1)-N(3)-C(4)	116.4(8)
Pd(1)-N(3)-C(2)	123.3(4)	Pt(1)-N(3)-C(4)	123.1(7)
N(1)-C(2)-N(3)	121.0(6)	N(1)-C(2)-N(3)	123.0(1)
C(2)-N(3)–C(4)	121.7(6)	C(2)-N(3)–C(4)	121.0(2)

In contrast to **10**, the two central methylene groups, C(2D) and C(3D), in **11** are pointing to the opposite side of the PtN$_4$ plane, deviations from the PtN$_4$ plane being -0.53(1) Å C(2D) and -0.46(1) Å C(3D). The external angles at N(3) (M(1)-N(3)-C(4), 114.8(5)° Pd and 116.4(8)° Pt; M(1)-N(3)-C(2), 123.3(4)° Pd and 123.1(7)° Pt) are not equal. Hence, O(4) is closer to M(1) as compared to N(2). Distances and angles within the 1-MeIC ligand are not unusual. The crystal packing is similar for **10** and **11**. The perchlorate anions are involved in numerous hydrogen bonding interactions to the dien, O(4) and N(2)H$_2$ groups of 1-MeIC. Additionally, there are a few short contacts between the perchlorate anions and the methylene groups of the dien ligand.

2.3.9 Theoretical Calculations

Molecular geometries of [(dien)M(1-MeIC-*N3*)]$^{2+}$ (M = Pt or Pd) complexes have also been computed in order to get an insight into the gas phase structures of these complexes. The views of the optimized structures of the N(3) linkage isomers of [(dien)M(1-MeIC)]$^{2+}$ (M = Pt and Pd) are given in Figure 37.
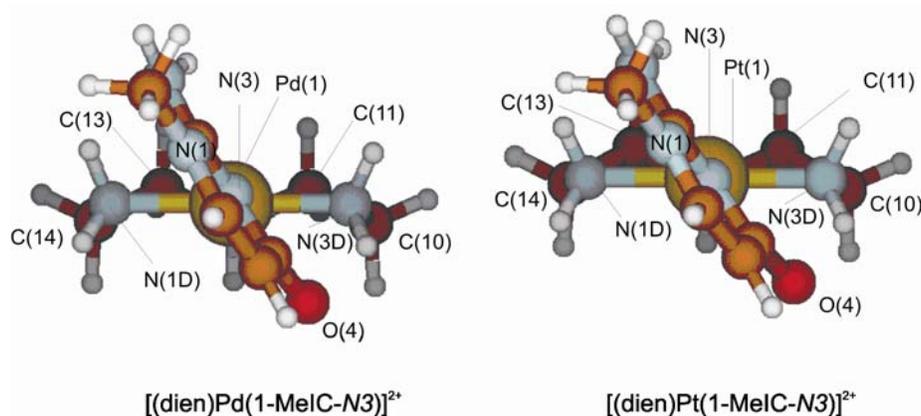
Figure 37 Optimized computed structures of N(3) isomers of [(dien)M(1-MeIC)]$^{2+}$
(M = Pt and Pd) with atom numbering schemes.

The two N(3) linkage isomers of (dien)M^{II} are very similar. The 1-MeIC plane is tilted by 58.3° (Pd) and 54.9° (Pt) relative to the MN$_4$ coordination plane. This is in sharp contrast to the angles obtained between the MN$_4$ coordination and 1-MeIC for the X-ray characterized compounds **10** and **11,** viz. 73.9° (Pd) and 75.7° (Pt). This discrepancy might be explained if we take into account the presence of counter anions as well as crystal packing forces in the solid state structures. Both NH$_2$ groups of the dien ligands are involved in hydrogen bond formation with O(4) as well as N(2)H$_2$ of 1-MeIC. Though, the latter is rather weak.

Hydrogen bond lengths are for O(4)···NH$_2$(dien), 2.829 Å (Pd) and 2.808 Å (Pt) whereas, those involving the N(2)H$_2$ of 1-MeIC and dien-NH$_2$ are 3.456 Å (Pd) and 3.344 Å (Pt). The exocyclic NH$_2$ group of 1-MeIC has also undergone pyramidalization.[110,111,126] In the dien puckers, the central methylene groups C(11) and C(13) are below the MN$_4$ plane. Deviations of carbon atoms from the mean-squares planes for the Pd complex are 0.06 Å (C10) and -0.54 Å (C11), as

opposed to -0.52 Å (C13) and 0.12 Å (C14). These deviations are comparable to those for the Pt complex. The M(1)-N(dien) distances range from 2.06 Å in M(1)-N(2D) Å to 2.08 – 2.12 Å in M(1)-N(1D) or M(1)-N(3D), and are likewise normal. The external angles at N(3), (M(1)-N(3)-C(4) and M(1)-N(3)-C(2) are 119.0˚ and are equal. Thus, O(4) is at the same distance to M(1) as N(2). The distances and angles within the 1-MeIC ring have normal values.

2.3.10 Deamination of [(dien)Pt(1-MeIC-*N3*)]$^{2+}$

Deamination reactions of N(3) platinated 1-MeIC were carried out essentially in a similar manner described by Šponer et al.[149] The starting compound, [(dien)Pt(1-MeIC-*N3*)]$^{2+}$, was dissolved in D_2O, pD of the sample was adjusted to 12.7 and the reaction was followed at ambient temperature over time by ^{1}H NMR spectroscopy. A typical ^{1}H NMR spectrum (Figure 38) obtained after five days, pD 12.3 consisted of two intense sets of resonances, A'' and B''.
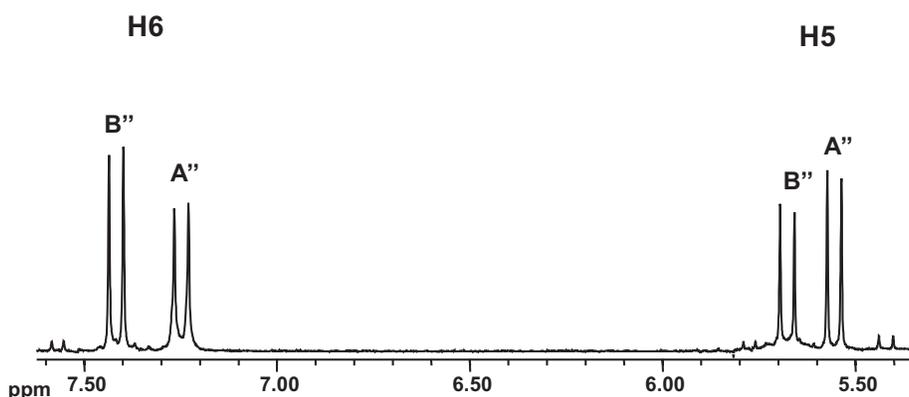
Figure 38 Lowfield section of ^{1}H NMR spectrum (D_2O, pD 12.3) of [(dien)Pt(1-MeIC-*N3*)]$^{2+}$ after 5 days. The set of resonances A'' is due to [(dien)Pt(1-MeIC-*N3*)]$^{2+}$ and B'' is assigned to the deamination product [(dien)Pt(1-MeU-*N3*)]$^{2+}$.

Signal set A'' was due to the starting compound, [(dien)Pt(1-MeIC-*N3*)]$^{2+}$ and correspondingly, the set of resonances B'' was assigned to the deamination product, [(dien)Pt(1-MeU-*N3*)]$^{2+}$, by comparison with a sample obtained from a reaction between [(dien)Pt(D_2O)]$^{2+}$ and 1-MeU.

2.3.11 Summary

1-MeIC was synthesized and the pK_a value (calculated for H_2O) was found to be 4.02. 1-MeICH$^+$ **9** was isolated and characterized by X-ray crystallography. Reactions with (dien)Pd^{II} and (dien)Pt^{II} were carried out and the crystal structure analyses of [(dien)Pd(1-MeIC-*N3*)](ClO$_4$)$_2$ **10** and [(dien)Pt(1-MeIC-*N3*)](ClO$_4$)$_2$ **11** are reported. Under alkaline conditions, [(dien)Pt(1-MeIC-*N3*)]$^{2+}$ undergoes a significant amount of deamination to give [(dien)Pt(1-MeU-*N3*)]$^{2+}$.

Ab initio calculations have been performed for [(dien)Pd(1-MeIC-*N3*)]$^{2+}$ and [(dien)Pt(1-MeIC-*N3*)]$^{2+}$. The calculations show pyramidalization of the NH$_2$ group of 1-MeIC in the complexes when the heterocyclic ligand forms a dihedral angle < 90˚ with the Pt and Pd coordination planes.

2.4   Pt^II Complexes of Unsubstituted Guanine

2.4.1 Introduction

Guanine (Chart 17) is one of the four main nucleobases present in nucleic acids (*e.g.*, DNA and RNA). It is also found in the scales of certain fish, the guano of sea-birds, and the liver and pancreas of mammals.[161,162] Among vertebrate species, the range in guanine content in DNA is quite narrow, 20 – 22%. RNA is generally richer in guanine than DNA, the guanine content of transfer and ribosomal RNA isolated from a variety of sources varies from about 26 to 34%.[163]
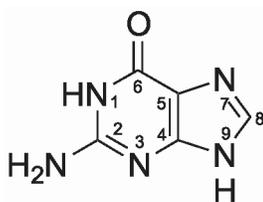
Chart 17 Schematic representation of guanine.

2.4.1.1   Tautomerism and Acidity

Of the common nucleic acid components, guanine has the largest number of possible tautomeric forms (oxo-hydroxy, amino-imino, N(1)H-N(3)H, N(7)H-N(9)H).[163] Many theoretical studies have been carried out to study tautomeric equilibria of guanine and calculations mostly show the existence of four low-energy tautomers (amino-oxo and amino-hydroxy) with the amino-oxo form having hydrogen at N(7) as their most stable gas-phase tautomer.[164-168] The imino tautomers are shown to be energetically less stable.[169] Experimental results are in agreement with the theoretical data.

Recently, four tautomeric forms of guanine were detected in the gas phase.[170,171] Additionally, the other tautomeric forms are also present. However, their energies as well as the free energies are considerably higher. In the solid state, guanine is (Chart 18) protonated at N(1) and N(9) positions.[172] However, in solution a

tautomeric equilibrium exists with the proton distribution between N(7) and N(9) positions.[163]
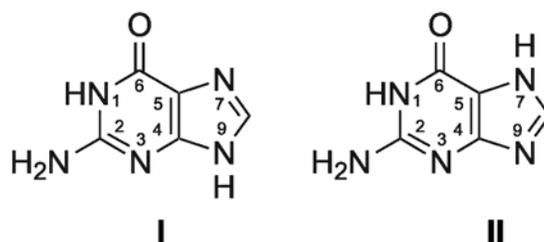
Chart 18 The two preferred tautomeric forms of guanine.

The pK_a values[163] for a number of guanine derivatives are summarized in Table 10. The pK_1 value is for the protonation of guanine either at O(6) or N(3), pK_2 is for the deprotonation taking place at N(7) or N(9) positions. Finally, pK_3 is for the deprotonation of N(1) position.

Table 10 pK_a values of guanine derivatives

Compound	pK_1	pK_2	pK_3
Guanine[173]	3.0	9.3	12.3
1-Methylguanine[173]	3.1	10.5	-
7-Methylguanine[173]	3.5	10.0	-
9-Methylguanine[174]	2.9	9.8	-
7,9-Dimethylguanine[173]	7.2	-	-

2.4.2 Aim of the Project

In recent years, interactions between the transition metals and nucleic acids or their constituent bases have been a subject of considerable research. Many studies of metal ion interactions with nucleic acids or their constituent bases have been complicated by the availability of numerous metal binding sites. Various spectroscopic (IR, visible)[175,176] and physical methods[177] have been employed in order to determine the metal binding site(s).

The present study was undertaken with the objective of synthesizing (dien)Pt[II] complexes of unsubstituted guanine in which the metal binding site(s) could be unequivocally established and to investigate the physical properties of these complexes which might be useful in assigning the metal binding sites. In particular, we wanted to synthesize the metal complexes of guanine with the Pt[II] entity attached to the N(9) position. This way we would like to generate platinated nucleobase analogs (Chart 19) which, when incorporated into a suitable backbone,[51,88] might give rise to artificial, cationic oligonucleotide analogs with the ability to recognize natural nucleobases via hydrogen bond formation.
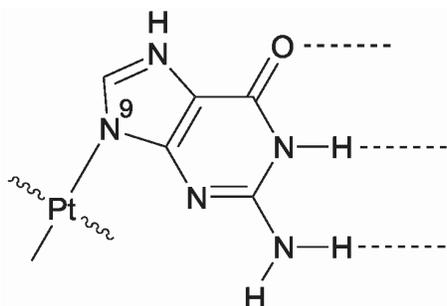
Chart 19 N(9) platinated form of guanine.

Metal complex formation with guanine has previously been studied by other groups.[178-181] For GH$_2^+$, there are examples of X-ray characterized Zn[182] or Cu[183] compounds with N(9) coordination.

2.4.3 1:1 Complexes of (dien)Pt[II] and Guanine

The reaction of (dien)Pt[II] with guanine was performed on a preparative scale. 1:1 mixtures of guanine and [(dien)Pt(H$_2$O)]$^{2+}$ were stirred at 40 °C for a few hours. Excess guanine was removed by filtration, the solution was rotary-evaporated to dryness and a ^{1}H NMR spectrum of the yellow solid was obtained in D$_2$O.

A typical spectrum (Figure 39) in D$_2$O at pD 7.0, consists of two major aromatic H(8) guanine resonances (singlets each). The most intense signal (A) with platinum satellites ($^3J_{Pt-H}$ ~ 20.4 Hz) is due to the N(9) linkage isomer and the other resonance (B) was assigned to the N(7),N(9) dinuclear species. The

assignment was done by comparison with the spectra of the isolated compounds, the structures of which have been established by X-ray crystallography. Additionally, there were two minor signals due to the formation of some side products. However, it was not possible to identify these side products.
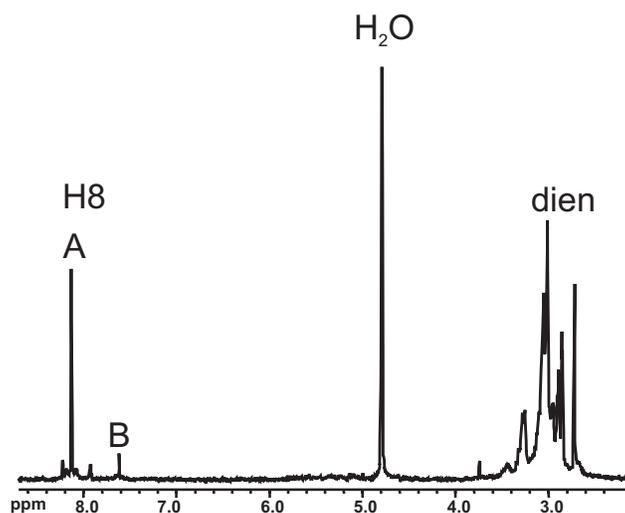
Figure 39 A section of ^{1}H NMR spectrum (D$_2$O, pH* 7.0) of (dien)Pt^{II} complex of guanine. Peak A is assigned to the [(dien)Pt(GH$_2$-*N9*)]$^{2+}$ and B is assigned to the [(dien)Pt(GH-*N7,N9*)]$^{3+}$.

2.4.4 Solution Studies of [(dien)Pt(GH$_2$-*N9*)]$^{2+}$

pD dependent ^{1}H NMR spectroscopic measurements (Figure 40) for this compound[63] have been carried out previously. However, in absence of the crystal structure, the absolute identification of the compound was not possible.

In the course of the present work, a number of samples were prepared at different pD's. Typically, the crystals were dissolved in D$_2$O, were treated with acid and/or base over a wide pH* range and ^{1}H NMR spectra were recorded. This was done to ensure that the pD-dependence performed previously corresponded to this compound. Relevant pK_a values are 6.51 ± 0.01 (H$_2$O) and 10.53 ± 0.05 (H$_2$O) for the deprotonations of N(7) and N(1) positions, respectively.
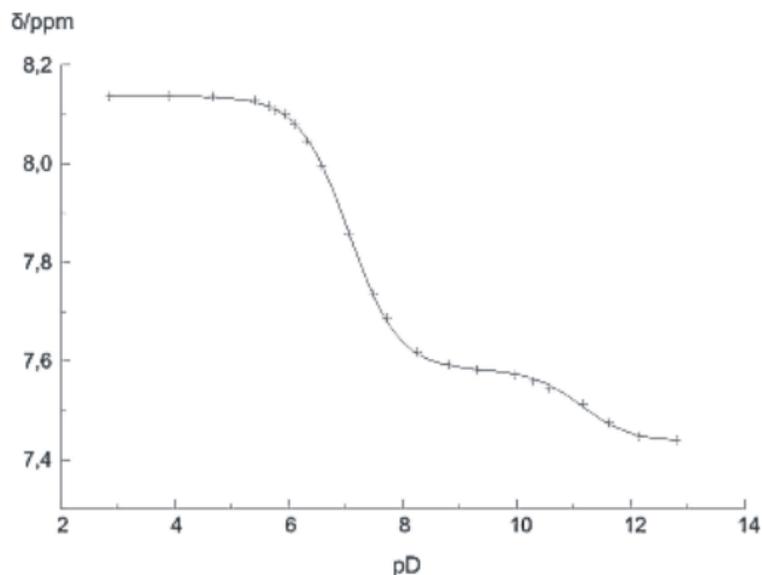
Figure 40 pD dependence (δ, ppm) of H8 resonance for [(dien)Pt(GH$_2$-*N9*)]$^{2+}$ in D$_2$O.[63]

2.4.5 Characterization of [(dien)Pt(GH$_2$-*N9*)]$^{2+}$ (12a), (12b)

Preparative work has yielded three complexes of guanine, out of which two are bonded to the metal via N(9). Views of the molecular cations of [(dien)Pt(GH$_2$-*N9*)]Cl(ClO$_4$) **12a** and 2{[(dien)Pt(GH$_2$-*N9*)](ClO$_4$)$_2$ · 2H$_2$O} **12b** are illustrated in the Figures 41 and 42, respectively. Selected bond distances and angles for **12a** and **12b** are given in Tables 11 and 12, respectively.
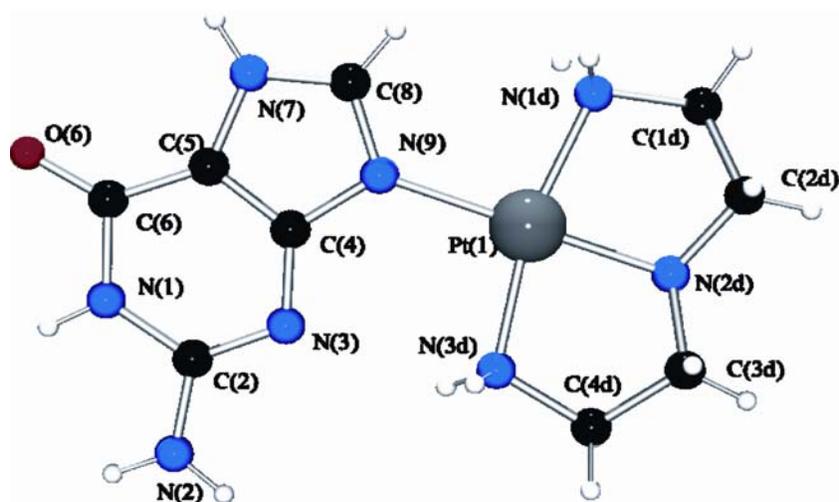
Figure 41 View of cation of [(dien)Pt(GH$_2$-*N9*)]Cl(ClO$_4$) (12a) with atom numbering scheme.
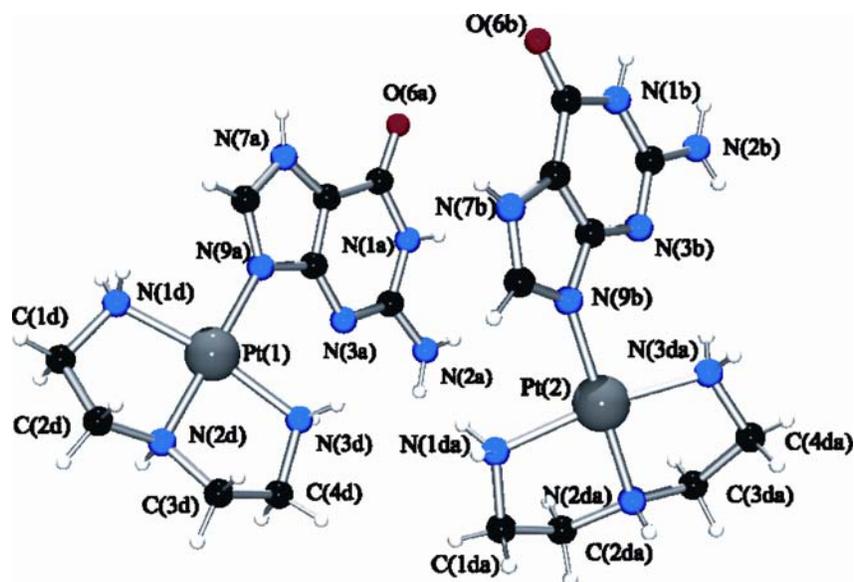
Figure 42 View of cations of 2{[(dien)Pt(GH$_2$-*N9*)](ClO$_4$)$_2$ · 2H$_2$O} (12b) with atom numbering scheme.

In **12a** and **12b**, (dien)Pt^{II} entities are coordinated to the guanine base via N(9) positions. Each cation exhibits a slightly distorted square-planar geometry with the four equatorial coordination sites occupied by the tridentate dien chelate, its terminal amino groups in *trans* positions, and the endocyclic nitrogen atom N(9) of the guanine base. The geometries of the (dien)Pt^{II} groups in both compounds are normal, including the deviations of some of the angles from ideal square-planar coordination geometry of the Pt due to the strain by the tridentate ligand.[106,159,160] Angles between the Pt coordination plane and the guanine ligand are 12.7° (Pt(1), **12a**), 25.8° (Pt(1), **12b**) and 39.3° (Pt(2), **12b**).

Carbon atoms of the ethylene groups of the dien ligands do not display a uniform pattern relative to the PtN$_4$ plane. In **12b,** the deviations of carbon atoms from the least-squares plane formed by the PtN$_4$ plane are -0.51(1) Å C(2d), -0.60(1) Å C(3d), 0.17(1) Å C(1d), -0.01(1)Å C(4d), -0.66(1) Å C(2da), -0.59(1) Å C(3da), -0.07(1) Å C(1da), and 0.05(1) Å C(4da). Thus, the two halves of the dien ligands undergo marked distortions from the case of a symmetrical distribution of the two carbon atoms of an ethylenediamine ring. In **12a**, the dien ligand adopts a sting-ray geometry[106] with the central methylene groups C(2d) and C(3d) pointing

in the same direction, yet being below the PtN_4 plane. Deviations of carbon atoms from the least-squares plane formed by the PtN_4 plane are -0.55(1) Å C(2d), -0.52(1) Å C(3d) and 0.07(1) Å C(1d) and 0.09 (1) Å C(4d). There are no significant differences in bond lengths and bond angles for **12a** and **12b**. The guanine ligands do not display any unusual features. Structural data are well within those of related compounds.[182,183]

Table 11 Selected distances (Å) and angles (º) for [(dien)Pt(GH$_2$-*N9*)]Cl(ClO$_4$) (12a)

[(dien)Pt(GH$_2$-*N9*)]Cl(ClO$_4$) (12a)			
Pt(1)N$_4$/GH	12.7(1)	Pt(1)-N(1d)	2.040(6)
Pt(1)-N(9)	2.058(5)	Pt(1)-N(2d)	2.005(5)
Pt(1)-N(3d)	2.042(6)		
N(1d)-Pt(1)-N(3d)	166.3(2)	Pt(1)-N(1d)-C(1d)	109.4(4)
N(1d)-Pt(1)-N(9)	95.7(2)	Pt(1)-N(2d)-C(2d)	108.4(4)
N(2d)-Pt(1)-N(3d)	83.4(2)	Pt(1)-N(2d)-C(3d)	109.3(2)
N(2d)-Pt(1)-N(9)	178.2(2)	Pt(1)-N(3d)-C(4d)	109.1(4)
N(1d)-Pt(1)-N(2d)	83.7(2)	Pt(1)-N(9)-C(4)	126.6(4)
N(3d)-Pt(1)-N(9)	97.3(2)	Pt(1)-N(9)-C(8)	126.8(4)
C(2)-N(3)-C(4)	113.7(5)	N(7)-C(8)-N(9)	112.2(6)
C(2)-N(1)-C(6)	124.1(5)	C(4)-N(9)-C(8)	106.2(5)
C(5)-N(7)-C(8)	107.1(5)		

Table 12 Selected distances (Å) and angles (º) for 2{[(dien)Pt(GH$_2$-*N9*)](ClO$_4$)$_2$ · 2H$_2$O} (12b)

2{[(dien)Pt(GH$_2$-*N9*)](ClO$_4$)$_2$ · 2H$_2$O} (12b)					
	"a"	"b"		"a"	"b"
PtN$_4$/GH	25.8 (1)	39.3(1)	Pt-N(1D)	2.040(9)	2.054(8
Pt-N(9)	2.032(8)	2.047(9)	Pt-N(2D)	2.010(1)	2.022(9)
Pt-N(3D)	2.040(1)	2.035(6)			

Pt-N(1D)-C(1D)	107.9(8)	108.3(7)	Pt-N(2D)-C(3D)	107.8(6)	108.0(7)
Pt-N(2D)-C(2D)	108.6(8)	105.4(8)	Pt-N(3D)-C(4D)	109.6(6)	109.4(5)
N(1D)-Pt-N(3D)	167.4(5)	167.3(3)	Pt-N(9)-C(4)	127.5(7)	125.0(6)
N(1D)-Pt-N(9)	95.1(4)	95.6(4)	Pt-N(9)-C(8)	127.2(7)	129.4(9)
N(2D)-Pt-N(3D)	84.3(4)	83.3(3)	N(7)-C(8)-N(9)	111.4(9)	113.0(1)
N(2D)-Pt-N(9)	178.3(4)	176.9(5)	C(2)-N(3)-C(4)	113.4(1)	112.5(8)
N(1D)-Pt-N(2D)	83.9(4)	85.0(3)	C(2)-N(1)-C(6)	127.0(1)	125.0(1)
N(3D)-Pt-N(9)	96.8(4)	95.8(3)	C(5)-N(7)-C(8)	109.0(1)	108.4(9)
			C(4)-N(9)-C(8)	105.2(9)	106.0(1)

Pt denotes Pt(1) in "a" and Pt(2) in "b". D denotes dien ligand.

In **12a**, the purine bases of the adjacent complexes (Figure 43) are hydrogen bonded to each other in a Hoogsteen fashion. The hydrogen bond formation occurs between O(6)···N(7), where O(6) of the purine base acts as an acceptor while the N(7) site acts as a donor for the O(6a) of the adjacent purine base, the distance being 2.722(7) Å between the heavy atoms.
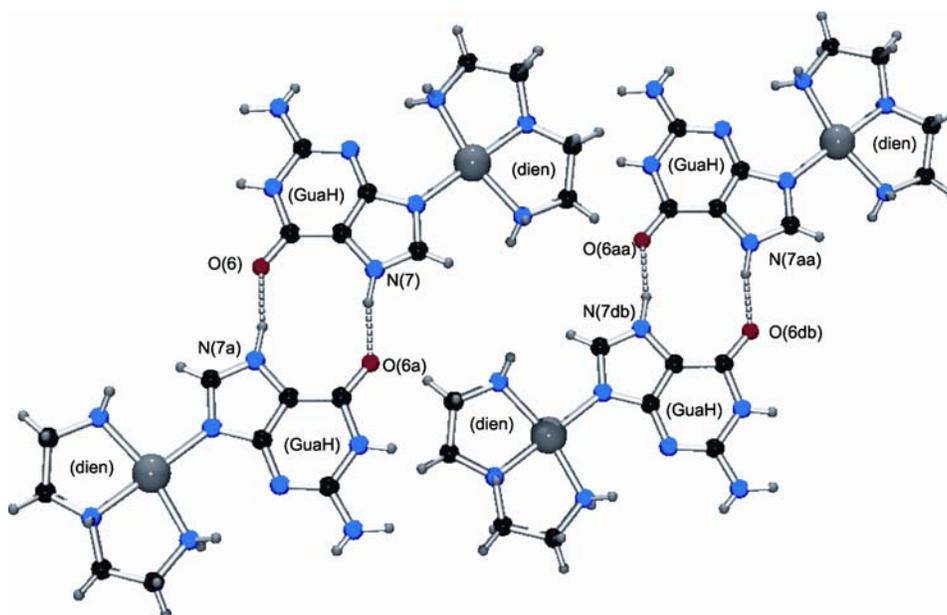
Figure 43 In 12a, purine rings of the adjacent complexes are bonded to each other in a Hoogsteen fashion. The anions are omitted for clarity.

In **12b**, the purine bases are linked by additional hydrogen bonding between the dien-NH_2 and O(6) of guanine base for *e.g.*, N(1)-H···O(6), 2.94(1) Å and N(1)-H···O(6), 2.84(1) Å. The purine rings of the adjacent complexes stack such that the pyrimidine ring of one complex overlays the N(1)-C(6) bond on another (Figure 44) at a distance of 3.19 Å to form a ladder structure. A network of hydrogen bonding exists between the chloride, dien-NH_2 and perchlorates.
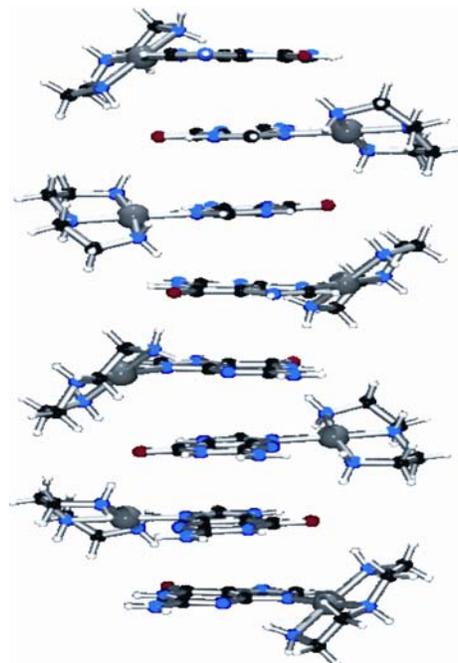
Figure 44 In 12b, purine rings of the adjacent complexes stack such that the pyrimidine ring of one complex overlays the N(1)-C(6) bond on another to form a ladder. The anions are omitted for clarity.

2.4.6 Solution Studies of [(dienPt)$_2$(GH-*N7,N9*)]$^{3+}$ (13)

[(dienPt)$_2$(GH-*N7,N9*)]$^{3+}$ was prepared by taking a solution of 2 equivalent of [(dien)Pt(D_2O)]$^{2+}$ and 1 equivalent of guanine and adjusting the pH* to 10.0. The solution was kept at 40 °C for a few hours. Excess guanine was removed by filtration, the solution was rotary-evaporated to dryness and a ^{1}H NMR spectrum of the colorless compound was obtained in D_2O. Initially, a typical spectrum at pD 7.0, consists of an aromatic singlet H(8) guanine resonance at 7.62 ppm.

pD dependent ^{1}H NMR spectroscopic measurements (Figure 45) have been previously performed for this compound[63] and the structure of the compound has been speculated upon.
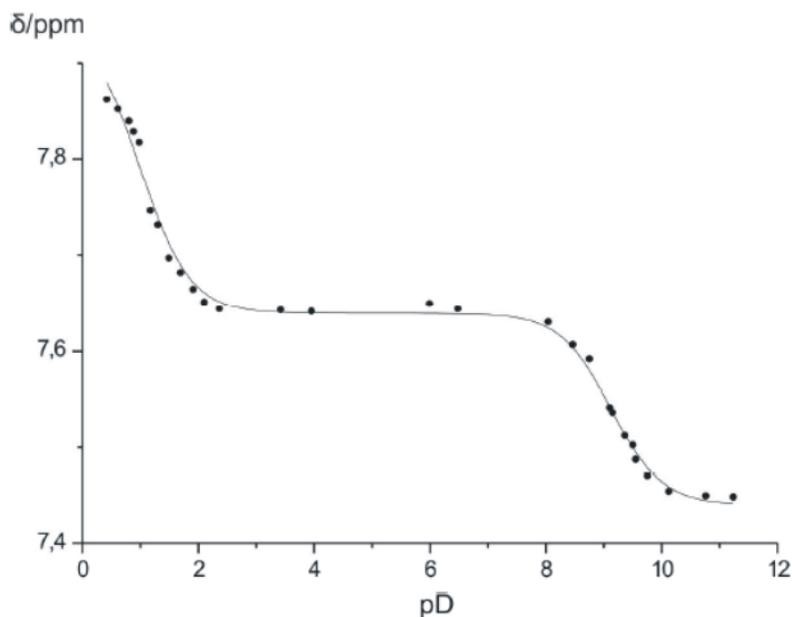
Figure 45 pD dependence (δ, ppm) of H8 resonance for [(dienPt)$_2$(GH-*N7,N9*)]$^{3+}$ in D$_2$O.[63]

During the course of the present work, it was possible to isolate the compound and characterize it by X-ray crystallography. The crystals were dissolved in D$_2$O, were treated with acid and/or base over a wide pD range and ^{1}H NMR spectra were recorded. This was done to ensure that the pD-dependence performed previously corresponded to this compound. Relevant pK_a values are 0.52 ± 0.07 and 8.55 ± 0.06 for the protonated N(3) and deprotonated N(1) positions, respectively.

2.4.7 Characterization of [(dienPt)$_2$(GH-*N7,N9*)](ClO$_4$)$_3$ (13)

Figure 46 depicts the cation of compound **13**. Selected interatomic distances and angles are given in Table 13. In **13**, two (dien)Pt^{II} entities are coordinated to the guanine ligand via N(7) and N(9) positions. GH planes form angles of approximately 43° and 45° with the respective Pt(1) and Pt(2) coordination planes.
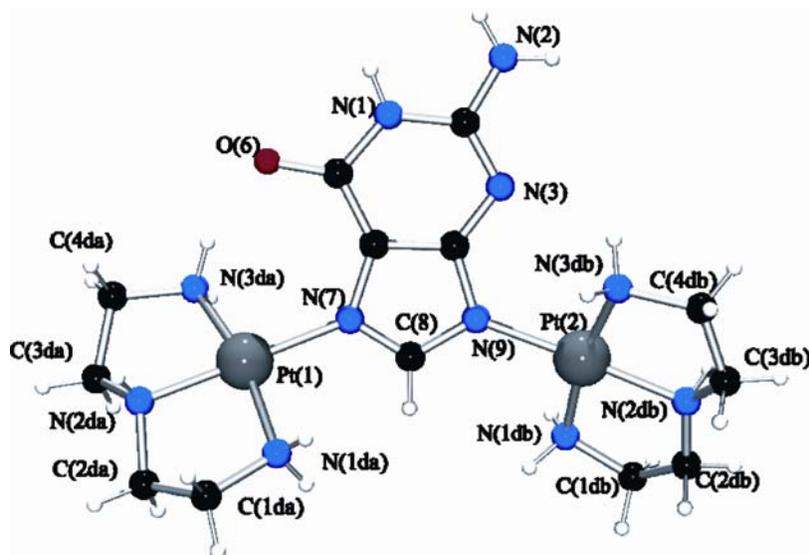
Figure 46 View of cation of [(dienPt)₂(GH-*N7,N9*)](ClO₄)₃ (13) with atom numbering scheme.

Angles about Pt deviate markedly from ideal square-planar[106,159,160] (*e.g.* N(1da)-Pt(1)-N(2da), 83.9(5)°; N(1da)-Pt(1)-N(3da), 166.8(5)°; N(1db)-Pt(2)-N(2db), 85.0(6)°; N(1db)-Pt(2)-N(3db), 168.9(4)°). The M-N(dien) distances range from 2.000(1) to 2.010(1) Å in Pt(1)-N(2da) or Pt(2)-N(2db), to 2.010(1) to 2.040(1) Å in Pt(1)-N(3da) or Pt(2)-N(3db), and are likewise normal.

Table 13 Selected distances (Å) and angles (º) for [(dienPt)₂(GH-*N7,N9*)](ClO₄)₃ (13)

[(dienPt)₂(GH-*N7,N9*)](ClO₄)₃ (13)			
Pt(1)···Pt(2)	5.983(1)	Pt(1)-N(7)	2.020(1)
Pt(2)-N(9)	2.020(1)		
N(2db)-Pt(2)-N(9)	175.7(5)	Pt(1)-N(7)-C(8)	126.9(11)
N(3db)-Pt(2)-N(9)	94.4(4)	C(5)-N(7)-C(8)	105.0(1)
N(1da)-Pt(1)-N(7)	95.4(4)	C(2)-N(3)-C(4)	114.4(1)
N(1db)-Pt(2)-N(9)	96.1(4)	N(7)-C(8)-N(9)	118.0(1)
N(2da)-Pt(1)-N(7)	177.4(4)	N(1)-C(2)-N(3)	125.0(1)
N(3da)-Pt(1)-N(7)	96.5(4)	N(3)-C(4)-N(9)	125.7(13)
Pt(2)-N(9)-C(8)	129.3(9)	N(1)-C(6)-C(5)	113.0(1)
N(7)-C(5)-C(4)	107.0(1)	C(4)-N(9)-C(8)	104.4(1)

Distances and angles within the GH ligand are not unusual. The geometries of the (dien)Pt^{II} entities are likewise not unusual and compare well with the published data. The dien ligands, "da" and "db", adopt the characteristic sting-ray geometries[106] with the central methylene groups C(2) and C(3) of the two dien ligands pointing to the same side of the PtN$_4$ plane, yet in opposite directions for "da" and "db".

Deviations of central methylene groups of the dien ligands from the least-squares planes formed by the PtN$_4$ planes are 0.56(2) Å (C2da), 0.56(2) Å (C3da), -0.25(2) Å (C2db) and -0.37(2) Å (C3db). The purine rings of the adjacent complexes stack such that the pyrimidine ring of one complex overlays the N(1)-C(6) bond on another at a distance of ca. 3.5 Å.

The dien ligands, perchlorate anions, N(1)H, N(2)H$_2$ and O(6) of the GH ligand are involved in numerous intramolecular and intermolecular short contacts. For example, the protons at N1d(a/b), N2d(a/b) and N3d(a/b) of dien ligands are hydrogen bonded to various oxygen atoms of different perchlorate anions, and O(6) of the GH ligand, whereas the N(1)H and N(2)H$_2$ in GH are hydrogen bonded to perchlorate anions. None of these contacts (2.9 – 3.1 Å) between heavy atoms is particularly short.

2.4.8 Theoretical Calculations

Molecular geometries of [(dien)Pt(GH$_2$-$N7$)]$^{2+}$ and [(dien)Pt(GH$_2$-$N9$)]$^{2+}$ complexes have been computed in an attempt to better understand the metal binding behavior of guanine. Figure 47 provides views of the optimized structures of [(dien)Pt(GH$_2$-$N7$)]$^{2+}$and [(dien)Pt(GH$_2$-$N9$)]$^{2+}$.

Calculations of relative energies of N(7) and N(9) linkage isomers for [(dien)Pt(GH$_2$)]$^{2+}$ reveal a preference of the Pt^{II} entity for N(7) site (ΔE = 8.4 kcal/mol). The theoretical results are not in agreement with the experimental observation. The experimental results reveal a preference of the Pt^{II} entity for the N(9) site.

$[(dien)Pt(GuaH_2-N7)]^{2+}$ $[(dien)Pt(GuaH_2-N9)]^{2+}$
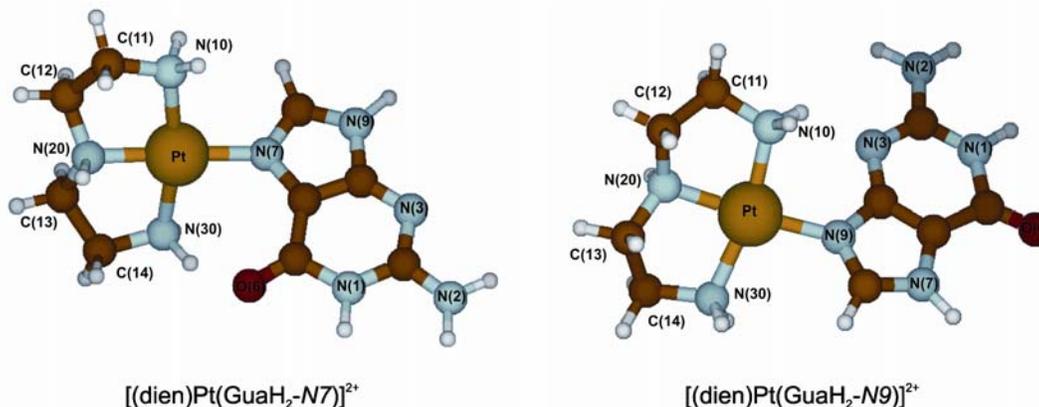
Figure 47 Optimized computed structures of $[(dien)Pt(GH_2-N7)]^{2+}$ and $[(dien)Pt(GH_2-N9)]^{2+}$ with atom numbering schemes.

The comparison between the two geometries shows that in the N(7) linkage isomer the guanine ring forms an angle of ca. 55° with the PtN_4 coordination plane. The NH_2 group of the dien ligand is involved in hydrogen bond formation with O(6), the hydrogen bond length being O(6)···NH_2(dien), 2.768 Å. On the other hand, in the N(9) linkage isomer the guanine ring is tilted at an angle of ca. 36° with respect to the Pt coordination plane. The low value of the dihedral angle between the PtN_4 and guanine planes is consistent with the values obtained for the solid state structures, viz. in the range of 12 to 40°.

Hydrogen bond formation takes place between the (dien)NH_2···N(3), 2.911 Å. There are no significant differences in the bond lengths and angles in the two linkage isomers (*e.g.* Pt(1)-N(10), 2.077 to 2.078 Å, Pt(1)-N(20), 2.064 to 2.068 Å, Pt(1)-N(30), 2.118 to 2.122 Å, N(10)-Pt(1)-N(20), 83.8° to 84.0°, N(20)-Pt(1)-N(30), 83.3° to 83.2° for N(7) and N(9) linkage isomers, respectively), except the Pt(1)-N(7), 2.075 Å and Pt(1)-N(9), 2.063 Å bond lengths. There is generally a good agreement between the calculated and the solid state geometry of the N(9) linkage isomer. The minor discrepancies might be due to the absence of counter anions and the crystal packing forces.

Finally, the calculations were also performed for the dinuclear compound, $[(dienPt)_2(GH-N7,N9)]^{3+}$. View of the optimized structure is presented in Figure 48.
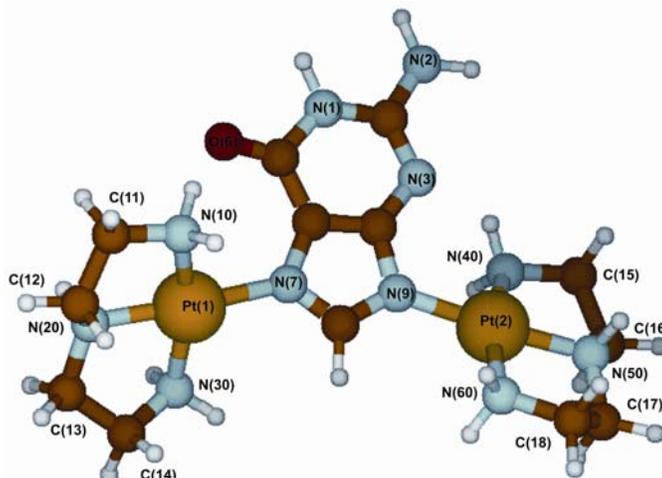
Figure 48 **View of the optimized computed structure of [(dienPt)$_2$(GH-*N7,N9*)]$^{3+}$ with atom numbering schemes.**

The guanine ring forms an angle of ca. 50° and 40° with the Pt(1)N$_4$ and Pt(2)N$_4$ coordination planes, respectively. The M-N(dien) distances range from 2.07 Å in Pt(1)-N(10) or Pt(2)-N(40) to 2.120 Å in Pt(1)-N(30) or Pt(2)-N(60), and are likewise normal. The dien ligands bonded to N(7) and N(9) positions of guanine have different geometries.

Deviations of carbon atoms of the dien ligand from the mean-squares planes formed by the Pt(1)N$_4$ plane are 0.05 Å (C11), -0.49 Å (C12), -0.84 Å (C13) and -0.21 Å (C14) and for Pt(2)N$_4$ plane are 0.11 Å (C15), -0.52 Å (C16), -0.55 Å (C17) and 0.83 Å (C18).

The angles and bond lengths of the guanine ring are usual. O(6), N(3) and NH$_2$ groups of the dien ligands are involved in hydrogen bonding. Hydrogen bond lengths are O(6)-NH$_2$(dien), 2.784 Å and N(3)-NH$_2$(dien), 2.939 Å. Additionally, there might be a weak interaction between N(2)···NH$_2$(dien), 3.541 Å.

In general there is a good agreement between the dinuclear compounds of (dien)Pt^{II} and the X-ray structure of **13**. However, the minor discrepancies are probably a consequence of crystal packing forces and the presence of the counter anions in the solid state structures.

2.4.9 Summary

Guanine (GH_2) exists in solution as two major tautomers, the keto form with N(7) carrying a proton (**I**) and the keto form with N(9) being protonated (**II**). (dien)Pt^{II} prefers binding to the N(9) position. The crystal structure analyses of [(dien)Pt(GH_2-*N9*)]Cl(ClO$_4$) **12a** and 2{[(dien)Pt(GH_2-*N9*)](ClO$_4$)$_2$ · 2H$_2$O} **12b** are reported. With an excess of (dien)Pt^{II} dinuclear species [(dienPt)$_2$(GH-*N7,N9*)]$^{3+}$ forms, which was isolated as a ClO$_4^-$ salt **13** and structurally characterized. Individual species have been identified by the pD dependence of the guanine resonances. pK_a values (calculated for H$_2$O) for deprotonation of the N(9) linkage isomer are 6.5 and 10.5, as well as 0.5 and 8.6 in the dinuclear complex [(dienPt)$_2$(GH-*N7,N9*)]$^{3+}$.

Ab initio calculations have been performed for [(dien)Pt(GH_2-*N7*)]$^{2+}$, [(dien)Pt(GH_2-*N9*)]$^{2+}$ and [(dienPt)$_2$(GH-*N7,N9*)]$^{3+}$. The calculations reveal that the N(7) linkage isomer is more stable than the N(9) linkage isomer by $\Delta E = 8.4$ kcal/mol. The reason of this binding preference might be the intramolecular hydrogen bonding between O(6) and the NH$_2$(dien) ligand in the N(7) linkage isomer. However, this observation is not in agreement with the experimental results. The experimental results reveal a preference of the (dien)Pt^{II} entity for the N(9) position.

2.4.10 Discussion

We were able to synthesize (dien)Pt^{II} complexes of unsubstituted guanine and to a large extent, we successfully identified the various metal binding site(s). However, our goal of synthesizing N(9) bound complexes of Pt^{II} on a preparative scale is still in its infancy.

2.5   Synthesis of Cationic Oligonucleotide Analogs using 9-Ethylguanine (9-EtGH)

2.5.1   Introduction

9-ethylguanine (9-EtGH) can exist in 10 different tautomeric forms.[184] However, at physiological pH, it exists primarily in the keto-amino form (Chart 20).
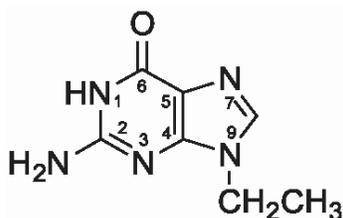
Chart 20   Schematic representation of 9-ethylguanine.

9-EtGH can undergo protonation at N(7) position (pK_s = 3.27) and deprotonation occurs at N(1) position (pK_s = 9.57).[174] In a highly acidic medium, a second protonation can occur at N(3) position.[185]

2.5.2   Aim of the Project

The objective of the present project was the synthesis of artificial oligonucleotide analogs. The synthesis of artificial oligonucleotide analogs can be divided into three parts.

(1)   Synthesis of Central Building Blocks

Hegmans et al.[186] have previously described a synthetic route (Chart 21) for the preparation of *trans*-[(NH$_3$)Pt(9-EtGH)I$_2$] starting out from *cis*-[(NH$_3$)$_2$Pt(9-EtGH-*N7*)Cl]Cl.[187] The use of KI and slightly acidic reaction conditions greatly increases the yield of the *trans* complex, thereby making this reaction useful for subsequent preparative work.

$$\underset{\underset{\displaystyle Cl}{|}}{\overset{\overset{\displaystyle NH_3}{|}}{H_3N-Pt-L}} \quad \xrightarrow[-NH_4Cl]{2I^-,\ H^+} \quad \underset{\underset{\displaystyle |}{|}}{\overset{\overset{\displaystyle |}{|}}{H_3N-Pt-L}} \quad \text{(Charges omitted)}$$
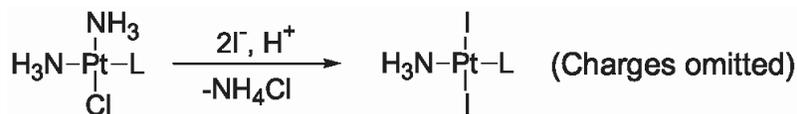
L = pym-*N1*, pu-*N9*, pu-*N7*

Chart 21 Synthetic strategy for the preparation of *trans*-(NH₃)Pt(9-EtGH)I₂.

(2) Choice of the Bridging Ligands

The distance between the Pt^{2+} centers or the nucleobases should be around 3.4 Å. Therefore, the bridging ligand can either be short (*e.g.*, hydrazine) or a long flexible molecule like ethylenediamine. During the course of the present work, the following bridging ligands were used *i.e.*, pyrazine, ethylenediamine and 4,4'-bipyridine (Chart 22).
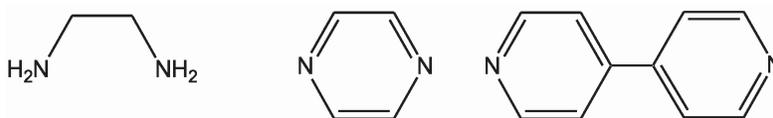
Chart 22 The bridging ligands, ethylenediamine, pyrazine, 4,4'-bipyridine (from left to right).

With pyrazine, the distance between the Pt^{2+} centers is around 7 Å.[188] Therefore, the hydrogen bonding of cationic oligonucleotides can occur only with every second nucleobase in DNA or RNA. When 4,4'-bipyridine is used as a bridging ligand, the distance between the Pt^{2+} centers is around 11.1 Å.[189] Hence, the hydrogen bonding is only possible with every third or fourth nucleobase in DNA or RNA.

(3) Synthesis of the Terminus

The terminus of the cationic oligonucleotide is formed by an am(m)ine ligand *cis* to the nucleobase (Nb). Therefore, the ends can be capped by using precursor complexes of the type *cis*-[(NH₃)₂Pt(Nb)Cl]⁺ or [(en)Pt(Nb)Cl]⁺.

2.5.3 Synthesis of the Building Blocks

2.5.3.1   Synthesis of *cis*-[(NH₃)₂Pt(9-EtGH-*N7*)Cl]Cl (14)

Synthesis of **14** was carried out according to the synthetic procedure reported in the literature.[187] 1:1 mixtures of *cis*-[(NH₃)₂PtCl₂] and 9-EtGH were kept at 40 °C for 48 h. The crude product was a mixture of *cis*-[(NH₃)₂Pt(9-EtGH-*N7*)Cl]Cl and *cis*-[(NH₃)₂Pt(9-EtGH-*N7*)₂]Cl₂ complexes. The yellow-white precipitate was washed with DMF to get pure compound **14**.

During the course of the present work, we have also isolated the 2:1 complex (*cis*-[(NH₃)₂Pt(9-EtGH-*N7*)₂](NO₃)₂) as an impurity of 1:1 (*cis*-[(NH₃)₂Pt(9-EtGH-*N7*)Cl]Cl) complex. *cis*-[(NH₃)₂Pt(9-EtGH-*N7*)₂](NO₃)₂ **19** has been characterized by X-ray crystallography. A view of the molecular cation is given in Figure 49. Selected interatomic distances and angles are listed in Table 14.
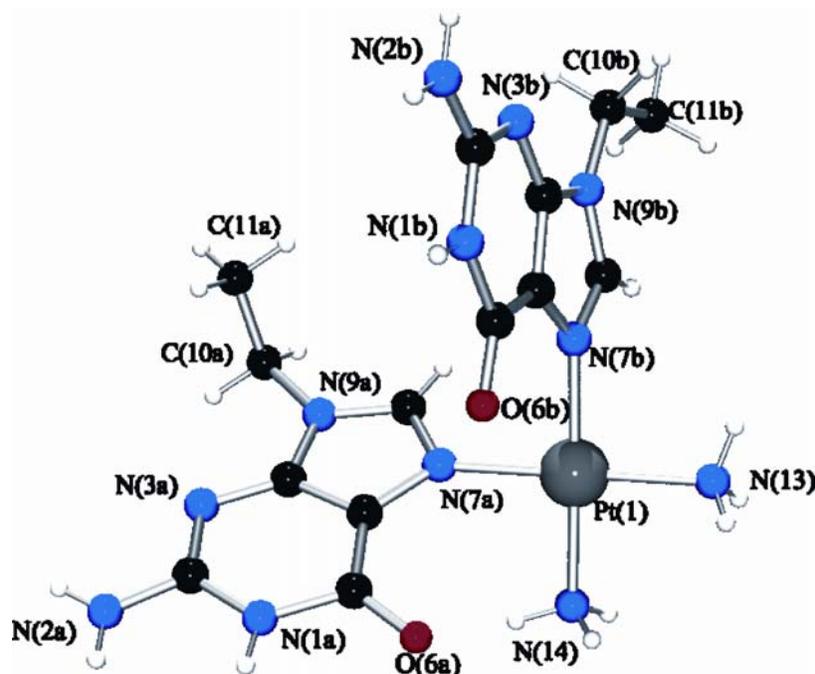
Figure 49 View of cation of *cis*-[(NH₃)₂Pt(9-EtGH-*N7*)₂](NO₃)₂ (19) with atom numbering scheme.

As can be seen from Figure 49, the neutral 9-ethylguanine ligands are coordinated to Pt through N(7). The two purine bases are oriented in a way that the exocyclic oxygens are at the same side of the Pt coordination plane, hence in

a *head*-to-*head* fashion. The review of the published structures on bis(guanine)-*cis*-diam(m)ineplatinum(II) complexes shows that the two purine bases are always in a *head*-to-*tail* orientation,[190-193] with an exception of only a few structures.[194,195] In all these cases, Pt is coordinated through N7 of the guanine ligand.

Table 14 Selected distances (Å) and angles (º) for *cis*-[(NH₃)₂Pt(9-EtGH-*N7*)₂](NO₃)₂ (19)

cis-[(NH₃)₂Pt(9-EtGH-*N7*)₂](NO₃)₂ (19)			
Pt(1)-N(7a)	2.020(7)	Pt(1)-N(13)	2.026(6)
Pt(1)-N(7b)	2.000(1)	Pt(1)-N(14)	2.019(9)
N(7a)-Pt(1)-N(13)	179.0(3)	N(7b)-Pt(1)-N(13)	91.4(3)
N(7a)-Pt(1)-N(14)	90.03(3)	N(7b)-Pt(1)-N(14)	178.6(3)
Pt(1)N₄/9-EtGH(a)	52.6(1)	Pt(1)N₄/9-EtGH(b)	75.7(1)
N(7a)-Pt(1)-N(7b)	88.4(4)	N(13)-Pt(1)-N(14)	89.8(3)
Pt(1)-N(7a)-C(5a)	122.1(7)	C(5a)-N(7a)-C(8a)	106.3(8)
Pt(1)-N(7b)-C(5b)	128.8(8)	C(5b)-N(7b)-C(8b)	105.0(1)

The geometry about the Pt is normal and similar to the other published structures. [194,195] There are no significant differences in bond lengths and angles within the G ligands. The differences in the relative orientation of the ethyl groups determine the degree of base overlap.[194] The ethyl group of guanine ligand "b" is roughly coplanar with the endocyclic atoms of the ring, while the CH₃ group of the ethyl group of the ligand "a" is substantially outside the plane of the rest of the ring and is bent towards the ring "b". Therefore, the intermolecular base-base distance is too large for any stacking interactions.

The hydrogen bonding takes place between O(6) of purines and NH₃ groups, N(13)···O(6a), 2.983(9) Å, N(13)···O(6b), 2.98(1) Å and N(13)···O(6b), 2.970(9) Å. The exocyclic amino groups act as proton donors in hydrogen bonds with O(6) and N(3), the distances being 3.15(1) Å, 2.97(1) Å, for N(2b)H₂···O(6) and N(2b)H₂···N(3b)respectively. Additionally, there is extensive hydrogen bonding

involving O(6) of guanine, NH_3 groups and oxygens of the nitrates. None of these contacts (2.8 – 3.3 Å) between heavy atoms is particularly short.

2.5.3.2   Synthesis of *trans*-[(NH₃)Pt(9-EtGH-*N7*)I₂] (15)

15 was prepared according to the method described in the literature. [186] 1:4 solution mixtures of **14** and KI were kept at 35 °C for 4 days. The reaction was done in a slightly acidic medium as in this condition high yields of the *trans* complex are obtained.

2.5.4 Ethylenediamine as a Bridging Ligand

Qu et al.[196] have reported the synthesis and properties of complexes (Figure 50) containing bidentate coordination spheres [{*cis*-[(NH₃)PtCl₂}₂-(diamine)]Cl₂ and monodentate coordination spheres [{*trans*-[(NH₃)₂PtCl}₂-(diamine)]Cl₂ where diamine = 1,4-butanediamine or 2,5-dimethyl-2,5-hexadiamine. These complexes serve as novel types of intra- and interstrand crosslinks suggesting that different DNA binding modes may have different biological effects.[196]
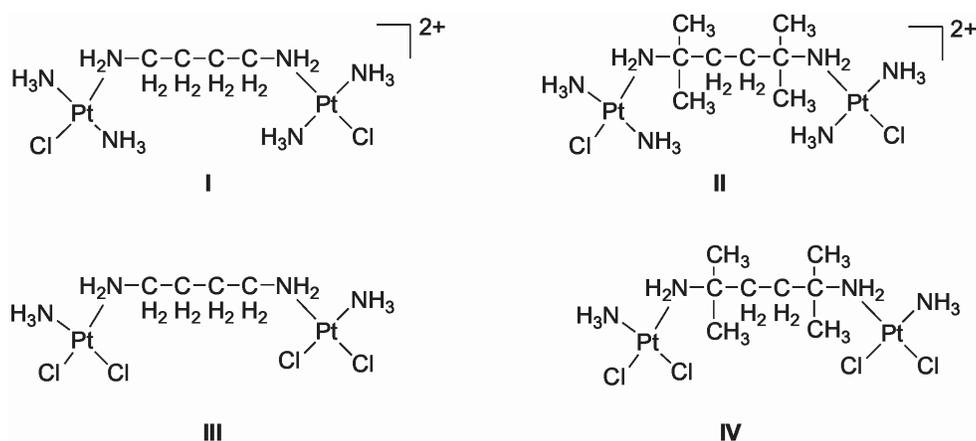
Figure 50 Structures of bis(platinum) complexes containing monodentate (I, II) and bidentate (III, IV) coordination spheres.[196]

The reactions of *trans*-[(NH₃)Pt(9-EtGH-*N7*)I₂] with ethylenediamine in aqueous solution were unsuccessful due to the poor solubility of the starting materials. To circumvent this problem, reactions were carried out with *cis*-[(NH₃)₂Pt(9-EtGH-*N7*)Cl]Cl instead of *trans*-[(NH₃)Pt(9-EtGH-*N7*)I₂] and followed by ^{1}H NMR

spectroscopy. The ^{1}H NMR spectra revealed the presence of a number of linkage isomers and proved difficult to interpret.

2.5.5 Pyrazine as a Bridging Ligand

The coordination chemistry of pyrazine (pyrz) and related ligands with Pt has been extensively investigated.[188,197,198] The pyrazine-bridged dinuclear Pt(II) complexes, [{cis-$(NH_3)_2$PtCl}$_2$-(μ-pyrz)]Cl_2, and its derivatives have been reported to possess anticancer properties. The Pt···Pt distance is 6.82 Å[188] and the compounds have the flexibility to cross-link with a minimal distortion of the DNA molecule. With pyrazine as a bridging ligand, the hydrogen bonding of the cationic oligonucleotides can take place only with every second nucleobase in DNA or RNA.

The single pot aqueous reaction of trans-[(NH_3)Pt(9-EtGH-N7)I_2], $AgNO_3$ and pyrazine in a 1:2:3 proportion at room temperature produced the complex trans-[(NH_3)Pt(9-EtGH-N7)(pyrz)$_2$]$^{2+}$ **16**. Recrystallization of **16** from 1:1:1 mixture of acetone, MeOH and water, afforded yellow crystals suitable for X-ray crystallography. **16** was characterized by elemental analysis, ^{1}H NMR spectroscopy and X-ray crystallography. The Raman spectrum was not obtained as the compound decomposed under the laser beam.
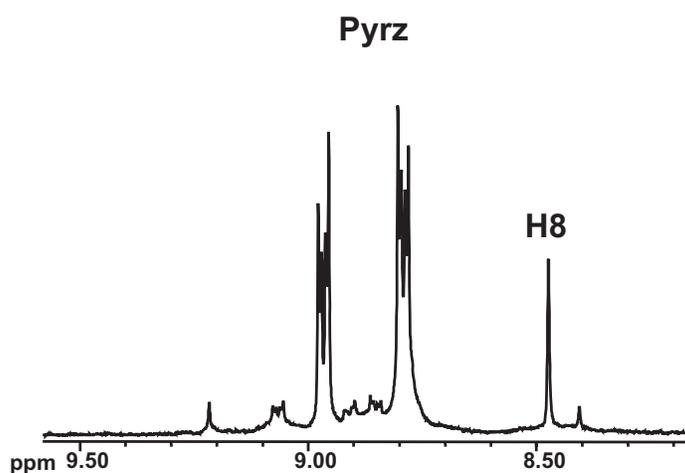
Figure 51 A section of ^{1}H NMR spectrum for the reaction of 15 with AgNO$_3$ and pyrazine (1:2:3, D$_2$O, pH* 4.3).

A representative ^{1}H NMR spectrum for the H8 and pyrazine protons region is shown in Figure 51. Chemical shifts of the individual ^{1}H resonances of the compound **16** are listed and assigned in the Experimental Section. Additionally, there were ^{195}Pt satellites present for the pyrazine signals. The coupling constant is $^3J_{Pt-H}$ ~ 46 Hz.

2.5.5.1   Solution Studies of 16

In the course of the present work, pK_a values of **16** were determined (Figure 52) using pH dependent ^{1}H NMR spectroscopic measurements. pK_a (H$_2$O) for *trans*-[(NH$_3$)Pt(9-EtGH-*N7*)(pyrz)$_2$]$^{2+}$/*trans*-[(NH$_3$)Pt(9-EtG-*N7*)(pyrz)$_2$]$^+$ is 8.13 ± 0.07. Contrary to the expectations, the pyrazine signals are shifted upfield, this might be due to the protonation of guanine.
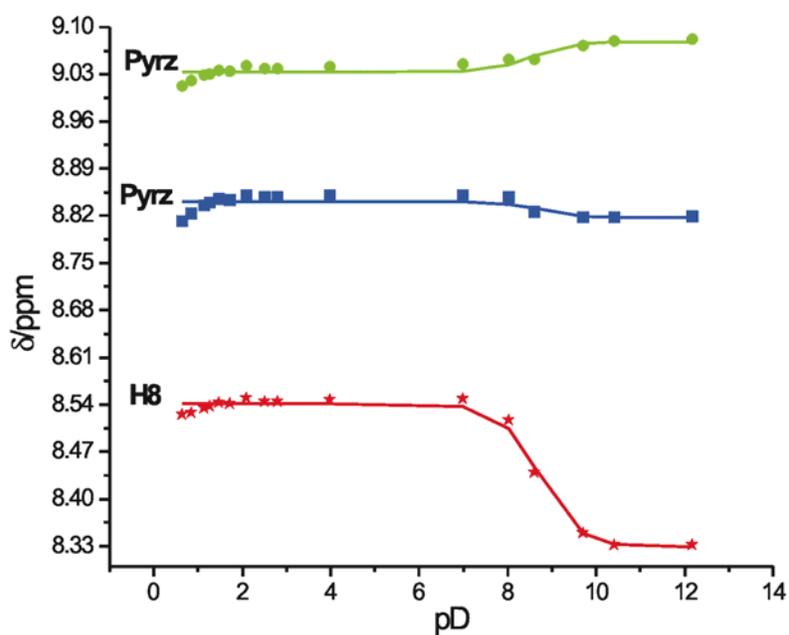
Figure 52 pD dependence (δ, ppm) of H8 and pyrazine protons for 16 in D$_2$O.

2.5.5.2   Characterization of *trans*-[(NH$_3$)Pt(9-EtGH-*N7*)(pyrz)$_2$](NO$_3$)$_2$ · H$_2$O (**16**)

The view of the molecular cation is shown in Figure 53. A selection of bond lengths and angles is given in Table 15.
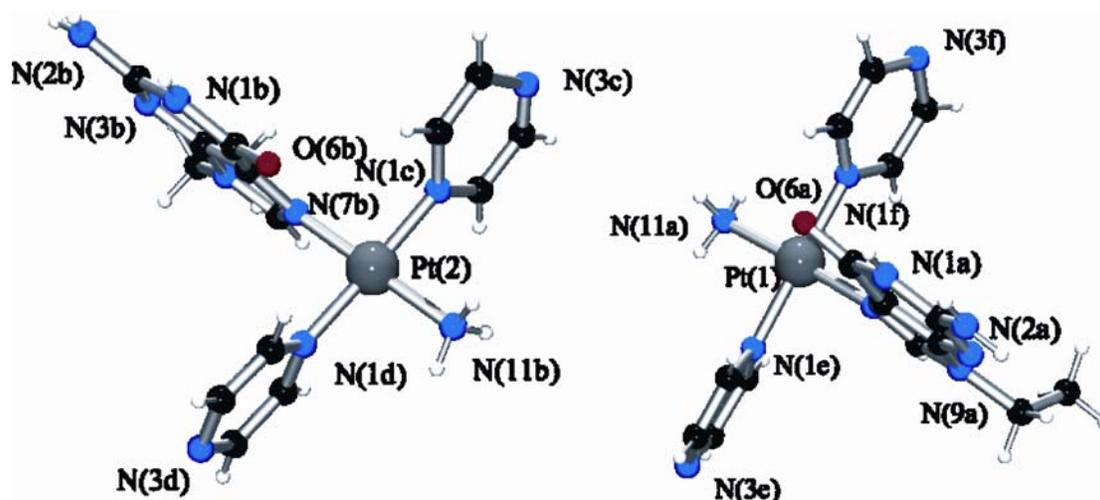
Figure 53 **View of cations of *trans*-[(NH₃)Pt(9-EtGH-*N7*)(pyrz)₂](NO₃)₂ · H₂O (16) with atom numbering scheme. Only one of the two positions of the disordered ethyl chains is shown.**

The coordination around the platinum atoms is square planar. The angles around the Pt atom are close to the expected values for this situation. The dihedral angles between the heterocycles "a" and "b" and $Pt(1)N_4$ and $Pt(2)N_4$ coordination planes are 78.0(1)° and 85.2(1)°, respectively.

Table 15 Selected distances (Å) and angles (⁰) for
***trans*-[(NH₃)Pt(9-EtGH-*N7*)(pyrz)₂](NO₃)₂ · H₂O (16)**

trans-[(NH₃)Pt(9-EtGH-*N7*)(pyrz)₂](NO₃)₂ · H₂O (16)			
Pt(1)-N(7a)	2.030(1)	Pt(1)-N(11b)	2.050(1)
Pt(1)-N(7b)	2.020(1)	Pt(1)-N(1e)	2.010(1)
Pt(1)-N(11a)	2.040(1)	Pt(1)-N(1f)	2.010(1)
Pt(2)-N(1d)	2.000(1)	Pt(2)-N(1c)	2.000(1)
N(1e)-Pt(1)-N(1f)	178.1(5)	N(7a)-Pt(1)-N(11a)	177.0(5)
N(1e)-Pt(1)-N(7a)	88.0(5)	N(1f)-Pt(1)-N(11a)	89.8(5)
N(1e)-Pt(1)-N(11a)	90.1(5)	N(7a)-Pt(1)-N(11a)	177.0(5)
N(1f)-Pt(1)-N(7a)	92.2(5)	N(7b)-Pt(2)-N(11b)	178.1(5)
N(1c)-Pt(2)-N(1d)	176.6(5)	N(1c)-Pt(2)-N(11b)	90.2(5)

N(1c)-Pt(2)-N(7b)	89.5(4)	N(1d)-Pt(2)-N(7b)	90.0(5)
N(1d)-Pt(2)-N(11b)	90.5(5)	Pt(1)-N(1e)-C(1e)	123.0(1)
Pt(1)-N(1f)-C(1f)	125.0(1)	Pt(1)-N(1e)-C(4e)	120.0(1)
Pt(1)-N(1f)-C(5f)	120.0(1)	Pt(2)-N(1c)-C(2c)	120.0(1)
Pt(2)-N(1d)-C(1d)	122.0(1)	Pt(2)-N(1c)-C(5c)	124.0(1)
Pt(2)-N(1d)-C(5d)	122.0(1)	Pt(2)-N(7b)-C(5b)	127.8(9)
Pt(1)-N(7a)-C(5a)	126.2(8)	Pt(2)-N(7b)-C(8b)	125.3(9)
Pt(1)-N(7a)-C(8a)	128.0(1)	C(5b)-N(7b)-C(8b)	107.0(1)
C(5a)-N(7a)-C(8a)	107.0(1)	C(4b)-N(9b)-C(8b)	108.0(1)
C(2c)-N(1c)-C(5c)	117.1(1)	C(1c)-N(3c)-C(4c)	119(2)
C(2f)-N(3f)-C(4f)	114.0(1)	C(2e)-N(3e)-C(5e)	117.1(1)
C(2d)-N(3d)-C(4d)	117.0(1)	C(1d)-N(1d)-C(5d)	117.1(1)
C(1e)-N(1e)-C(4e)	118.0(1)	C(1f)-N(1f)-C(5f)	117.0(1)

Pt-N distances are normal. The binding of pyrazine to platinum through the nitrogen atom slightly increases the internal C-N-C angles, which vary from 117.1(1)° to 119(2)°. In free pyrazine, these angles are 115.1°.[199] The bond distances and angles in the different pyrazine rings are as expected. In the crystal, the stacking interactions occur between the pyrazine rings at a distance of ca. 3.48 Å.

The cations are arranged in a form of chains and the nitrate anions are located in between these chains. The nitrate anions are involved in extensive intermolecular hydrogen bonding interactions to the N(1)H, N(2)H_2 of the purine bases as well as to the NH_3 ligands.

The hydrogen bonding distances between the heavy atoms are N(1)-H···O, 2.89(1) Å, N(11)-H···O, 3.26(1) Å, N(11)-H···O, 2.75(3) Å, N(11)-H···O, 3.15(1) Å, N(11)-H···O, 2.75(3) Å, N(11)-H···O, 3.16(2) Å, N(11)-H···O, 3.21(3) Å, N(11)-H···O, 2.82(2) Å, N(11)-H···O, 3.20(3) Å, N(11)-H···O, 2.95(2) Å, N(2)-H···O, 2.96(2) Å and N(2)-H···O, 3.26(2) Å. Additionally, the water molecules also participate in hydrogen bonding.

2.5.5.3   Reactions with *cis*-[(NH₃)₂Pt(9-EtGH-*N7*)Cl]Cl (14)

The reaction between **14,** AgNO$_3$ and pyrazine at 1:1.5:1 ratio in water was carried out to obtain the complex *cis*-[(NH$_3$)$_2$Pt(9-EtGH-*N7*)(pyrz)]$^{2+}$. AgNO$_3$ was added to the reaction mixture slowly, in order to have constantly an excess of **14**. The reaction was monitored by ^{1}H NMR spectroscopy. A representative ^{1}H NMR spectrum is shown in Figure 54.
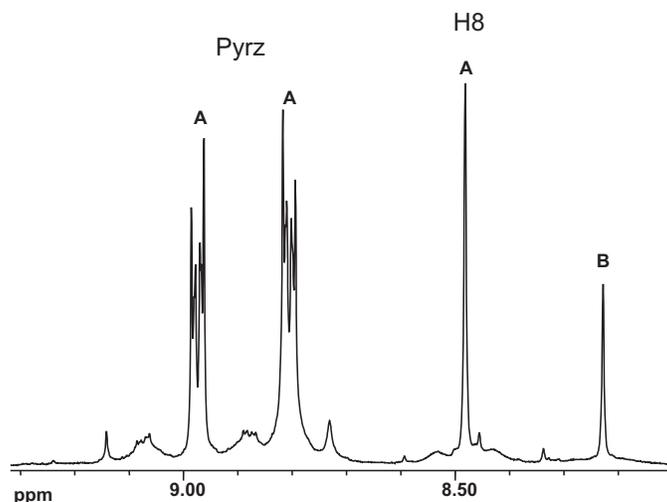
Figure 54 A section of ^{1}H NMR spectrum for the reaction of 14 with AgNO$_3$ and pyrazine (1:1:1.5, D$_2$O, pH* 5.4). Assignment of resonances (A)–(B) was made on the basis of their pD dependence.

During the course of the reaction, two new sets of H8 and pyrazine peaks were observed. The products were identified by a ^{1}H NMR pH titration (Figure 55) on a similar solution. Of these, peak B is due to the complex **14**. The most intense set of resonances A was assigned to the desired complex *cis*-[(NH$_3$)$_2$Pt(9-EtGH-*N7*)(pyrz)]$^{2+}$. There are ^{195}Pt satellites present for the pyrazine ($^3J_{Pt-H}$ ~ 43 Hz) and H8 protons ($^3J_{Pt-H}$ ~ 21 Hz). The integrals are consistent with this interpretation.

The pK_a values were determined from H8 ^{1}H NMR shifts. Relevant pK_a values are 8.48 ± 0.04 and 8.36 ± 0.06 for *cis*-[(NH$_3$)$_2$Pt(9-EtGH-*N7*)(H$_2$O)]$^{2+}$/*cis*-[(NH$_3$)$_2$Pt(9-EtGH-*N7*)(H$_2$O)]$^+$ and   *cis*-[(NH$_3$)$_2$Pt(9-EtGH-*N7*)(pyrz)]$^{2+}$/*cis*-[(NH$_3$)$_2$Pt(9-EtGH-*N7*)(pyrz)]$^+$, respectively.
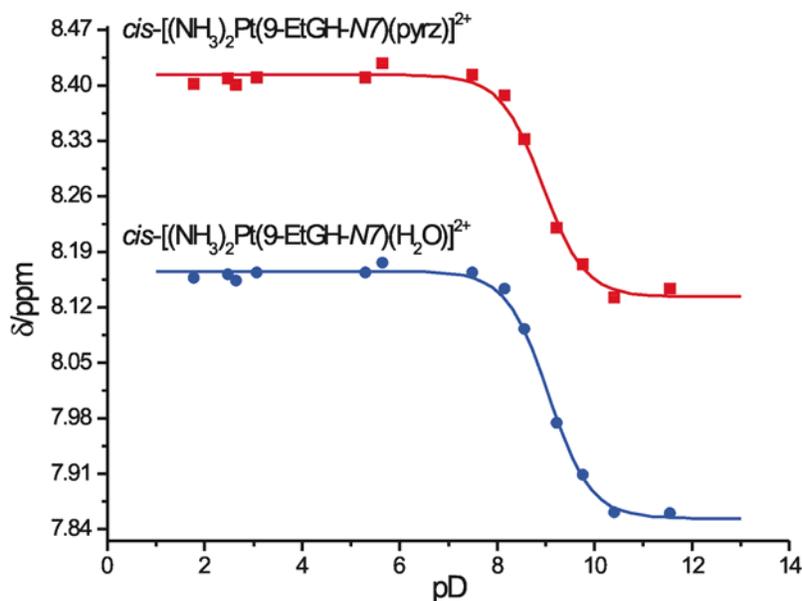
Figure 55 pD dependence (δ, ppm) of H8 protons of guanine ligand in
***cis*-[(NH$_3$)$_2$Pt(9-EtGH-*N7*)(pyrz)]$^{2+}$ and *cis*-[(NH$_3$)$_2$Pt(9-EtGH-*N7*)(H$_2$O)]$^{2+}$**
in D$_2$O.

A similar reaction was performed with excess of **14,** and only one species corresponding to the compound *cis*-[(NH$_3$)$_2$Pt(9-EtGH-*N7*)(pyrz)]$^{2+}$ was detected in the ^{1}H NMR spectrum.

2.5.6 4,4'-bipyridine as a Bridging Ligand

A number of cationic, tetranuclear, Pt^{II}- and Pd^{II}- based macrocyclic squares have been prepared and characterized using difunctional chelating ligands, for example, 4,4'-bipyridine and dicyanobenzene.[189] The X-ray crystallography establishes the dimension of the 4,4'-bipy and related squares to be ca. 11 Å, based on the M···M interatomic distances.[189] Using 4,4'-bipy as a bridging ligand, the hydrogen bonding of the cationic oligonucleotides can take place only with every third or fourth nucleobase in DNA or RNA. The pK_a value of protonated 4,4'-bipy is 3.87 ± 0.12.

2.5.6.1   Reactions with *trans*-[(NH$_3$)Pt(9-EtGH-*N7*)I$_2$] (15)

The reaction of **15** with AgNO$_3$ and 4,4'-bipy at 1:2:3 ratio was done at room temperature as well as at 40 °C. After 3 days, AgI and insoluble 4,4'-bipy were filtered off and ^{1}H NMR spectra of the products were recorded. For the reaction

performed at 40 °C, a number of linkage isomers were formed in the reaction mixture. The ^1H NMR spectrum was complicated and hence, interpretation was difficult.

A typical ^1H NMR spectrum for the reaction carried out at room temperature is shown in Figure 56. As can be seen, only a single product was detected corresponding to the set of resonances A. This set of resonances was assigned to the compound *trans*-[(NH$_3$)Pt(9-EtGH-*N7*)(bipy)$_2$]$^{2+}$. Additionally, there was uncoordinated or free 4,4'-bipy present. However, it was not possible to remove the excess bipy from the mixture. The free bipy was identified on the basis of its pD-dependent chemical shifts.
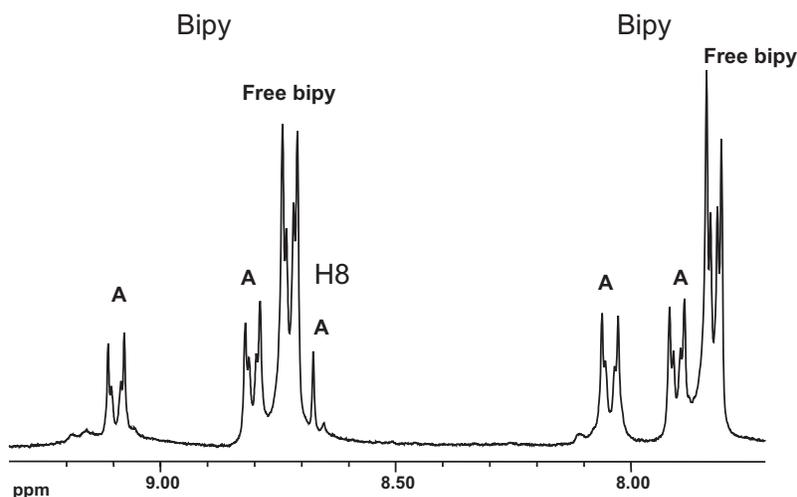
Figure 56 A section of ^1H NMR spectrum for the reaction of 15 with AgNO$_3$ and 4,4'-bipy (1:2:3, D$_2$O, pH* 5.8). The set of resonances A was assigned to the complex *trans*-[(NH$_3$)Pt(9-EtGH-*N7*)(bipy)$_2$]$^{2+}$.

^1H NMR peak assignments are as follows: δ = 9.09 (m, bipy), 8.80 (m, bipy), 8.72 (m, free bipy), 8.78 (s, H8), 8.04 (m, bipy), 7.90 (m, bipy), 7.82 (m, free bipy), 4.15 (q, methylene), 1.46 (t, methyl) ppm.

2.5.6.2   Reactions with *cis*-[(NH$_3$)$_2$Pt(9-EtGH-*N7*)Cl]Cl (14)

The reactions of **14** with 4,4'-bipy in different proportions, viz. 1:2, 1:1 and 1:0.5 were carried out at room temperature and monitored by ^1H NMR spectroscopy. A typical spectrum is shown in Figure 57.

Four species labeled A, B, C and free bipy were detected during the time course of the reaction. Of these, B and free bipy are due to **14** and uncoordinated 4,4'-bipyridine. These species were identified on the basis of their pD dependence.
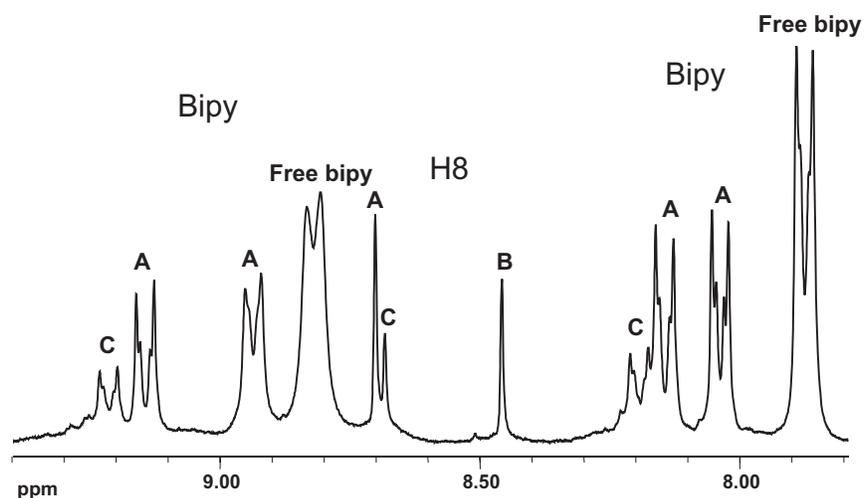
Figure 57 A section of ^{1}H NMR spectrum for the reaction of 14 with 4,4'-bipy (1:1, D_2O, pH* 5.6). The set of resonances A was assigned to the complex cis-[($NH_3)_2$Pt(9-EtGH-$N7$)(bipy)]$^{2+}$, C to the bridged complex [{cis-($NH_3)_2$Pt(9-EtGH-$N7$)}$_2$-(µ-bipy)]$^{2+}$ and B is the complex 14.

For the complex cis-[($NH_3)_2$Pt(9-EtGH-$N7$)(bipy)]$^{2+}$, four sets of resonances were expected for the coordinated 4,4'-bipy. Hence, the set of resonances A has been assigned to this complex. The two sets of resonances C for the coordinated 4,4'-bipy are due to the bridged complex [{cis-($NH_3)_2$Pt(9-EtGH-$N7$)}$_2$-(µ-bipy)]$^{2+}$. Out of the three H8 signals present, the most intense signal A has been assigned to cis-[($NH_3)_2$Pt(9-EtGH-$N7$)(bipy)]$^{2+}$ and C is due to the complex [{cis-($NH_3)_2$Pt(9-EtGH-$N7$)}$_2$-(µ-bipy)]$^{2+}$ based on the relative intensities and the species distribution in the reaction mixture.

2.5.7 Synthesis of the Terminus

Attempts to prepare and isolate Pt_3^{6+} compounds using $trans$-[(NH_3)Pt(9-EtGH-$N7$)(pyrz)]$^{2+}$ and **14** at 1:2 ratio have till this date been unsuccessful. The spectra obtained are complicated and difficult to interpret.

2.5.8 Summary

Reactions with *trans*-[(NH$_3$)Pt(9-EtGH-*N7*)I$_2$] have been carried out using three different bridging ligands, ethylenediamine, pyrazine and 4,4'-bipyridine. The reactions with ethylenediamine were unsuccessful. With pyrazine, initial success was achieved as far as the synthesis of the middle part of the artificial oligonucleotides is concerned. However attempts to use these blocks in order to synthesize Pt$_3^{6+}$ compounds have been unsuccessful. The reactions with 4,4'-bipyridine as a bridging ligand were also promising though the isolation of product has not been successful so far. The complexes *trans*-[(NH$_3$)Pt(9-EtGH-*N7*)(pyrz)$_2$](NO$_3$)$_2$ **16** and *cis*-[(NH$_3$)$_2$Pt(9-EtGH-*N7*)$_2$](NO$_3$)$_2$ **19** have been characterized by X-ray crystallography.

2.6   Pt^{2+} Complexes of 7-Methylguanine (7-MeGH)

2.6.1   Introduction

Treatment of cells by alkylating agents such as alkylsulfates, alkylmethanesulfonates or nitrosoureas can result in cell death, mutagenesis and carcinogenesis.[200,201] These effects are believed to be due to the alkylation of nucleic acids. The main DNA targets of such compounds are the N(3) of adenine, O(6) and N(7) sites of guanine.[200,201] Guanine, methylated at the N(7) position, is by far the main product of DNA alkylation.[202] The presence of 7-MeGH is necessary to optimize the activity of important functional regions of rRNA and tRNA.[203-205] The methylation leads to a pronounced change in the hydrogen bonding and acid-base properties of the guanine nucleobase.[206]

The relative degree and position of alkylation can lead to a drastic change in the metal binding behavior of the available heteroatoms in purine bases.[207,208] Studies of metal coordination to 7-MeGH (Chart 23) have been very limited. Metal complex formation with 7-MeGH has been studied by other groups,[209-214] and there are examples of X-ray structurally characterized metal compounds with N1,N3,N9,[209] N9,[209,213,214] N1,N9[209] or N1[209] coordination.
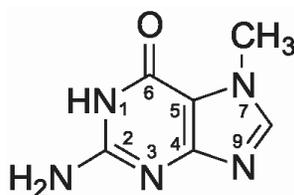
Chart 23 Schematic representation of 7-methylguanine.

2.6.2   Aim of the Project

We were interested in the metal binding behavior of 7-MeGH and specifically the attachment of a Pt^{II} entity to the N(9) position. Therefore, we wanted to synthesize the 1:1 complex *cis*-[(NH$_3$)$_2$Pt(7-MeGH-*N9*)Cl]Cl on a preparative

scale. This 1:1 complex was to be used in the synthesis of central building blocks in order to generate the artificial oligonucleotides (ref. section 2.5).

2.6.3 Reactions with (dien)Pt^{II}

A number of NMR scale reactions were carried out to study the metal binding behavior of 7-MeGH. The reaction of 7-MeGH with $[(dien)Pt(D_2O)]^{2+}$ was performed in a 1:1 proportion at pD 4.0 for a day at 40 °C. The reaction was monitored by ^1H NMR spectroscopy. Only one species was detected in the reaction mixture. The H(8) signal was assigned to the N(9) linkage isomer by comparison with the spectrum of the isolated compound $[(dien)Pt(7-MeGH-N9)]^{2+}$ **18**. The structure of this compound has been established by X-ray crystallography. Also, there were well resolved ^{195}Pt satellites ($^3J_{Pt-H}$ ~ 15.5 Hz) present for the H8 signal. The pK_a value for $[(dien)Pt(7-MeGH-N9)]^{2+}/[(dien)Pt(7-MeG-N9)]^+$ is 8.16 ± 0.04 as determined by pD dependent (Figure 58) ^1H NMR spectroscopic measurements. Below pD 1.0, protonation takes place either at N(3) or O(6).
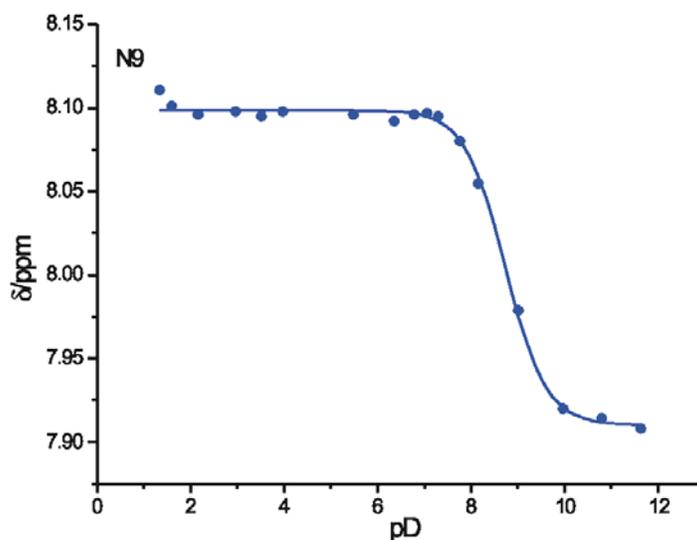
Figure 58 pD dependence (δ, ppm) of H8 proton for $[(dien)Pt(7-MeGH-N9)]^{2+}$.

2.6.4 Characterization of $[(dien)Pt(7-MeGH-N9)](NO_3)(ClO_4)$ (**18**)

The view of the molecular cation is shown in Figure 59. Selected bond lengths and angles are listed in Table 16. As can be seen, the (dien)Pt^{II} entity is

coordinated to 7-MeGH via N9 position. The angle between the Pt coordination plane and the guanine ligand is 12.0(1)°. The geometries of the (dien)Pt^{II} group is usual, including the deviations of some of the angles from ideal square-planar coordination geometry of the Pt due to the strain exercised by the tridentate ligand.[106,159,160]
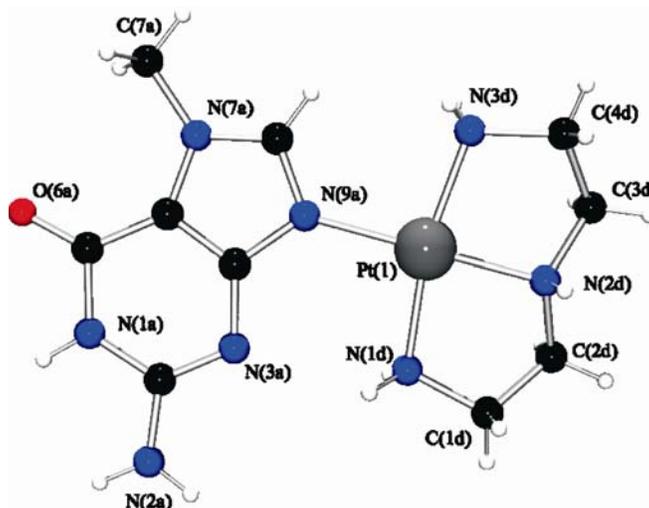
Figure 59 View of the cation of [(dien)Pt(7-MeGH-*N9*)](NO$_3$)(ClO$_4$) (18) with atom numbering scheme.

Carbon atoms of the ethylene group do not display a uniform pattern as far as positions relative to the PtN$_4$ plane is concerned,[106] deviations being -0.15(1) Å C(1d), 0.53(1) Å (C2d), 0.67 (1) Å (C3d) and 0.03 (1) Å (C4d). The bond lengths and bond angles in the 7-MeGH have normal values.

Table 16 Selected distances (Å) and angles (º) for [(dien)Pt(7-MeGH-*N9*)](NO$_3$)(ClO$_4$) (18)

[(dien)Pt(7-MeGH-*N9*)](NO$_3$)(ClO$_4$) (18)			
Pt(1)-N(9a)	2.032(5)	Pt(1)-N(2d)	2.005(6)
Pt(1)-N(1d)	2.040(6)	Pt(1)-N(3d)	2.042(6)
Pt(1)-N(9a)-C(8a)	124.9(4)	Pt(1)-N(1d)-C(1d)	107.3(4)
N(3d)-Pt(1)-N(9a)	95.3(2)	N(2d)-Pt(1)-N(9a)	179.3(2)
N(1d)-Pt(1)-N(2d)	83.9(2)	Pt(1)-N(2d)-C(2d)	108.1(4)
N(1d)-Pt(1)-N(3d)	166.3(2)	Pt(1)-N(2d)-C(3d)	106.8(4)

N(1d)-Pt(1)-N(9a)	96.6(2)	Pt(1)-N(3d)-C(4d)	108.7(4)
Pt(1)-N(9a)-C(4a)	129.9(4)	C(4a)-N(9a)-C(8a)	105.2(5)
N(2d)-Pt(1)-N(3d)	84.2(2)	C(2a)-N(1A)-C(6a)	125.0(5)

The perchlorate and nitrate anions are involved in intermolecular hydrogen bonding with the N(1a), N(2a), dien-NH$_2$ and dien-NH, viz. N(1d)-H⋯O(12), 3.18(1) Å, N(2d)-H⋯O(11), 3.16(1) Å, N(2d)-H⋯O(13), 3.12(1) Å, N(3d)-H⋯O(21), 3.00(1) Å, N(3d)-H⋯O(23), 3.18(1) Å, N(3d)-H⋯O(22), 3.09(1) Å, N(3d)-H⋯O(22), 2.92(1) Å, N(2a)-H⋯O(21), 3.12(1) Å, N(2a)-H⋯O(12), 3.03(1) Å and N(1a)-H⋯O(21), 2.88(1) Å. Additionally, N(3a) and O(6a) also participate in hydrogen bonding. There is an intramolecular hydrogen bond N(1d)-H⋯N(3a) 2.87(1) Å and O(6) is involved in intermolecular hydrogen bonding to N(1d)-H⋯O(6a) 3.02(1) Å. The purine rings of the adjacent complexes are stacked so that the pyrimidine ring of one complex overlays the N(1)-C(6) bond on another at a mean stacking distance of 3.42 Å.

2.6.5 Reactions with *cis*-[(NH$_3$)$_2$Pt^{II}]

On the NMR scale, reaction of *cis*-[(NH$_3$)$_2$PtCl$_2$] with 7-MeGH (1:1) gave at least three major products, one of which was later isolated in analytically pure form as a chloride salt: *cis*-[(NH$_3$)$_2$Pt(7-MeGH-*N9*)$_2$]$^{2+}$ **20**. The second compound *cis, cis*-[{(NH$_3$)$_2$Pt}$_2$(7-MeGH-*N3,N9*)Cl$_2$]$^{2+}$ was isolated as a chloride salt as well, but it was contaminated with **20**.

A typical ^{1}H NMR spectrum is shown in Figure 60. Peak B (8.10 ppm) was assigned to the complex *cis*-[(NH$_3$)$_2$Pt(7-MeGH-*N9*)$_2$]$^{2+}$ on the basis of the pD dependent ^{1}H NMR spectroscopic measurements for the isolated compound **20**. The signal A (7.87 ppm) was due to the free ligand by comparison with the spectrum obtained for the ligand at a similar pH.

There are well resolved [195]Pt satellites present for the signals C (8.53 ppm) and D (8.25 ppm). The coupling constants are $^3J_{Pt-H}$ ~ 13.8 Hz and $^3J_{Pt-H}$ ~ 16.9 Hz for the signals C and D, respectively. The signal C was assigned to the compound

cis, *cis*-[{(NH$_3$)$_2$Pt}$_2$(7-MeGH-*N3*,*N9*)Cl$_2$]$^{2+}$ **21** by comparison with the spectrum of the isolated compound. Although the isolated compound was contaminated with complex **20**, the peaks were well separated. Peak D is assigned to the desired complex *cis*-[(NH$_3$)$_2$Pt(7-MeGH-*N9*)Cl]$^+$. Besides this, there were also other linkage isomers present in the reaction mixture. However, it was not possible to identify these complexes.
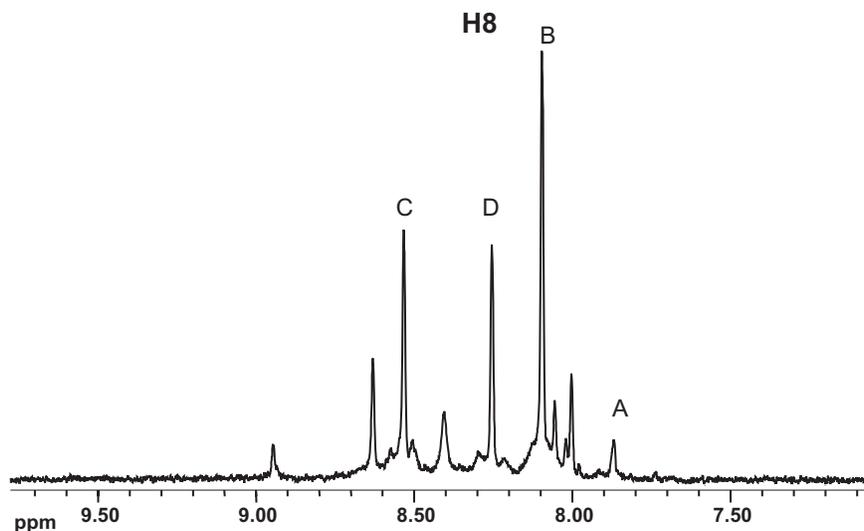
Figure 60 Lowfield section of ^{1}H NMR spectrum (D$_2$O, pH* 3.0, H8 resonances only) of reaction mixture (1:1) *cis*-[(NH$_3$)$_2$PtCl$_2$] and 7-MeGH after 2 days at 30 °C. The signal A has been assigned to the free ligand and B is due to the 2:1 complex (20). Peak C is assigned to N3,N9 dinuclear species and D is due to the N9 linkage isomer.

2.6.6 Characterization of *cis*, *cis*-[{(NH$_3$)$_2$Pt}$_2$(7-MeGH-*N3*,*N9*)Cl$_2$]Cl$_2$ · 3H$_2$O (**21**)

The complex was isolated during the course of the present work to synthesize the N(9) linkage isomer on a preparative scale. Figure 61 provides a view of the cation of *cis*, *cis*-[{(NH$_3$)$_2$Pt}$_2$(7-MeGH-*N3*,*N9*)Cl$_2$]Cl$_2$ · 3H$_2$O **21**. Selected bond lengths and angles are listed in Table 17.

Two *cis*-[(NH$_3$)$_2$PtCl]$^+$ entities are bound to 7-MeGH through N3 and N9 positions. The coordination spheres of the Pt(1) and Pt(2) are square-planar with the angles near 90° and the normal distances to the Cl ligands.[215]
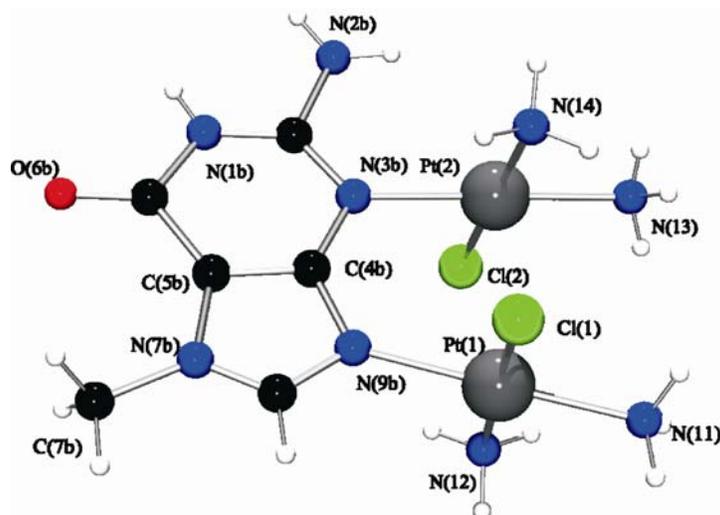
Figure 61 View of the cation of *cis, cis*-[{(NH$_3$)$_2$Pt}$_2$(7-MeGH-*N3,N9*)Cl$_2$]Cl$_2$ · 3H$_2$O (21) with atom numbering scheme. The water molecules and anions have been omitted for clarity.

The Cl ligands are oriented in mutually opposite directions to prevent steric hindrance. Pt-N distances are as usual. Distances and angles within the purine base are likewise normal.[209,214] The dihedral angles between the purine base and the Pt coordination planes are 86.3(2)° and 86.8(1)° for Pt(1) and Pt(2), respectively.

Table 17 Selected distances (Å) and angles (º) for *cis, cis*-[{(NH$_3$)$_2$Pt}$_2$(7-MeGH-*N3,N9*)Cl$_2$]Cl$_2$ · 3H$_2$O (21)

cis, cis-[{(NH$_3$)$_2$Pt}$_2$(7-MeGH-*N3,N9*)Cl$_2$]Cl$_2$ · 3H$_2$O (21)			
Pt(1)···Pt(2)	3.1603(9)	Pt(1)-Cl(1)	2.292(4)
Pt(2)-N(3b)	2.06(1)	Pt(1)-N(11)	2.04(1)
Pt(2)-N(13)	2.03(1)	Pt(1)-N(12)	2.05(1)
Pt(2)-N(14)	2.05(1)	Pt(1)-N(9b)	2.06(1)
Pt(2)-Cl(2)	2.298(4)		
Pt(1)N$_4$/7-MeGH	86.3(2)	Pt(2)N$_4$/7-MeGH	86.8(1)
Cl(1)-Pt(1)-N(9B)	90.5(3)	Pt(2)-N(3b)-C(4b)	120.6(9)
N(13)-Pt(2)-N(14)	89.1(5)	C(2b)-N(3b)-C(4b)	113.0(1)
Cl(2)-Pt(2)-N(3b)	88.4(3)	C(5b)-N(7b)-C(7b)	124.0(1)
N(3b)-Pt(2)-N(14)	92.5(5)	C(5b)-N(7b)-C(8b)	105.0(1)
N(3b)-Pt(2)-N(13)	178.5(4)	C(7b)-N(7b)-C(8b)	132.0(1)

Cl(1)-Pt(1)-N(12)	174.8(3)	C(4b)-N(9b)-C(8b)	102.0(1)
Pt(1)-N(9b)-C(4b)	129.7(9)	N(7b)-C(8b)-N(9b)	122.0(1)
Pt(1)-N(9b)-C(8b)	128.5(9)	N(7b)-C(5b)-C(6b)	135.0(1)
Cl(1)-Pt(1)-N(11)	88.0(3)	N(1b)-C(2b)-N(3b)	132.0(1)
N(11)-Pt(1)-N(12)	90.8(4)	N(3b)-C(4b)-N(9b)	130.0(1)
N(9b)-Pt(1)-N(11)	178.4(4)	N(9b)-C(4b)-C(5b)	109.0(1)
Cl(2)-Pt(2)-N(13)	90.1(4)	N(3b)-C(4b)-C(5b)	123.0(1)
Cl(2)-Pt(2)-N(14)	179.0(4)	N(7b)-C(5b)-C(4b)	105.0(1)
Pt(2)-N(3b)-C(2b)	128.0(1)	C(4b)-C(5b)-C(6b)	122.0(1)
		N(1b)-C(2b)-N(2b)	114.0(1)

In the crystal lattice, the adjacent complexes are (Figure 62) linked via intermolecular hydrogen bonding between the Cl of one and the NH_3 group of the other complex to form a zig zag ladder. The hydrogen bonding distances are N(12b)-H⋯Cl(2c), 3.43(1) Å and N(14)-H⋯Cl(1b), 3.39(1) Å. The chloride anions are involved in additional hydrogen bonding with N(1b)-H⋯Cl(4), 3.26(1) Å, N(11)-H⋯Cl(3), 3.32(1) Å, N(11)-H⋯Cl(4), 3.54(1) Å, N(11)-H⋯Cl(3), 3.36(1) Å, N(12)-H⋯Cl(3), 3.47(1) Å, N(13)-H⋯Cl(3), 3.36(1) Å, N(13)-H⋯Cl(3), 3.32(1) Å and N(13)-H⋯Cl(4), 3.36(1) Å. The water molecules are also participating in hydrogen bonding interactions.
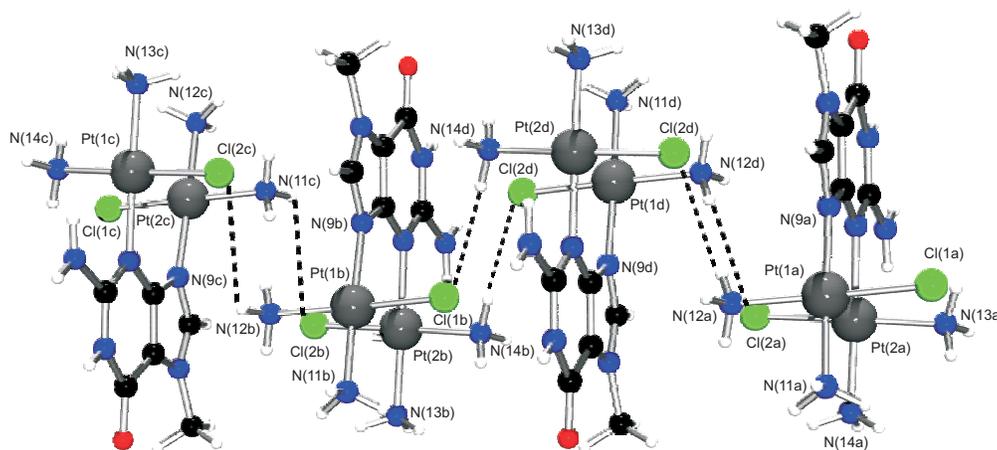
Figure 62 The adjacent complexes are linked via hydrogen bonding in *cis, cis*-[{(NH₃)₂Pt}₂(7-MeGH-*N3,N9*)Cl₂]Cl₂ · 3H₂O (21) to form a zig zag ladder. The water molecules and anions have been omitted for clarity.

2.6.7 Characterization of *cis*-[(NH$_3$)$_2$Pt(7-MeGH-*N9*)$_2$]Cl$_2$ · nH$_2$O (n = 2, 3) (20)

The reaction of 7-MeGH with an excess of *cis*-[(NH$_3$)$_2$Pt^{II}] at 30 °C led to the formation and isolation of the compound **20**. This complex has been characterized by X-ray crystallography. Two crystals have been measured for this complex with a varying number of water molecules, i.e. two and three water molecules. For both the crystals, the molecular geometries of the cations are similar. Figure 63 gives a view of the cation and Table 18 lists selected distances and angles.
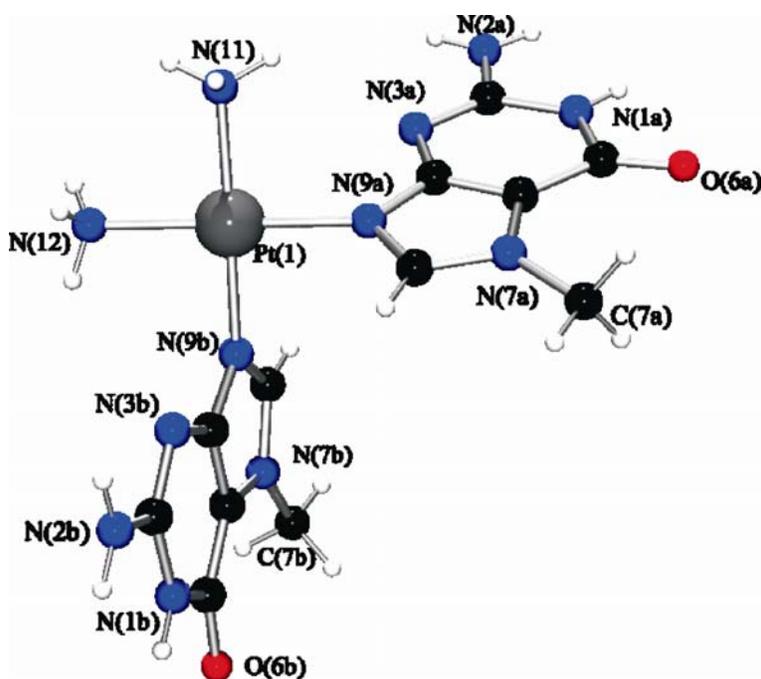
Figure 63 Molecular structure of *cis*-[(NH$_3$)$_2$Pt(7-MeGH-*N9*)$_2$]Cl$_2$ · nH$_2$O (20) with atom numbering scheme. The water molecules and anions have been omitted for clarity.

Pt is bound via the N9 positions of the two purine bases which are oriented in a *head-to-tail* fashion. Pt has square-planar coordination geometry with the angles close to 90°. The Pt-N distances are usual. There are no significant differences in bond lengths and angles within the two purine ligands except for the two internal angles, Pt(1)-N(9)-C(4) and Pt(1)-N(9)-C(8), at N9. For the two ligands, the variations in the internal angles at N9 are about 4°.

Table 18 Selected distances (Å) and angles (º) for *cis*-[(NH$_3$)$_2$Pt(7-MeGH-*N9*)$_2$]Cl$_2$ · nH$_2$O (20)

cis-[(NH$_3$)$_2$Pt(7-MeGH-*N9*)$_2$]Cl$_2$ · nH$_2$O (n = 2, 3) (20)			
Pt(1)-N(11)	2.050(7)	Pt(1)-N(9b)	2.018(6)
Pt(1)-N(12)	2.040(6)	Pt(1)-N(9a)	2.013(7)
Pt(1)N$_4$/9-EtGH(a)	70.2(1)	Pt(1)N$_4$/9-EtGH(b)	74.6(1)
N(11)-Pt(1)-N(12)	88.8(3)	N(12)-Pt(1)-N(9b)	178.9(3)
N(11)-Pt(1)-N(9a)	177.6(3)	N(9a)-Pt(1)-N(9b)	90.5(3)
N(11)-Pt(1)-N(9b)	90.1(3)	Pt(1)-N(9b)-C(4b)	126.2(6)
N(12)-Pt(1)-N(9a)	90.5(3)	Pt(1)-N(9b)-C(8b)	127.8(6)
Pt(1)-N(9a)-C(4a)	130.6(6)	N(1b)-C(2b)-N(3b)	123.5(9)
Pt(1)-N(9a)-C(8a)	123.9(7)	C(4b)-N(9b)-C(8b)	106.0(7)
N(1a)-C(2a)-N(3a)	122.8(1)	C(4a)-N(9a)-C(8a)	105.5(7)

The angles between the Pt coordination plane and the purine bases "a" and "b" are 70.2(1)° and 74.6(1)°, respectively. The *head-to-tail* orientation permits the purine bases of the adjacent complexes to undergo stacking interactions to form a ladder like structure with a mean stacking distance of 3.5 Å. Additionally, the O6 carbonyl oxygen forms an intermolecular hydrogen bond to the NH$_3$ ligand at a distance of 3.07(1) Å. The water molecules and chloride anions are involved in numerous hydrogen bonding interactions with NH$_3$, N1(H) and N(2)H$_2$ groups. None of the contacts (3.0 – 3.4 Å) between heavy atoms is particularly short.

2.6.8 Solution Studies of 20

During the course of the present work, the pK_a values were determined by pH dependent (Figure 64) ^{1}H NMR spectroscopic measurements. Typically, 1:1 reaction mixtures were treated with acid and/or base over a wide pH* range and ^{1}H NMR spectra were recorded. For the complex *cis*-[(NH$_3$)$_2$Pt(7-MeGH-*N9*)$_2$]$^{2+}$, the pK_a values (H$_2$O) are 8.00 ± 0.08 and 1.86 ± 0.45 corresponding to the deprotonations and protonations occurring in two purine bases.[216] At least for the deprotonation of the two guanine ligands, the two steps overlap.
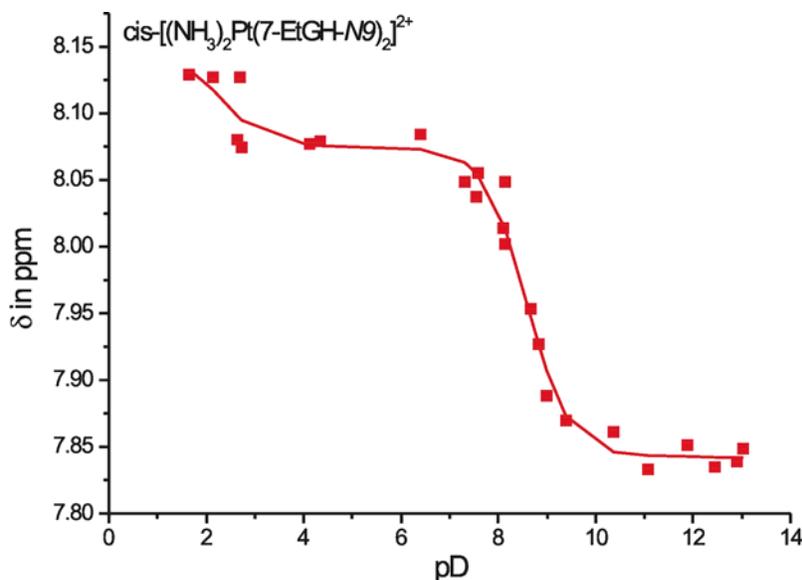
Figure 64 pD dependence (δ, ppm) of H8 proton for *cis*-[(NH$_3$)$_2$Pt(7-MeGH-*N9*)$_2$]$^{2+}$.

2.6.9 Summary

Reactions with [(dien)Pt^{II}] were carried out to study the metal binding behavior of the ligand 7-MeGH. The crystal structure analysis of [(dien)Pt(7-MeGH-*N9*)](NO$_3$)ClO$_4$ **18** is reported. Reactions with *cis*-[(NH$_3$)$_2$Pt^{II}] were carried out in order to synthesize *cis*-[(NH$_3$)$_2$Pt(7-MeGH-*N9*)Cl]Cl on a preparative scale. However, attempts to isolate this compound were unsuccessful. The pK_a values for the complex *cis*-[(NH$_3$)$_2$Pt(7-MeGH-*N9*)$_2$]$^{2+}$ are 8.00 ± 0.08 and 1.86 ± 0.45. The complexes *cis*-[(NH$_3$)$_2$Pt(7-MeGH-*N9*)$_2$]Cl$_2 \cdot$ nH$_2$O (n = 2 or 3) **20** and *cis, cis*-[{(NH$_3$)$_2$Pt}$_2$(7-MeGH-*N3,N9*)Cl$_2$]Cl$_2 \cdot$ 3H$_2$O **21** have been characterized by X-ray crystallography.

3. Summary

The central idea behind the present project was the synthesis of the cationic di-
and trinucleotide analogs with a positively charged Pt^{2+} backbone. The
nucleobases can attach to the metal centers either through

a) N1 (unsubstituted isocytosine base), via

b) N9 (unsubstituted guanine base),

c) N7 (9-EtGH) or

d) N9 (7-MeGH)

These ligands were also studied with regard to the effects of metallation on
hydrogen bonding properties and tautomerism.

Isocytosine exists in solution as two major tautomeric forms **1a** and **1b** with the
N(1) position and the N(3) position carrying the acidic proton, respectively. In the
solid state, both tautomers coexist in a 1:1 ratio. Our results reveal that it is
possible to shift the equilibrium between **1a** and **1b** by adding a co-hydrogen
bonding partner that selectively interacts with one of the two tautomers. The two
tautomers **1a** and **1b** can be individually crystallized in the presence of the
isocytosinium cation and neutral 1-MeC, respectively. In both compounds, the
two partners are involved in triple hydrogen bond formation.
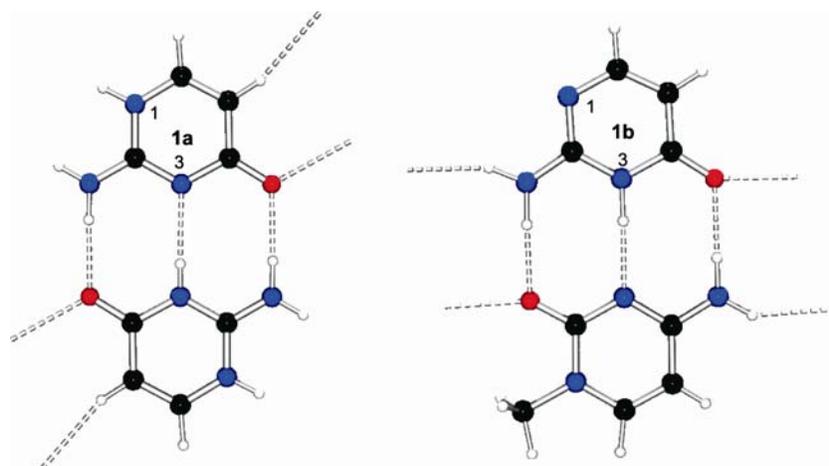
**Figure 65 Individual tautomers 1a and 1b can be cocrystallized in presence of a suitable
hydrogen bonding partner.**

Reactions with a series of Pd^{II} and Pt^{II} am(m)ine entities, (dien)Pd^{II}, (dien)Pt^{II}, *cis*-$(NH_3)_2Pt^{II}$ and *trans*-$(NH_3)_2Pt^{II}$ have been carried out and were followed by ^1H NMR spectroscopy. It was found that these metals have an apparent preference for the N(3) site. The crystal structure analyses of [(dien)Pd(ICH-*N3*)]$(NO_3)_2$ **2** and [(dienM)$_2$(IC-*N1,N3*)]$(ClO_4)_3$ (M = Pd^{II}, **3** and Pt^{II}, **4**) are reported. In strongly acidic medium [(dienPt)$_2$(IC-*N1,N3*)]$^{3+}$ is converted to [(dien)Pt(ICH-*N1*)]$^{2+}$, hence to the Pt^{II} complex of tautomer **1b**.

DFT calculations have been carried out for tautomer compounds of composition [(NH_3)_3Pt(ICH)]$^{2+}$, *cis*- and *trans*-[(NH_3)_2PtCl(ICH)]$^+$, *trans*-[(NH_3)_2Pt(ICH)_2]$^{2+}$, as well as (dien)Pd^{II}, (dien)Pt^{II} and (tmeda)Pt^{II} linkage isomers. Without exception, N(3) linkage isomers are more stable. The experimental results are in agreement with the theoretical calculations. The calculations suggest that the intramolecular hydrogen bonding between the ICH tautomers and the co-ligands at M play an important role. However, it is the inherently stronger M-N3 bond which is the determining factor for the preferential complexation of **1a**. The calculations furthermore show a marked pyramidalization of the NH_2 group of ICH in the complex once the heterocycle forms a dihedral angle < 90° with the metal coordination plane.

[(NH_3)_3Pt(ICH-*N1*)]$^{2+}$ [(NH_3)_3Pt(ICH-*N3*)]$^{2+}$

trans-[(NH_3)_2PtCl(ICH-*N1*)]$^+$ *trans*-[(NH_3)_2PtCl(ICH-*N3*)]$^+$
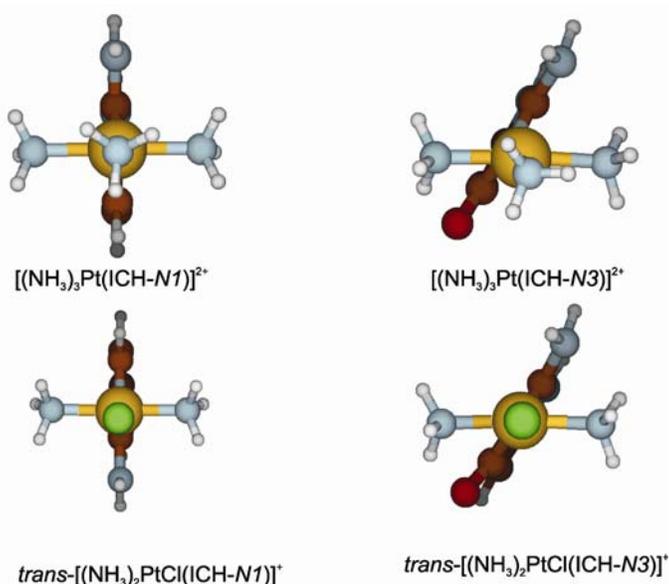
Figure 66 Optimized computed structures of N(1) and N(3) linkage isomers of [(NH_3)_3Pt(ICH)]$^{2+}$ and *trans*-[(NH_3)_2PtCl(ICH)]$^+$.

The low abundance of Pt^{II} and Pd^{II} complexes of isocytosine with N(1) coordination in solution reflects the enormous influence metal coordination can have on the tautomer equilibria. The efforts to coordinate isocytosine at N(1) position by changing the co-ligands at Pt^{II} have likewise not been successful. These findings are in qualitative agreement with the results obtained from the computational studies.

In order to synthesize the metal complexes of guanine with the Pt^{II} entity attached to the N(9) position, at first, it was important to unequivocally establish the metal binding site(s) of guanine. Therefore, (dien)Pt^{II} complexes of unsubstituted guanine were synthesized and individual species have been identified by the pD dependence of the guanine resonances. With (dien)Pt^{II}, the coordination occurs preferentially at the N9 position. The complexes, [(dien)Pt(GH$_2$-*N9*)]Cl(ClO$_4$) **12a**, 2{[(dien)Pt(GH$_2$-*N9*)](ClO$_4$)$_2 \cdot$ 2H$_2$O} **12b** and [(dienPt)$_2$(GH-*N7,N9*)](ClO$_4$)$_3$ **13** have been characterized by X-ray crystallography.

DFT calculations have been carried out for [(dien)Pt(GH$_2$-*N7*)]$^{2+}$, [(dien)Pt(GH$_2$-*N9*)]$^{2+}$ and [(dienPt)$_2$(GH-*N7,N9*)]$^{3+}$. The calculations show that the N(7) linkage isomer is more stable than the N(9) linkage isomer by ΔE = 8.4 kcal/mol. This observation is not in accordance with the experimental results where the preferential coordination site is N9. The reason for the preference of the N(7) linkage isomer might be the intramolecular hydrogen bonding between O(6) and the NH$_2$(dien) ligand.

Using 9-EtGH as a ligand, the complex *trans*-[(NH$_3$)Pt(9-EtGH-*N7*)I$_2$] was synthesized according to the known literature methods. Starting out from *trans*-[(NH$_3$)Pt(9-EtGH-*N7*)I$_2$], a number of reactions have been carried out using three different bridging ligands, ethylenediamine, pyrazine and 4,4'-bipyridine.

The reactions with ethylenediamine were not successful. The reactions with pyrazine were successful as far as the synthesis of the middle part of the artificial

oligonucleotides is concerned. Attempts to prepare and isolate [(NH$_3$)$_5$Pt$_3$(9-EtGH)$_3$(pyrz)$_2$]$^{6+}$ compounds using these middle blocks have till date been unsuccessful. The reactions carried out with 4,4'-bipyridine as a bridging ligand led to the synthesis of the desired product in solution although the isolation of product has not been possible. The complexes *trans*-[(NH$_3$)Pt(9-EtGH-*N7*)(pyrz)$_2$](NO$_3$)$_2$ **16** and *cis*-[(NH$_3$)$_2$Pt(9-EtGH-*N7*)$_2$](NO$_3$)$_2$ **19** have been characterized by X-ray crystallography.

The metal binding behavior of 7-MeGH has been studied using (dien)Pt^{II} and *cis*-[(NH$_3$)$_2$Pt^{II}]. Attempts have been made to obtain the 1:1 *cis*-[(NH$_3$)$_2$Pt(7-MeGH-*N9*)Cl]Cl on a preparative scale. However, it has not been possible to isolate this compound. The crystal structure analyses of [(dien)Pt(7-MeGH-*N9*)](NO$_3$)(ClO$_4$) **18**, *cis*-[(NH$_3$)$_2$Pt(7-MeGH-*N9*)$_2$]Cl$_2$ · nH$_2$O (n = 2 or 3) **20** and *cis, cis*-[{(NH$_3$)$_2$Pt}$_2$(7-MeGH-*N3*,*N9*)Cl$_2$]Cl$_2$ · 3H$_2$O **21** are reported.

The (dien)M^{II} (M = Pd and Pt) complexes of 1-MeIC were also synthesized and it was found that under alkaline conditions, [(dien)Pt(1-MeIC-*N3*)]$^{2+}$ undergoes deamination to give the corresponding complex [(dien)Pt(1-MeU-*N3*)]$^{2+}$. The 1-MeICH$^+$ **9**, [(dien)Pd(1-MeIC-*N3*)](ClO$_4$)$_2$ **10** and [(dien)Pt(1-MeIC-*N3*)](ClO$_4$)$_2$ **11** were characterized by X-ray crystallography.

4. Zusammenfassung

Die zentrale Idee hinter dem aktuellen Projekt war die Synthese kationischer Di-
und Trinukleotik-Analoga mit einem positiv geladenen Pt^{2+}-Rückgrat. Die
Nukleobasen können hierbei entweder über

a) N1 (unsubstituiertes Isocytosin),

b) N9 (unsubstituiertes Guanin),

c) N7 (9-EtGH) oder über

d) N9 (7-MeGH)

an das Metall koordinieren. Diese Liganden wurden auch mit Hinblick auf die
Einflüsse ihrer Metallierung auf ihre Wasserstoffbrückenbindungseigenschaften
sowie ihre Tautomerisierung untersucht.

Isocytosin existiert in Lösung in zwei tautomeren Formen **1a** und **1b**, in denen
N(1) oder N(3) das saure Proton trägt. Im Festkörper liegen beide Tautomere im
Verhältnis 1:1 vor. Unsere Ergebnisse zeigen, dass es möglich ist, das
Gleichgewicht zwischen den Tautomeren durch Zufügen selektiv
wechselwirkender Wasserstoffbrückenbindungspartner zu verschieben. Die
beiden Tautomere **1a** und **1b** können mit Isocytosinium und 1-MeC getrennt
voneinander kokristallisiert werden. In beiden Festkörperstrukturen liegen
zwischen den beiden beteiligten Molekülen jeweils drei Wasserstoffbrücken vor.
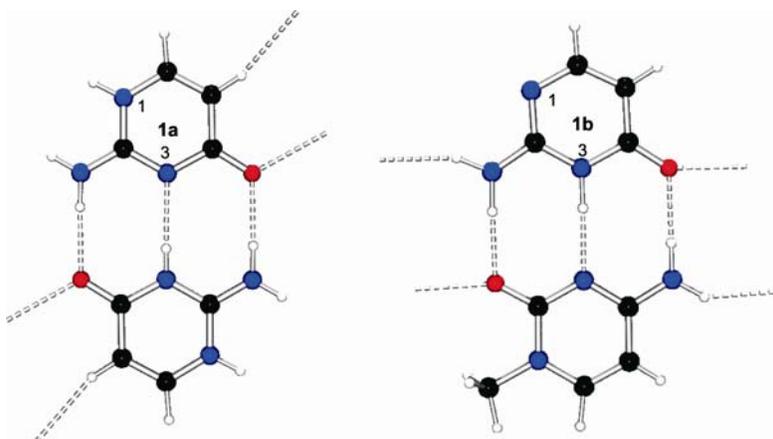
**Abbildung 1 Die zwei Tautomere 1a und 1b können einzeln in Gegenwart eines geeigneten
Wasserstoff-brückenbindungs partners kokristallisiert werden.**

Reaktionen dieser Liganden mit einer Reihe von Pd[II] und Pt[II] Am(m)in-Komplexen, (dien)Pd[II], (dien)Pt[II], *cis*-$(NH_3)_2$Pt[II] und *trans*-$(NH_3)_2$Pt[II] wurden ^{1}H-NMR-spektroskopisch untersucht. Es zeigte sich, dass diese Metalle eine Koordination an N(3) bevorzugen. Die Kristallstrukturen von [(dien)Pd(ICH-*N3*)]$(NO_3)_2$ **2** und [(dienM)$_2$(IC-*N1*,*N3*)]$(ClO_4)_3$ (M = Pd[II], **3** und Pt[II], **4**) werden beschrieben. In stark saurem Medium reagiert [(dienPt)$_2$(IC-*N1*,*N3*)]$^{3+}$ zu [(dien)Pt(ICH-*N1*)]$^{2+}$, also zum Pt[II] Komplex des Tautomers **1b**.

DFT-Berechnungen wurden für [$(NH_3)_3$Pt(ICH)]$^{2+}$, *cis*- und *trans*-[$(NH_3)_2$PtCl(ICH)]$^{+}$, *trans*-[$(NH_3)_2$Pt(ICH)$_2$]$^{2+}$ und für bindungsisomeren ICH-komplexe mit, (dien)Pd[II], (dien)Pt[II] und (tmeda)Pt[II] ausgeführt. In allen Fällen war die Koordination an N(3) gegenüber N(1) energetisch bevorzugt. Die experimentellen Ergebnisse unterstützen die theoretischen Befunde. Die Berechnungen legen nahe, dass dieser Befund vor allem durch die energetische Bevorzugung der Metall-N3-Bindung gegenüber der Metall-N1-Bindung hervorgerufen wird. Intramolekulare Wasserstoffbrücken zwischen den Coliganden am Metall und dem ICH-Tautomer unterstützen diesen Effekt zusätzlich. Die Berechnungen zeigen außerdem eine deutliche Pyramidalisierung der exozyklischen NH_2-Gruppe an, sobald die Nukleobase einen Diederwinkel < 90° zur Koordinationsebene des Metalls einnimmt.
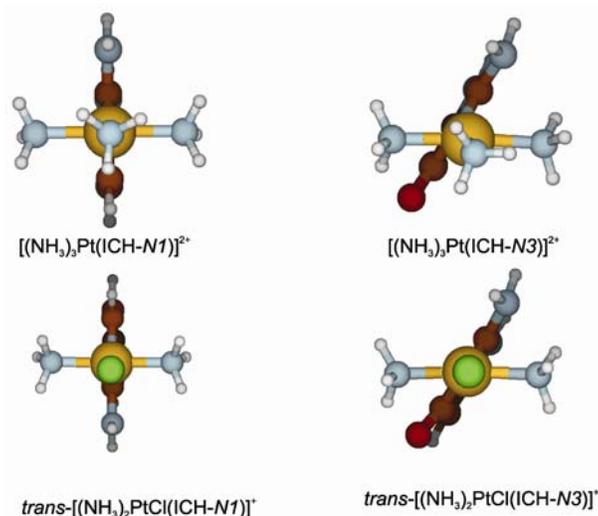
Abbildung 2 Optimierte berechnete Strukturende N(1) und N(3)-Bindungsisomere von [$(NH_3)_3$Pt(ICH)]$^{2+}$ und *trans*-[$(NH_3)_2$PtCl(ICH)]$^{+}$.

Das geringe Vorkommen der Pt^{II} und Pd^{II} Komplexe des Isocytosins mit einer koordinativen Bindung über N(1) in Lösung belegt den enormen Einfluss, den Metallkoordination auf Tautomeren-Gleichgewichte haben kann. Demgemäß waren die Bemühungen, durch Variation der Coliganden am Pt^{II} das Isocytosin über N(1) zu koordinieren, nicht erfolgreich. Dies kann als Bestätigung der theoretischen Berechnungen aufgefasst werden.

Um Metallkomplexe des Pt^{II} mit Guanin über dessen N(9) Position zu synthetisieren, war es zunächst erforderlich, die bevorzugte Koordination des Guanins zu ermitteln. Dazu wurden $(dien)Pt^{II}$ Komplexe des unsubstituierten Guanins dargestellt und einzelne Spezies dann über die pH-Abhängigkeit ihrer ^{1}H-NMR-Resonanzen identifiziert. $(dien)Pt^{II}$ koordiniert bevorzugt an N(9) des Guanins. Die Komplexe [(dien)Pt(GH$_2$-*N9*)]Cl(ClO$_4$) **12a**, 2{[(dien)Pt(GH$_2$-*N9*)](ClO$_4$)$_2$ · 2H$_2$O} **12b** und [(dienPt)$_2$(GH-*N7,N9*)](ClO$_4$)$_3$ **13** wurden kristallographisch charakterisiert.

DFT-Berechnungen wurden für [(dien)Pt(GH$_2$-*N7*)]$^{2+}$, [(dien)Pt(GH$_2$-*N9*)]$^{2+}$ und [(dienPt)$_2$(GH-*N7,N9*)]$^{3+}$ durchgeführt. Die Rechnungen zeigen, dass der über N(7)-koordinierende Komplex um $\Delta E = 8,4$ kcal/mol stabiler ist als das N(9)-Bindungsisomer. Dieser Befund steht nicht im Einklang mit den experimentellen Befunden, wonach das N(9)-Bindungsisomer bevorzugt ist. Als Grund für die Bevorzugung der N(7)-Position in der Gasphase ist die intramolekulare Wasserstoffbrücke zwischen O(6) und der NH$_2$(dien)-Gruppe des Coliganden zu betrachten.

Mit 9-EtGH als Ligand wurde der Komplex *trans*-[(NH$_3$)Pt(9-EtGH-*N7*)I$_2$] entsprechend der in der Literatur bekannten Methoden dargestellt. Ausgehend von *trans*-[(NH$_3$)Pt(9-EtGH-*N7*)I$_2$] wurden drei verschiedene verbrückende Liganden untersucht: Ethylendiamin, Pyrazin und 4,4'-Bipyridin.

Die Umsetzungen mit Ethylendiamin waren nicht erfolgreich; mit Pyrazin waren sie nur im Hinblick auf die Synthese des Mittelstücks der künstlichen

Oligonukleotide erfolgreich. Versuche, $[(NH_3)_5Pt_3(9-EtGH)_3(pyrz)_2]^{6+}$ mit diesem „Mittelteil" zu synthetisieren und zu isolieren, sind bis heute fehlgeschlagen. Die Umsetzungen mit 4,4'-Bipyridin als verbrückendem Liganden führten zur Synthese des Zielproduktes in Lösung, aber dessen Isolierung gelang bis heute nicht erfolgreich. Die Komplexe *trans*-$[(NH_3)Pt(9-EtGH-N7)(pyrz)_2](NO_3)_2$ **16** und *cis*-$[(NH_3)_2Pt(9-EtGH-N7)_2](NO_3)_2$ **19** konnten kristallographisch charakterisiert werden.

Das Metallbindungsverhalten von 7-MeGH wurde an (dien)Pt^{II} und *cis*-$[(NH_3)_2Pt^{II}]$ untersucht. Dabei wurde versucht, den 1:1 Komplex *cis*-$[(NH_3)_2Pt(7-MeGH-N9)Cl]Cl$ im präparativen Maßstab zu isolieren. Dies gelang allerdings nicht. Die Kristallstrukturen von $[(dien)Pt(7-MeGH-N9)](NO_3)(ClO_4)$ **18**, *cis*-$[(NH_3)_2Pt(7-MeGH-N9)_2]Cl_2 \cdot nH_2O$ (n = 2 oder 3) **20** und *cis, cis*-$[\{(NH_3)_2Pt\}_2(7-MeGH-N3,N9)Cl_2]Cl_2 \cdot 3H_2O$ **21** werden beschrieben.

(dien)M^{II} (M = Pd und Pt) Komplexe von 1-MeIC wurden synthetisiert und es wurde gefunden, dass $[(dien)Pt(1-MeIC-N3)]^{2+}$ unter alkalischen Bedingungen desaminiert wird und $[(dien)Pt(1-MeU-N3)]^{2+}$ bildet. 1-MeICH$^+$ **9**, $[(dien)Pd(1-MeIC-N3)](ClO_4)_2$ **10** und $[(dien)Pt(1-MeIC-N3)](ClO_4)_2$ **11** konnten kristallographisch charakterisiert werden.

5. Experimental Section

5.1 Materials

Isocytosine (ICH), pyrazine and 4,4'-bipyridine were purchased from Sigma; K_2PtCl_4 and K_2PdCl_4 from Heraeus; guanosine from Sigma-Aldrich; guanine from Merck; 9-MeGH, 9-EtGH and 7-MeGH from Prof. W. Pfleiderer, Fa. Chemogen, Konstanz; [(dien)PtI]I[217], [(dien)PdI]I[105], *trans*-[(NH$_3$)$_2$PtCl$_2$][218], *cis*-[(NH$_3$)$_2$PtCl$_2$][218], 1-methylcytosine (1-MeC)[150], 1-methylthymine (1-MeT)[219] and the complexes, *trans*-[(NH$_3$)$_2$Pt(9-EtGH-*N7*)Cl]Cl[187,220], *trans*-[(NH$_3$)$_2$Pt(1-MeC)Cl]Cl[221], *cis*-[(NH$_3$)$_2$Pt(1-MeC)Cl]Cl[222] and *trans*-[(NH$_3$)$_2$Pt(1-MeT)Cl][223] were prepared according to the methods given in the literature; [(dien)PdBr]Br[105] was prepared in an analogous manner as [(dien)PdI]I. Deuterated solvents DMSO-*d$_6$*, D_2O were obtained from Deutero GmbH, Kastellaun (Germany).

5.2 Instrumentation and Measurements

5.2.1 NMR-Spectroscopy

^{1}H NMR Spectra were recorded on Varian FT-NMR Mercury 200 (200.13 MHz), and DRX 400 (400.13 MHz) instruments at 23 °C. In D_2O, spectra were measured with presaturation of the water resonance using sodium-3-(trimethylsilyl)propanesulfonate (TSP, δ = 0 ppm) as internal reference.

Spectra in DMSO-*d$_6$* were recorded without the presaturation of the water signal using the resonance of DMSO-*d$_5$* (δ = 2.50 ppm relative to tetramethylsilane (TMS)) as reference. DMSO-*d$_6$* was dried over 4-Å-molecular sieves for a week before use or a freshly opened bottle was used.

5.2.2 Vibrational Spectra

Infrared spectra (KBr pellets) were recorded on a Bruker IFS 28 FT spectrometer in the region between 4000 cm^{-1} to 250 cm^{-1}.

Raman spectra were recorded on a Coderg T800 with Ar^+-Laser (514.5 nm) or Kr^+-Laser (647.1 nm) excitation.

5.2.3 Elemental Analysis

Elemental analysis (C H N) was performed with a Leco Elemental Analyzer CHNS-932.

5.2.4 pK_a values

pH* values refer to uncorrected pH meter readings (Metrohm 6321; combination glass electrode) in D_2O solutions. pH* values were adjusted by addition of DNO_3 or NaOD solutions; pD values were obtained by adding 0.4 to the uncorrected pH meter reading. The pK_a values were determined using pH dependent ^1H NMR spectroscopic measurements in D_2O. pK_a values were evaluated with a Newton-Gauss[224] non-linear least-squares fit method that deals with the changes in chemical shifts of all non-exchangeable protons with the change in pD of the solution. The obtained acidity constants were then transformed to the values valid for H_2O according to the literature.[225]

5.2.5 Computational Details

The *ab initio* molecular orbital calculations were performed using the *Gaussian* 98 package.[226] A combination of Becke's three-parameter hybrid functional[101] with Lee-Yang-Parr's exchange functional[102,103] was applied for all structures. The structures of the two tautomers were optimized using two different basis sets LANL2DZ and 6-31+G*. The metals in the Pd and Pt complexes have been described with the LANL2DZ basis set, including effective core potentials, while the 6-31G* basis set has been used for C, N, O, and H atoms. Additionally, the wave functions were analyzed by the natural bond orbital (NBO) method,[116] a standard option of *Gaussian* 98. The NBO analysis explains the strength of hydrogen bonds in terms of donor-acceptor interactions between doubly occupied lone pair orbitals and unoccupied antibond orbitals. The total energy was calculated as the sum of the electronic energy and the zero-point vibrational

energy. Vibrational frequency calculations were carried out to ensure that the stationary points located on the potential energy surfaces by geometry optimization were minima.

5.2.6 X-ray Crystallography

X-ray intensity data were collected at room temperature or at 120 K for compounds on an Enraf-Nonius-KappaCCD diffractometer[227] using graphite-monochromated Mo Kα radiation (λ = 0.7107 Å). None of the crystals showed evidence of crystal decay during data collection. For data reduction and cell refinement, the programs DENZO and SCALEPACK (Nonius, 2000)[228] were used. Corrections for incident and diffracted beam absorption effects were applied using SADABS. The structures were solved by either conventional direct or Patterson methods and subsequent Fourier syntheses and refined by full-matrix least squares on *F*2 using the SHELXTL 5.1 program.[229] Hydrogen atoms were either located in a difference Fourier map and refined isotropically or were fixed in idealized positions and allowed to ride on the atom to which they were attached. Hydrogen atom thermal parameters were tied to those of the atom to which they were attached. Except for the disordered atoms, all non-hydrogen atoms in the structures were refined anisotropically. Crystallographic data and details of refinement are reported in X-ray Tables (ref. Appendix).

5.3   Syntheses of Complexes

5.3.1 [(dien)PdBr]Br (1)

A reaction mixture containing 5.0 g (28 mmol) of $PdCl_2$, 5.0 g (24 mmol) of dien·3HCl in 100 ml of water was refluxed for 8 h. An orange solution formed and some deposition of metallic palladium was observed. The solution was filtered and the filtrate was concentrated to a volume of 30 ml. LiBr (4.3 g, 50 mmol) was added to the concentrated solution to isolate [(dien)PdBr]Br. Yellow crystals of [(dien)PdBr]Br were isolated and characterized by X-ray crystallography. Yield 65%.

Elemental analysis (%) for $C_4N_3H_{13}Br_2Pd$ (369.4): C 13.0, H 3.5, N 11.4; found: C 13.1, H 3.5, N 11.4. IR ($\tilde{v}$ cm^{-1}): 3204 (s), 3127 (s), 3056 (s), 1591 (s), 1448 (m), 1384 (m), 1144 (s), 1084 (s), 1050 (s), 991 (w), 926 (w). ^{1}H NMR (200 MHz, D_2O): δ = 3.35 – 2.90 ppm (m; dien).

5.3.2   [(dien)Pd(ICH-*N3*)](NO$_3$)$_2$ (2)

A suspension of [(dien)PdBr]Br (79.8 mg, 0.22 mmol) in water (10 ml) was treated with AgNO$_3$ (73.4 mg, 0.43 mmol) for 5 h at 40 $^\circ$C with the exclusion of daylight. The solution was then cooled to room temperature, AgI was filtered off, and isocytosine (314.0 mg, 0.22 mmol) was added. The mixture was again stirred for 5 h at 40 $^\circ$C and kept for crystallization. Yellow crystals appeared after few weeks, which were later dried in air. A single crystal was picked and characterized by X-ray crystallography. Yield 20%.

Elemental analysis (%) for $C_8H_{18}N_8O_7Pd \cdot H_2O$ (462.7): C 20.7, H 4.4, N 24.2; found: C 20.2, H 4.2, N 24.0. No water was detected in the X-ray crystal structure, however. ^{1}H NMR spectra were recorded in D_2O and it was found that there was an immediate equilibration of the compound in solution to give four sets of resonances. ^{1}H NMR (200 MHz, D_2O, pD = 4.4): δ = 7.84 (d; ^3J = 7.6 Hz; H6), 7.69 (d; ^3J = 7.0 Hz; H6), 7.61 (d; ^3J = 7.8 Hz; H6), 7.48 (d; ^3J = 7.4 Hz; H6), 5.93 (d; ^3J = 7.8 Hz; H5), 5.91 (d; ^3J = 7.6 Hz; H5), 5.87 (d; ^3J = 7.4 Hz; H5), 5.73 (d; ^3J = 7.0 Hz; H5), 3.30 – 2.90 ppm (m; dien). IR ($\tilde{v}$ cm^{-1}): 3407 (s), 3135 (br), 1664 (s), 1606 (s, sh), 1381 (w, sh), 824 (s). Raman ($\tilde{v}$ cm^{-1}): 1230(3), 1045(10), 1039(8), 798(7), 612(4), 572(1), 546(2).

5.3.3   [(dienPt)$_2$(IC-*N1,N3*)](ClO$_4$)$_3$ · 2H$_2$O (3)

A suspension of [(dien)PtI]I (155.1 mg, 0.14 mmol) in D_2O (3 ml) was treated with AgClO$_4$ (95.5 mg, 0.28 mmol) for 5 h at 40 $^\circ$C with the exclusion of daylight. The solution was then cooled to room temperature, AgI filtered off, and divided into two parts. Isocytosine (7.7 mg, 0.22 mmol) was added to the first part of the solution. The mixture was again stirred for 5 h at 40 $^\circ$C. pD of the solution was

later adjusted to 5.6 and 100 µL of $[(dien)Pt(D_2O)]^{2+}$ solution was added to the mixture solution. The progress of the reaction was monitored by ^1H NMR spectroscopy. This procedure was repeated until only a single set of signals due to $[(dienPt)_2(IC-\textit{N1,N3})](ClO_4)_3$ was present. Colorless crystals were formed in the reaction mixture within 2 days at 3 °C. A single crystal was picked and characterized by X-ray crystallography. Yield 40%.

Elemental analysis (%) for $C_{12}H_{30}N_9O_{13}Pt_2Cl_3 \cdot 2H_2O$ (1040.97): C 13.9, H 3.3, N 12.1; found: C 13.7, H 3.2, N 12.1. ^1H NMR (200 MHz, D_2O, pD = 6.24): δ = 7.73 (d; ^3J = 7.0 Hz; H6), 5.77 (d; ^3J = 7.0 Hz; H5), 3.30 – 2.90 ppm (m; dien). IR ($\tilde{\nu}$ cm^{-1}): 3410 (s, br), 3271 (m, sh), 1633 (s, sh), 1563 (m), 1458 (s), 1409 (s), 1304 (s), 843 (m). Raman ($\tilde{\nu}$ cm^{-1}): 1496(3), 1409(1), 1235(8), 934(10), 801(7).

5.3.4 $[(dienPd)_2(IC-\textit{N1,N3})](ClO_4)_3$ (4)

A suspension of $[(dien)PdBr]Br$ (50.0 mg, 0.14 mmol) in D_2O (1.0 ml) was treated with $AgClO_4$ (55.7 mg, 0.27 mmol) for 5 h at 40 °C with the exclusion of daylight. The solution was then cooled to room temperature, AgBr filtered off, and divided into two parts. Isocytosine (7.5 mg, 0.07 mmol) was added to the first part of the solution. The mixture was again stirred for 5 h at 40 °C. pD of the solution was later adjusted to 7.6 and 150 µL of $[(dien)Pd(D_2O)]^{2+}$ solution was added to the mixture. The progress of the reaction was monitored by ^1H NMR spectroscopy. This procedure was repeated until only a single set of signals due to $[(dienPd)_2(IC-\textit{N1,N3})](ClO_4)_3$ was present. Yellow crystals were formed in the reaction mixture within 1 day at 3 °C. A single crystal was picked and characterized by X-ray crystallography. Yield 45%.

Elemental analysis (%) for $C_{12}H_{30}N_9O_{13}Pd_2Cl_3$ (827.62): C 17.4, H 3.7, N 15.2; found: C 17.4, H 3.5, N 15.1. Two molecules of water were detected in the X-ray crystal structure, however. ^1H NMR (200 MHz, D_2O, pD = 6.42): δ = 7.70 (d; ^3J = 7.0 Hz; H6), 5.73 (d; ^3J = 7.0 Hz; H5), 3.35 – 2.90 ppm (m; dien). IR ($\tilde{\nu}$ cm^{-1}):

3400 (s, br), 3266 (m, sh), 1620 (s, sh), 1563 (s), 1450 (m), 1400 (m), 1300 (s), 840(w). Raman ($\tilde{v}$ cm^{-1}): 1409(2), 1237(8), 955(2), 936(10), 801(5), 455(7).

5.3.5   [(dien)Pt(ICH-*N1*)]$^{2+}$ (5a) and [(dien)PtCl]ClO$_4$ (5b)

[(dienPt)$_2$(IC-*N1, N3*)](ClO$_4$)$_3$ was dissolved in D$_2$O and the pD of the solution was adjusted to 1.2 by addition of DCl. The progress of the reaction was monitored by ^{1}H NMR spectroscopy. A new set of resonances started to appear immediately after addition of DCl. The solution was then heated at 40 °C for four hours. With time, the signals for the dinuclear complex disappeared and a single set of resonances was present. This set of resonances was assigned to the N(1) linkage isomer on the basis of a pD-dependence. Furthermore, ^{195}Pt satellites are present for the H6 proton of the ICH ligand. Till date, it has not been possible to isolate the compound from solution. From the reaction mixture, colorless crystals were picked but X-ray crystallography revealed that the crystals were the compound [(dien)PtCl]ClO$_4$ **5b**.

^{1}H NMR for **5a** (200 MHz, D$_2$O, pD = 1.41): δ = 7.87 (d; ^3J = 7.6 Hz; H6), 5.90 (d; ^3J = 7.6 Hz; H5), 3.33 – 2.90 ppm (m; dien).

Elemental analysis (%) for **5b** C$_4$H$_{13}$N$_3$O$_4$PtCl$_2$ · H$_2$O (451.17): C 10.6, H 3.4, N 9.3; found: C 10.9, H 3.7, N 9.8. No water molecule was detected in the crystal structure, however.

5.3.6   ICH · (1-MeC) · 2H$_2$O (6)

1-MeC (50.0 mg, 0.40 mmol) and ICH (44.4 mg, 0.40 mmol) were dissolved in a minimum amount of water. The solution was warmed at 30 °C until a clear solution was obtained. The solution was concentrated on a water bath and kept for crystallization in air. Colorless crystals appeared after one week. A single crystal was picked and characterized by X-ray crystallography.

Elemental analysis (%) for $C_9H_{12}N_6O_2$ (anhydrous sample): C 45.7, H 5.1, N 35.6; found: C 45.5, H 5.0, N 35.2. Raman ($\tilde{v}$ cm^{-1}): 1263(8), 1216(2), 781(6), 774(10), 629(6).

5.3.7 [ICH · ICH$_2$]NO$_3$ (7)

ICH (50.0 mg, 0.45 mmol) was dissolved in water and pH* of the solution was adjusted to 4.3 with the addition of HNO_3. Colorless crystals were isolated and characterized by X-ray crystallography.

Elemental analysis (%) for $C_8H_{11}N_7O_5$ (285.24): C 33.7, H 3.8, N 34.7; found: C 34.0, H 3.8, N 35.0. Raman ($\tilde{v}$ cm^{-1}): 1231(5), 1209(5), 1046(4), 1038(3), 796(10), 790(5).

5.3.8 1-MeIC (8)

4.0 g (0.04 mol) of isocytosine, 70.0 ml of hexamethyldisilazane (HMDS) and 5.8 ml of trimethylchlorosilane (TMCS) were added to a 250 ml round-bottom flask. The mixture was stirred and refluxed at 140 °C with until the solution became transparent. The reaction mixture was cooled to 40 °C and 28 ml of methyliodide (CH_3I) was slowly added to the flask. The solution was again heated to reflux at 80 °C, with stirring, overnight. The reaction mixture was treated with 230 ml of 6N acetic acid at room temperature to hydrolyze the trimethylsilyl protecting group. The solution was evaporated to dryness under reduced pressure to yield a crude slightly yellow product. The crude product was washed with a large amount of water and redissolved in ethanol, kept at 4 °C for a day. White crystalline product precipitated out of the solution which was later purified over the sephadex G25 column. Yield 60%.

Elemental analysis (%) for $C_5H_7N_3O$ (125.10): C 48.0, H 5.6, N 33.6; found: C 47.5, H 5.7, N 33.6. ^{1}H NMR (200 MHz, D_2O, pD = 4.0): δ = 7.56 (d; H6), 5.98 (d; H5), 3.53 ppm (s; CH$_3$). Raman ($\tilde{v}$ cm^{-1}): 1451(1), 1408(1), 1289(8), 982(1), 972(1), 796(10), 615(2), 552(1).

5.3.9 [1-MeICH](NO$_3$)$_3$(ClO$_4$) (9)

20.2 mg (0.16 mmol) of 1-methylisocytosine was dissolved in 2 ml of H$_2$O and pH of the solution was adjusted with the help of HNO$_3$, HClO$_4$ and NaOH to 4.5 (pK_a value of 1-methylisocytoine). Colorless crystals appeared after a few days which were characterized by X-ray crystallography.

Elemental analysis (%) for C$_{20}$H$_{32}$N$_{15}$O$_{17}$Cl (790.01): C 30.4, H 4.1, N 26.6; found: C 30.0, H 4.0, N 27.0. Raman ($\tilde{v}$ cm^{-1}): 1508(9), 1473(1), 1290(1), 1272(6), 1249(6), 1207(1), 1047(10), 798(5), 790(8), 772(7), 719(1), 623(1), 607(3), 555(3), 547(4).

5.3.10 [(dien)Pd(1-MeIC-*N3*)](ClO$_4$)$_2$ (10)

To a suspension of **1** (25.0 mg, 0.07 mol) in 1 ml of water, AgClO$_4$ was added. The reaction mixture was stirred at 40 °C with the exclusion of daylight for 4 h and AgBr was filtered off. To the clear solution, 1-methylisocytosine (4.2 mg, 0.03 mmol) was added and the reaction mixture was stirred at 40 °C for few hours. The solution was rotary-evaporated to near dryness. The residue was redissolved in a minimum quantity of water. Pale yellow crystals appeared at 4 °C after one day, which were later dried under vacuum. A single crystal was picked and characterized by X-ray crystallography. Yield 75%.

Elemental analysis (%) for C$_9$H$_{20}$N$_6$O$_9$PdCl$_2$ (533.6): C 20.3, H 3.8, N 15.7; found: C 20.0, H 3.5, N 15.5. ^{1}H NMR (200 MHz, D$_2$O, pD = 2.0): δ = 7.49 (d; ^3J = 7.6 Hz; H6), 5.90 (d; ^3J = 7.6 Hz; H5), 3.52 (s, CH$_3$), 3.35 – 2.90 ppm (m; dien). Raman ($\tilde{v}$ cm^{-1}): 1464(1), 1273(1), 935(10), 840(1), 791(3), 633(2), 576(4).

5.3.11 [(dien)Pt(1-MeIC-*N3*)](ClO$_4$)$_2$ (11)

Addition of AgClO$_4$ (71.6 mg, 0.36 mmol) to a suspension of [(dien)PtI]I (100.4 mg, 0.180 mmol) in 5 ml of water resulted in the immediate precipitation of AgI. The mixture was stirred at 40 °C with the exclusion of daylight for 4 h and AgI was filtered off. To the clear solution, 1-methylisocytosine (22.0 mg, 0.18 mmol)

was added and the reaction mixture was stirred at 40 $^\circ$C for 2 days. The solution was evaporated at room temperature to a volume of 2.0 ml. Colorless crystals appeared at 4 $^\circ$C after a few days, which were later dried under vacuum. A single crystal was picked and characterized by X-ray crystallography. Yield 65%.

Elemental analysis (%) for $C_9H_{20}N_6O_9PtCl_2$ (622.3): C 17.4, H 3.2, N 13.5; found: C 17.0, H 3.2, N 13.1. ^{1}H NMR (200 MHz, D_2O, pD = 6.2): δ = 7.73 (d; ^3J = 7.6 Hz; H6), 5.77 (d; ^3J = 7.6 Hz; H5), 3.59 (s, CH_3), 3.35 – 2.90 ppm (m; dien). Raman ($\tilde{v}$ cm^{-1}): 1464(1), 1408(1), 1264(8), 933(10), 811(2), 790(3), 634(2), 546(4).

5.3.12 [(dien)Pt(GH$_2$-*N9*)](Cl)ClO$_4$ (12a) and 2{[(dien)Pt(GH$_2$-*N9*)](ClO$_4$)$_2$ · 2H$_2$O} (12b)

A suspension of [(dien)PtI]I (276.0 mg, 0.50 mmol) in H_2O (13 ml) was treated with $AgClO_4$ (221.0 mg, 0.98 mmol) for 5 h at 40 $^\circ$C with the exclusion of daylight. The mixture was then cooled to room temperature and AgI was filtered off. pH of the solution was adjusted to 4.1 with the addition of 0.1 M NaOH or 0.01 M HCl and 72.0 mg (0.48 mmol) guanine was added. The reaction mixture was stirred at 40 $^\circ$C for 8 h. Excess guanine was removed by filtration. The solution was rotary-evaporated to dryness. The residue was dissolved in 1:1 solution of $CH_3OH:H_2O$. Very fine, colorless crystals appeared after 2 days at 3 $^\circ$C. A single crystal was picked and characterized by X-ray crystallography. Yield 15%.

Elemental analysis (%) for **12b** $C_9H_{18}N_8O_9Cl_2Pt$ (648.28): C 16.7, H 2.8, N 17.3; found: C 16.6, H 2.7, N 17.3. Four water molecules were detected in the crystal structure, however. ^{1}H NMR (200 MHz, D_2O, pD = 3.3): δ = 8.15 (s; H8), 3.35 - 2.90 ppm (m; dien).

5.3.13 [(dienPt)$_2$(GH-*N7,N9*)](ClO$_4$)$_3$ (13)

A suspension of [(dien)PtI]I (845.0 mg, 1.53 mmol) in H_2O (20 ml) was treated with $AgClO_4$ (671.0 mg, 2.98 mmol) for 5 h at 40 $^\circ$C with the exclusion of daylight.

The reaction mixture was then cooled to room temperature and AgI was filtered off. 116.0 mg (0.77 mmol) guanine was added and pH of the solution was adjusted to 10.0 with the addition of 0.1 M NaOH. The solution was stirred at 40 °C for 8 h. Excess guanine was removed by filtration. The solution was rotary-evaporated to a volume of 10.0 ml. Yield 250 mg. Colorless crystals appeared within 2 days at 3 °C, which were later air dried. A single crystal was picked and characterized by X-ray crystallography.

Elemental analysis (%) for $C_{13}H_{30}N_{11}OPt_2 \cdot 2.5ClO_4$ (995.24): C 15.7, H 3.0, N 15.5; found: C 15.7, H 3.0, N 15.4. The compound was isolated at basic pH hence, deprotonation at N(1) position might have led to formation of an associated structure. ^{1}H NMR (200 MHz, D_2O, pD = 10.4): δ = 7.47 (s; H8), 3.35 – 2.90 ppm (m; dien). ^{1}H NMR (200 MHz, DMSO-d_6): δ = 11.18 (s, N(1)H), 7.67 (s; H8), 7.21 (s, dien(NH)), 6.45 (s, NH_2), 5.89 (s, dien-NH_2), 3.11 – 2.78 (m, dien).

5.3.14 cis-[(NH$_3$)$_2$Pt(9-EtGH-N7)Cl]Cl (14)

A solution of cis-[(NH$_3$)$_2$PtCl$_2$] (900.0 mg, 3.0 mmol) and 9-EtGH (537.0 mg, 3.0 mmol) in 45 ml of water was stirred at 40 °C for 48 h. The reaction mixture was cooled to room temperature and a yellow-white precipitate was filtered. The precipitate was washed with 3 ml of DMF to remove the yellow component. The white residue was dried in air. Yield 65%.

Elemental analysis (%) for $C_7H_{15}N_7OPtCl_2$ (479.2): C 17.7, H 3.3, N 20.3; found: C 17.3, H 3.2, N 20.3. ^{1}H NMR (200 MHz, D_2O, pD = 6.6): δ = 8.24 (s; H8), 4.14 (q; methylene), 1.43 ppm (t, CH_3). ^{1}H NMR (200 MHz, DMSO-d_6): δ = 10.90 (s, N(1)H), 8.37 (s; H8), 6.92 (s, NH_2), 4.59 (s, Pt-NH_3), 4.27 (s, Pt-NH_3), 4.10 (q, methylene), 1.33 ppm (t, CH_3). IR ($\tilde{v}$ cm^{-1}): 349 [ν(Pt-Cl)].

5.3.15 *trans*-[(NH₃)Pt(9-EtGH-*N7*)I₂] (15)

To a suspension of **14** (150.0 mg, 0.31 mmol) in 150 ml of water was added KI (208.0 mg, 1.25 mmol) which was dissolved in 10 ml of water. The pH of the reaction mixture was adjusted to 2.0 by the addition of 1 M HNO_3. The mixture was stirred at 35 °C for 4 days. The solution was then rotary-evaporated to near dryness, and a brown precipitate was filtered off, washed with water to remove NH_4Cl and dried. Yield 45%.

Elemental analysis (%) for $C_7H_{12}N_6OPtI_2$ (645.1): C 12.5, H 2.0, N 12.7; found: C 12.4, H 1.9, N 12.6. ^1H NMR (200 MHz, DMSO-d_6): δ = 11.20 (s, N(1)H), 8.57 (s; H8), 6.86 (s, NH_2), 4.59 (s, Pt-NH_3), 4.03 (q, CH_2), 1.35 ppm (t, CH_3).

5.3.16 *trans*-[(NH₃)Pt(9-EtGH-*N7*)(pyrz)₂](NO₃)₂ · H₂O (16)

A suspension of 150.0 mg of **15** (0.23 mmol), $AgNO_3$ (79.2 mg, 0.47 mmol) and pyrazine (56.0 mg, 0.70 mmol) in 200 ml of water was stirred at room temperature for 6 days with the exclusion of daylight. After that, AgI was filtered off and the solution was rotary-evaporated to dryness. The yellow residue was dissolved in 1:1:1 solution of $CHCl_3$:CH_3OH:H_2O. Yellow crystals appeared within 2 days at 3 °C, which were later air dried. A single crystal was picked and characterized by X-ray crystallography. Yield 35%.

Elemental analysis (%) for $C_{15}H_{20}N_{12}O_7Pt \cdot H_2O$ (693.50): C 25.8, H 3.2, N 24.2; found: C 25.7, H 3.2, N 24.0. ^1H NMR (200 MHz, D_2O, pD = 4.3): δ = 8.47 (s; H8), 8.79 (m, pyrz), 8.97 (m, pyrz), 4.05 (q; CH_2), 1.35 ppm (t, CH_3). A Raman spectrum was not obtained as the compound decomposed under the laser light.

5.3.17 *trans*-[(NH₃)Pt(9-EtGH-*N7*)(4,4'-bipyridine)₂](NO₃)₂ (17)

15 (100 mg, 0.155 mmol), $AgNO_3$ (52.7 mg, 0.36 mmol) and 4,4'-bipyridine (72.6 mg, 0.46 mmol) were dissolved in 50 ml of water. The reaction mixture was stirred at room temperature with the exclusion of daylight for four days. AgI was filtered off and the solution was rotary-evaporated to dryness. ^1H NMR of the

yellow solid in DMSO-d_6 confirmed the presence of the desired compound along with free 4,4'-bipyridine. The compound was dissolved in a number of solvents (methanol, acetone, chloroform) in order to get rid of unreacted 4,4'-bipyridine. However, these attempts were unsuccessful.

^{1}H NMR (200 MHz, DMSO-d_6) of **17**: δ = 11.29 (s, N(1)H), 8.92 (d; bipy), 8.78 (m, bipy) 8.16 (d, bipy), 7.89 (m, bipy), 6.91 (s, NH$_2$), 5.10 (s, Pt-NH$_3$), 3.95 (q, CH$_2$), 1.29 (t, CH$_3$).

5.3.18 [(dien)Pt(7-MeGH-*N9*)](NO$_3$)(ClO$_4$) (18)

A suspension of [(dien)PtI]I (50 mg, 0.05 mmol) in D$_2$O (1 ml) was treated with AgClO$_4$ (18.8 mg, 0.09 mmol) for 5 h at 40 °C with the exclusion of daylight. The solution was then cooled to room temperature, AgI was filtered off, and to this solution 7.5 mg (0.05 mmol) of 7-methylguanine (7-MeGH) was added. The mixture was stirred at 40 °C for one day. Colorless crystals were isolated from the reaction mixture within 2 days at 3 °C. A single crystal was picked and characterized by X-ray crystallography.

Elemental analysis (%) for C$_{10}$H$_{20}$N$_9$O$_8$ClPt·2H$_2$O (660.89): C 18.2, H 3.7, N 19.1; found: C 18.1, H 3.7, N 19.0. No water molecules were detected in the X-ray structure, however. ^{1}H NMR (200 MHz, D$_2$O, pD = 2.4): δ = 8.10 (s; H8), 3.97 (s; CH$_3$), 3.35, 3.29, 3.12, 3.09, 2.93, 2.90 ppm (m; dien). A Raman spectrum was not obtained as the compound decomposed under the laser light.

5.3.19 *cis*-[(NH$_3$)$_2$Pt(7-MeGH-*N9*)$_2$]Cl$_2$ (20)

A solution of *cis*-[(NH$_3$)$_2$PtCl$_2$] (150.0 mg, 0.5 mmol) and 7-MeGH (165.2 mg, 1.0 mmol) in 45 ml of water was stirred at 40 °C for 48 h. The reaction mixture was cooled to room temperature and a white precipitate was filtered off. The precipitate was dried in air. Yield 85%.

Elemental analysis (%) for C$_{12}$H$_{20}$N$_{12}$O$_2$PtCl$_2$ (630.36): C 22.7, H 3.2, N 26.7; found: C 22.4, H 3.2, N 26.5. ^{1}H NMR (200 MHz, D$_2$O, pD = 2.3): δ = 8.12 (s;

H8), 3.98 (s, CH$_3$). IR ($\tilde{\nu}$ cm^{-1}): 3440 (m, br), 3141 (w), 1701 (s), 1630 (s, sh), 1384 (s). Raman ($\tilde{\nu}$ cm^{-1}): 1579(4), 1559(3), 1516(4), 1363(10), 1275(4), 1049(6), 719(2), 689(1), 650(4), 563(1).

6. Appendix

6.1 Theoretical and Computational Aspects of *ab initio* Procedures

The *ab initio* molecular orbital calculations done in this thesis dealt mainly with the geometry optimizations to locate the lowest energy molecular structure in close proximity to the specified starting structures. Additionally, vibrational frequency calculations were carried out to ensure that the stationary points located on the potential energy surfaces by geometry optimization were minima. Calculations were done using the *Gaussian* 98 suite of programs.[226]

6.1.1 Geometry Optimizations

Geometry optimizations[230] strive to locate a minimum on the potential energy surface in order to predict equilibrium structures of molecular systems. This can be understood in terms of the values of potential energy surfaces. These surfaces indicate the way in which the energy of a molecular system varies with small changes in its structure. Hence, a potential energy surface is a mathematical relationship linking the molecular structure and the resultant energy. In Figure 67, the potential energy surface considers only two of the degrees of freedom within the molecule, and plots the energy above the plane defined by them, creating a surface. Each point corresponds to a particular molecular structure, with the height of the surface at that point representing the energy of that structure.
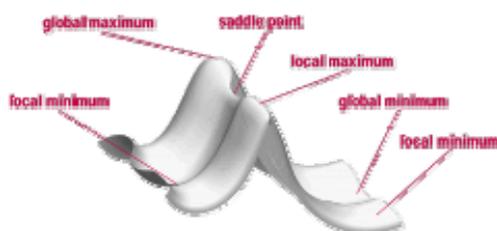

Figure 67 The potential energy surface.[230]

All the minima on a potential energy surface of a molecule correspond to stable stationary points where the forces on atoms are zero. The global minimum is the most stable conformation; the local minima, less stable conformations; and the saddle points are transition conformations between minima.

At both minima and saddle points, the first derivative of the energy is zero. Since the gradient is the negative of the forces, the forces are also zero at such points. A point on the potential energy surface where the forces are zero is called a stationary point. All successful optimizations locate a stationary point, although not always the one that was anticipated. Geometry optimizations usually locate the stationary point closest to the starting geometry.

Geometry optimizations are iterative and begin at some starting geometry. First, the single point energy calculation is performed on the starting geometry. Then the coordinates for some subset of atoms are changed and another single point energy calculation is performed to determine the energy of the new conformation. The first or second derivative of the energy (depending on the method) with respect to the atomic coordinates then determines how large and in what direction the next increment of geometry change should be. Then the change is made. Following the incremental change, the energy and energy derivatives are again determined and the process continues until convergence is achieved, at which point the minimization process terminates. A successive search for minimum finds a local minimum but not necessarily the lowest. A geometry optimization alone is not adequate to tell the nature of the stationary point that it finds. In order to characterize a stationary point, it is essential to perform a frequency calculation on the optimized geometry.

6.1.2 Vibrational Frequency Calculations

Energy calculations and geometry optimizations ignore the vibrations in molecular systems. In this way, these computations use an idealized view of nuclear position. In reality, the nuclei in molecules are constantly in motion. In

equilibrium states, these vibrations are regular and predictable, and molecules can be identified by their characteristic spectra.[230]

Gaussian can calculate the vibrational spectra of molecules in their ground state. Additionally, it can also describe the displacements a system undergoes in its normal modes. Molecular frequencies depend on the second derivative of the energy with respect to the nuclear positions.

The completed frequency calculation comprises of frequencies, intensities, the associated normal modes, the structure's zero point energy, and various thermochemical properties. The nature of the computations is such that the frequency calculations are valid only at stationary points on the potential energy surface. Therefore, frequency calculations should be performed only on the optimized structures. A frequency job should use the same theoretical model and basis set as the optimized geometry. Frequencies computed with a different basis sets or methods have no validity.

The frequency values which are less than zero are known as imaginary frequencies. The number of imaginary frequencies represents the sort of stationary point to which the given molecular structure corresponds. By definition, a structure which has *n* imaginary frequencies is an *nth* order saddle point. Thus, the minimum will have zero imaginary frequencies, and an ordinary transition structure will have one imaginary frequency since it is a first order saddle point.

6.2   Determination of pK_a values

NMR methods are widely used for the determination of pK_a values of nucleobases lying in the pH range of aqueous solutions (pH 0 – 14). For a single protonation-deprotonation step, the chemical shifts, δ, plotted against pD gives a sigmoidal curve. The resultant pD profile is then analysed by the equation[224]:

$$\delta_{exp} = \frac{\delta_A + \delta_B \cdot 10^{(pK_a - pH)}}{1 + 10^{(pK_a - pH)}} \qquad (1)$$

where δ_A and δ_B represent the chemical shifts for the deprotonated and neutral species, respectively. For a molecule with two deprotonation sites, pD profile is analysed by the equation:

$$\delta_{obs} = \frac{\delta_{Nb} + \delta_{NbH} \cdot 10^{(pK_{NbH}-pH)} + \delta_{NbH2} \cdot 10^{(pK_{NbH2}+pK_{NbH}-2pH)}}{1+10^{(pK_{NbH}-pH)} + 10^{(pK_{NbH2}+pK_{NbH}-2pH)}} \quad (2)$$

where, δ_{NbH2}, δ_{NbH} and δ_{Nb} represent the chemical shifts for the species which can be deprotonated twice (δ_{NbH2}), once (δ_{NbH}) and not any further (δ_{Nb}). The values pK_{NbH} and pK_{NbH2} are the negative logarithms of the acidity constants, NbH_2 and NbH, respectively.

The pK_a values obtained in this way can be transformed into pK_a values valid for H_2O solutions using the relationship[225]:

$$pK_a\left(H_2O\right) = \frac{pK_a\left(D_2O\right)-0.45}{1.015} \quad (3)$$

6.3   X-Ray Tables

X-ray Table 1. [(dien)PdBr]Br (**1**)

formula	$C_4H_{13}N_3Br_2Pd$
fw	369.39
space group	$P\bar{1}$
unit cell dimensions	a = 14.242(3) Å
	b = 4.9350(10) Å
	c = 13.551(3) Å
V (Å^3)	952.4(3)
Z	4
D$_{calc}$, (Mg/m^3)	2.576
μ (mm^{-1})	0.0022(3)
Reflns. collected	3048
Unique reflns. with |Fo| ≥ 4σ|Fo|	1563
2θ range	8.26-50.0
R$_1$, wR$_2$ [I > 2σ(I)]	0.0195, 0.0336
GOF	0.964

X-ray Table 2. [(dien)Pd(ICH-*N3*)](NO$_3$)$_2$ (**2**)

formula	$C_8H_{18}N_8O_7Pd$	
fw	444.72	
space group	$P\bar{1}$	
unit cell dimensions	a = 6.6310(13) Å	α = 65.80(3)°
	b = 10.651(2) Å	β = 87.08(3)°
	c = 12.214(3) Å	γ = 74.07(3)°
V (Å^3)	754.7(3)	
Z	2	
D$_{calc}$, (Mg/m^3)	1.957	
μ (mm^{-1})	1.285	
Reflns. collected	3463	
Unique reflns. with |Fo| ≥ 4σ|Fo|	2824	
2θ range	6.4-55.06	
R$_1$, wR$_2$ [I > 2σ(I)]	0.0345, 0.0863	
GOF	1.081	

X-ray Table 3. [(dienPt)$_2$(IC-*N1,N3*)](ClO$_4$)$_3$ · 2H$_2$O (**3**)

formula	C$_{12}$H$_{34}$N$_9$O$_{15}$Cl$_3$Pt$_2$	
fw	1040.97	
space group	*P*2$_1$/c	
unit cell dimensions	a = 14.598(3) Å	
	b = 11.601(2) Å	β = 129.54(1)°
	c = 21.769(7) Å	
V (Å^3)	2843.0(14)	
Z	4	
D$_{calc}$, (Mg/m^3)	2.423	
μ (mm^{-1})	1.109	
Reflns. collected	63424	
Unique reflns. with |Fo| ≥ 4σ|Fo|	6508	
2θ range	6.6-55.0	
R$_1$, wR$_2$ [I > 2σ(I)]	0.0306, 0.0712	
GOF	1.63	

X-ray Table 4. [(dienPd)$_2$(IC-*N1,N3*)](ClO$_4$)$_3$ · 2H$_2$O (**4**)

formula	C$_{12}$H$_{34}$N$_9$O$_{15}$Cl$_3$Pd$_2$	
fw	863.65	
space group	*P*2$_1$/c	
unit cell dimensions	a = 14.659(3) Å	
	b = 11.504(2) Å	β = 129.583(19)°
	c = 21.760(7) Å	
V (Å^3)	2828.1(14)	
Z	4	
D$_{calc}$, (Mg/m^3)	2.019	
μ (mm^{-1})	1.637	
Reflns. collected	49155	
Unique reflns. with |Fo| ≥ 4σ|Fo|	6471	
2θ range	6.0-55.0	
R$_1$, wR$_2$ [I > 2σ(I)]	0.0327, 0.0686	
GOF	1.15	

X-ray Table 5. [(dien)PtCl]ClO$_4$ (**5b**)

formula	C$_4$H$_{13}$N$_3$O$_4$Cl$_2$Pt
fw	433.15
space group	$P\overline{1}$
unit cell dimensions	a = 8.1414(16) Å α = 69.15(3)°
	b = 11.217(2) Å β = 86.27(3)°
	c = 13.247(3) Å γ = 78.88(3)°
V (Å^3)	1109.3(5)
Z	4
D$_{calc}$, (Mg/m^3)	2.594
μ (mm^{-1})	13.125
Reflns. collected	9720
Unique reflns. with |Fo| ≥ 4σ|Fo|	4956
2θ range	6.0-55.0
R$_1$, wR$_2$ [I > 2σ(I)]	0.0628, 0.1278
GOF	1.17

X-ray Table 6. ICH · (1-MeC) · 2H$_2$O (**6**)

formula	C$_9$H$_{16}$N$_6$O$_4$
fw	272.28
space group	$C2/c$
unit cell dimensions	a = 23.541(5) Å
	b = 7.4360(15) Å β = 93.88(3)°
	c = 14.529(3) Å
V (Å^3)	2537.5(9)
Z	8
D$_{calc}$, (Mg/m^3)	1.425
μ (mm^{-1})	0.114
Reflns. collected	4562
Unique reflns. with |Fo| ≥ 4σ|Fo|	2697
2θ range	5.6-55.8
R$_1$, wR$_2$ [I > 2σ(I)]	0.0335, 0.0629
GOF	0.627

X-ray Table 7. [ICH · ICH$_2$]NO$_3$ (**7**)

formula	C$_8$H$_{11}$N$_7$O$_5$
fw	285.24
space group	*C2/c*
unit cell dimensions	a = 20.617(5) Å
	b = 5.1570(10) Å β = 97.79(3)°
	c = 22.684(4) Å
V (Å^3)	2389.5(9)
Z	8
D$_{calc}$, (Mg/m^3)	1.586
μ (mm^{-1})	0.133
Reflns. collected	4327
Unique reflns. with |Fo| ≥ 4σ|Fo|	2637
2θ range	5.0-56.6
R$_1$, wR$_2$ [I > 2σ(I)]	0.0361, 0.0818
GOF	0.77

X-ray Table 8. [1-MeICH](NO$_3$)$_3$(ClO$_4$) (**9**)

formula	C$_{20}$H$_{32}$N$_{15}$O$_{17}$Cl
fw	790.06
space group	*P$\bar{1}$*
unit cell dimensions	a = 9.6476(19) Å α = 88.29(3)°
	b = 9.941(2) Å β = 86.06(3)°
	c = 18.783(4) Å γ = 64.63(3)°
V (Å^3)	1623.9(6)
Z	2
D$_{calc}$, (Mg/m^3)	1.616
μ (mm^{-1})	0.219
Reflns. collected	4327
Unique reflns. with |Fo| ≥ 4σ|Fo|	2637
2θ range	6.18-55.0
R$_1$, wR$_2$ [I > 2σ(I)]	0.0603, 0.1447
GOF	1.023

X-ray Table 9. [(dien)Pd(1-MeIC-*N3*)](ClO$_4$)$_2$ (**10**)

formula	C$_9$H$_{20}$N$_6$O$_9$Cl$_2$Pd
fw	533.63
space group	$P\bar{1}$
unit cell dimensions	a = 6.5670(13) Å α = 75.77(3)°
	b = 10.614(2) Å β = 87.05(3)°
	c = 14.099(3) Å γ = 77.42(3)°
V (Å^3)	929.7(4)
Z	2
D$_{calc}$, (Mg/m^3)	1.906
μ (mm^{-1})	1.343
Reflns. collected	4288
Unique reflns. with |Fo| ≥ 4σ|Fo|	2937
2θ range	6.4-55.0
R$_1$, wR$_2$ [I > 2σ(I)]	0.0720, 0.2116
GOF	1.34

X-ray Table 10. [(dien)Pt(1-MeIC-*N3*)](ClO$_4$)$_2$ (**11**)

formula	C$_9$H$_{20}$N$_6$O$_9$Cl$_2$Pt
fw	622.30
space group	$P\bar{1}$
unit cell dimensions	a = 6.5270(13) Å α = 75.93(3)°
	b = 10.663(2) Å β = 87.52(3)°
	c = 14.104(3) Å γ = 77.01(3)°
V (Å^3)	927.7(4)
Z	2
D$_{calc}$, (Mg/m^3)	2.228
μ (mm^{-1})	7.908
Reflns. collected	21612
Unique reflns. with |Fo| ≥ 4σ|Fo|	4263
2θ range	6.4-55.0
R$_1$, wR$_2$ [I > 2σ(I)]	0.0671, 0.1622
GOF	1.41

X-ray Table 11. [(dienPt)$_2$(GH-*N7,N9*)](ClO$_4$)$_3$ (**13**)

formula	C$_{13}$H$_{30}$N$_{11}$O$_{13}$Cl$_3$Pt$_2$
fw	1045.01
space group	*P*2$_1$/c
unit cell dimensions	a = 7.9690(16) Å
	b = 14.986(3) Å β = 106.90(3)°
	c = 25.261(6) Å
V (Å^3)	2886.5(12)
Z	4
D$_{calc}$, (Mg/m^3)	2.405
μ (mm^{-1})	10.038
Reflns. collected	3990
Unique reflns. with |Fo| ≥ 4σ|Fo|	3990
2θ range	4.4-46.8
R$_1$, wR$_2$ [I > 2σ(I)]	0.0462, 0.1001
GOF	0.89

X-ray Table 12. [(dien)Pt(GH$_2$-*N9*)](Cl)(ClO$_4$) (**12a**)

formula	C$_9$H$_{18}$N$_8$O$_5$Cl$_2$Pt
fw	584.29
space group	*P*2$_1$/c
unit cell dimensions	a = 8.1800(16) Å
	b = 19.454(4) Å β = 111.79(2)°
	c = 11.411(2) Å
V (Å^3)	1707.0(8)
Z	4
D$_{calc}$, (Mg/m^3)	2.274
μ (mm^{-1})	8.574
Reflns. collected	27195
Unique reflns. with |Fo| ≥ 4σ|Fo|	3913
2θ range	6.8-55.0
R$_1$, wR$_2$ [I > 2σ(I)]	0.0376, 0.0636
GOF	1.05

X-ray Table 13. 2{[(dien)Pt(GH$_2$-*N9*)](ClO$_4$)$_2$ · 2H$_2$O} (**12b**)

formula	C$_{18}$H$_{36}$N$_{16}$O$_{22}$Cl$_4$Pt$_2$
fw	1368.61
space group	*C2/c*
unit cell dimensions	a = 38.466(8) Å
	b = 11.210(2) Å β = 133.49(3)°
	c = 27.134(5) Å
V (Å^3)	8489(5)
Z	2
D$_{calc}$, (Mg/m^3)	2.129
μ (mm^{-1})	6.933
Reflns. collected	27635
Unique reflns. with |Fo| ≥ 4σ|Fo|	9515
2θ range	6.0-55.0
R$_1$, wR$_2$ [I > 2σ(I)]	0.0586, 0.1485
GOF	1.04

X-ray Table 14. *trans*-[(NH$_3$)Pt(9-EtGH-*N7*)(pyrz)$_2$](NO$_3$)$_2$ · H$_2$O(**16**)

formula	C$_{15}$H$_{22}$N$_{12}$O$_8$Pt
fw	693.51
space group	*P$\bar{1}$*
unit cell dimensions	a = 12.770(3) Å α = 104.56(3)°
	b = 14.437(3) Å β = 108.13(3)°
	c = 15.161(3) Å γ = 103.90(3)°
V (Å^3)	2412.0(13)
Z	4
D$_{calc}$, (Mg/m^3)	1.904
μ (mm^{-1})	5.884
Reflns. collected	21402
Unique reflns. with |Fo| ≥ 4σ|Fo|	10749
2θ range	6.0-55.0
R$_1$, wR$_2$ [I > 2σ(I)]	0.0728, 0.1842
GOF	1.32

X-ray Table 15. [(dien)Pt(7-MeGH-*N9*)](NO$_3$)(ClO$_4$) (**18**)

formula	C$_{10}$H$_{20}$N$_9$O$_8$ClPt
fw	624.88
space group	$P\overline{1}$
unit cell dimensions	a = 6.9590(14) Å α = 97.76(3)°
	b = 11.946(2) Å β = 96.47(3)°
	c = 11.964(2) Å γ = 92.56(3)°
V (Å^3)	977.4(3)
Z	2
D$_{calc}$, (Mg/m^3)	2.123
μ (mm^{-1})	7.375
Reflns. collected	7550
Unique reflns. with |Fo| ≥ 4σ|Fo|	4347
2θ range	6.4-55.0
R$_1$, wR$_2$ [I > 2σ(I)]	0.0386, 0.0958
GOF	1.15

X-ray Table 16. *cis*-[(NH$_3$)$_2$Pt(7-MeGH-*N9*)$_2$]Cl$_2$·3H$_2$O (**20a**)

formula	C$_{12}$H$_{26}$N$_{12}$O$_5$Cl$_2$Pt
fw	684.40
space group	*C2/c*
unit cell dimensions	a = 18.201(6) Å
	b = 21.417(6) Å β = 121.69(4)°
	c = 14.822(3) Å
V (Å^3)	4916(3)
Z	2
D$_{calc}$, (Mg/m^3)	1.833
μ (mm^{-1})	5.973
Reflns. collected	26925
Unique reflns. with |Fo| ≥ 4σ|Fo|	5636
2θ range	6.2-55.0
R$_1$, wR$_2$ [I > 2σ(I)]	0.0510, 0.1084
GOF	1.01

X-ray Table 17. *cis*-[(NH$_3$)$_2$Pt(7-MeGH-*N9*)$_2$]Cl$_2$·2H$_2$O (**20b**)

formula	C$_{12}$H$_{24}$N$_{12}$O$_4$Cl$_2$Pt
fw	666.39
space group	$P\overline{1}$
unit cell dimensions	a = 7.8340(16) Å α = 102.69(3)°
	b = 11.100(2) Å β = 100.49(3)°
	c = 13.252(3) Å γ = 90.02(3)°
V (Å^3)	1104.4(4)
Z	2
D$_{calc}$, (Mg/m^3)	1.992
μ (mm^{-1})	1.795
Reflns. collected	9818
Unique reflns. with |Fo| ≥ 4σ|Fo|	5011
2θ range	6.4-55.0
R$_1$, wR$_2$ [I > 2σ(I)]	0.0307, 0.0610
GOF	1.14

X-ray Table 18. *cis, cis*-[{(NH$_3$)$_2$Pt}$_2$(7-MeGH-*N3,N9*)Cl$_2$]Cl$_2$·3H$_2$O (**21**)

formula	C$_6$H$_{25}$N$_9$O$_4$Cl$_4$Pt$_2$
fw	819.29
space group	*C*2/c
unit cell dimensions	a = 13.525(3) Å
	b = 17.095(3) Å β = 110.15(3)°
	c = 19.292(4) Å
V (Å^3)	4187.5(17)
Z	8
D$_{calc}$, (Mg/m^3)	2.580
μ (mm^{-1})	13.889
Reflns. collected	16033
Unique reflns. with |Fo| ≥ 4σ|Fo|	4802
2θ range	6.4-55.0
R$_1$, wR$_2$ [I > 2σ(I)]	0.0631, 0.1262
GOF	1.14

X-ray Table 19. *cis*-[(NH$_3$)$_2$Pt(9-EtGH-*N7)*$_2$](NO$_3$)$_2$ (**19**)

formula	C$_{14}$H$_{24}$N$_{14}$O$_8$Pt
fw	711.56
space group	$P\bar{1}$
unit cell dimensions	a = 10.779(2) Å α = 64.08(3)°
	b = 11.926(2) Å β = 66.48(3)°
	c = 12.640(3) Å γ = 67.66(3)°
V (Å^3)	1297.7(4)
Z	2
D$_{calc}$, (Mg/m^3)	1.821
μ (mm^{-1})	5.473
Reflns. collected	4644
Unique reflns. with |Fo| ≥ 4σ|Fo|	4644
2θ range	4.6-55.0
R$_1$, wR$_2$ [I > 2σ(I)]	0.062, 0.147
GOF	1.46

7. References

(1)   Neidle, S. *Nucleic Acid Structure and Recognition*; Oxford University Press: Oxford, 2001.

(2)   Marincola, F. C.; Casu, M.; Saba, G.; Manettib, C.; Laia, A. *Phys. Chem. Chem. Phys.* **2000**, *2*, 2425.

(3)   Lippert, B. *J. Chem. Soc., Dalton Trans.* **1997**, 3971.

(4)   See various chapters in: Lippert, B. *(Ed.) Cisplatin: Chemistry and Biochemistry of a Leading Anticancer Drug*; Wiley-VCH, Weinheim, 1999.

(5)   Navarro, J. A. R.; Freisinger, E.; Lippert, B. *Inorg. Chem.* **2000**, *39*, 2301.

(6)   Krizanovic, O.; Sabat, M.; Beyerle-Pfnür, R.; Lippert, B. *J. Am. Chem. Soc.* **1993**, *115*, 5538.

(7)   Sundaralingam, M.; Carrabine, J. A. *J. Mol. Biol.* **1971**, *61*, 287.

(8)   Colombier, C.; Lippert, B.; Leng, M. *Nucleic Acids Res.* **1996**, *24*, 4519.

(9)   Brabec, V.; Sip, M.; Leng, M. *Biochemistry* **1993**, *32*, 11676.

(10)   Dalbiès, R.; Leng, M. *Proc. Natl. Acad. Sci. U.S.A.* **1994**, *91*, 8147.

(11)   Metzger, S.; Lippert, B. *J. Am. Chem. Soc.* **1996**, *118*, 12467.

(12)   Sigel, R. K. O.; Freisinger, E.; Metzger, S.; Lippert, B. *J. Am. Chem. Soc.* **1998**, *120*, 12000.

(13)   Sigel, R. K. O.; Sabat, M.; Freisinger, E.; Mower, A.; Lippert, B. *Inorg. Chem.* **1999**, *38*, 1481.

(14)   Dieter-Wurm, I.; Sabat, M.; Lippert, B. *J. Am. Chem. Soc.* **1992**, *114*, 357.

(15)   Schröder, G.; Sabat, M.; Baxter, I.; Kozelka, J.; Lippert, B. *Inorg. Chem.* **1997**, *36*, 490.

(16)   Lüth, M. S.; Freisinger, E.; Glahé, F.; Lippert, B. *Inorg. Chem.* **1998**, *37*, 5044.

(17)   Lüth, M. S.; Freisinger, E.; Glahé, F.; Müller, J.; Lippert, B. *Inorg. Chem.* **1998**, *37*, 3195.

(18)   Rauter, H.; Hillgeris, E. C.; Erxleben, A.; Lippert, B. *J. Am. Chem. Soc.* **1994**, *116*, 616.

(19)   Freisinger, E.; Rother, I. B.; Luth, M. S.; Lippert, B. *Proc. Natl. Acad. Sci. U. S. A.* **2003**, *100*, 3748.

(20)   Rauter, H.; Mutikainen, I.; Blomberg, M.; Lock, C. J. L.; AmoOchoa, P.; Freisinger, E.; Randaccio, L.; Zangrando, E.; Chiarparin, E.; Lippert, B. *Angew. Chem. Int. Ed. Engl.* **1997**, *36*, 1296.

(21)   Navarro, J. A.; Freisinger, E.; Lippert, B. *Inorg. Chem.* **2000**, *39*, 1059.

(22)   Rauter, H.; Mutikainen, I.; Blomberg, M.; Lock, C. J. L.; Amo-Ochoa, P.; Freisinger, E.; Randaccio, L.; Zangrando, E.; Chiarparin, E.; Lippert, B. *Angew. Chem. Int. Ed. Engl.* **1997**, *36*, 1296.

(23)   Meiser, C.; Freisinger, E.; Lippert, B. *J. Chem. Soc., Dalton Trans.* **1998**, 2059.

(24)   Witkowski, H.; Freisinger, E.; Lippert, B. *J. Chem. Soc., Chem. Commun.* **1997**, 1315.

(25)   Schröder, G.; Lippert, B.; Sabat, M.; Lock, C. J. L.; Faggiani, R.; Song, B.; Sigel, H. *J. Chem. Soc., Dalton Trans.* **1995**, 3767.

(26)   Šponer, J. E.; Leszczynski, J.; Glahé, F.; Lippert, B.; Šponer, J. *Inorg. Chem.* **2001**, *40*, 3269.

(27)   Šponer, J. E.; Glahé, F.; Leszczynski, J.; Lippert, B.; Šponer, J. *J. Phys. Chem. B* **2001**, *105*, 12171.

(28)   Šponer, J.; Šponer, J. E.; Gorb, L.; Leszczynski, J.; Lippert, B. *J. Phys. Chem. A* **1999**, *103*, 11406.

(29)   Šponer, J.; Sabat, M.; Gorb, L.; Leszczynski, J.; Lippert, B.; Hobza, P. *J. Chem. Phy. B* **2000**, *104*, 7335.

(30)   Munoz, J.; Šponer, J.; Hobza, P.; Orozco, M.; Luque, F. J. *J. Phys. Chem. B* **2001**, *105*, 6051.

(31)   Noguera, M.; Bertran, J.; Sodupe, M. *J. Phys. Chem. A* **2004**, *108*, 333.

(32)   Burda, J. V.; Zeizinger, M.; Leszczynski, J. *J. Chem. Phys.* **2004**, *120*, 1253.

(33)   Zeizinger, M.; Burda, J. V.; Šponer, J.; Kapsa, V.; Leszczynski, J. *J. Phys. Chem. A* **2001**, *105*, 8086.

(34)   Burda, J. V.; Šponer, J.; Leszczynski, J. *Phys. Chem. Chem. Phys.* **2001**, *3*, 4404.

(35)   Burda, J. V.; Šponer, J.; Hrabakova, J.; Zeizinger, M.; Leszczynski, J. *J. Phys. Chem. B* **2003**, *107*, 5349.

(36)   Burda, J. V.; Leszczynski, J. *Inorg. Chem.* **2003**, *42*, 7162.

(37)   Löwdin, P. O. *Adv. Quantum Chem.* **1965**, *2*, 213.

(38)   Blackburn, G. M. *Nucleic Acids in Chemistry and Biology*; IRL Press: Oxford, 1990.

(39)   Saenger, W. *Principles of Nucleic Acid Structure*; Springer-Verlag: New York, 1988.

(40)   Sinden, R. R. *DNA Structure and Function*; Academic Press: San Diego, 1994.

(41)   Topal, M. D.; Fresco, J. R. *Nature* **1976**, *263*, 285.

(42)   Robinson, H.; Gao, Y. G.; Bauer, C.; Roberts, C.; Switzer, C.; Wang, A. H. J. *Biochemistry* **1998**, *37*, 10897.

(43)   van Meervelt, L.; Moore, M. H.; Lin, P. K. T.; Brown, D. M.; Kennard, O. *J. Mol. Biol.* **1990**, *216*, 773.

(44)   Stone, M. J.; Nedderman, A. N. R.; Williams, D. H.; Lin, P. K. T.; Brown, D. M. *J. Mol. Biol.* **1991**, *222*, 711.

(45)   Brown, D. M.; Hewlins, M. J. E.; Schell, P. *J. Chem. Soc.* **1968**, 1925.

(46)   Gdaniec, Z.; Ban, B.; Sowers, L. C.; Fazakerley, V. *Eur. J. Biochem.* **1996**, *242*, 271.

(47)   Sower, L. C.; Goodman, M. F.; Eritja, R.; Kaplan, B. E.; Fazakerley, G. C. *J. Mol. Biol.* **1989**, *205*, 437.

(48)   Orozco, M.; Hernandez, B.; Luque, F. J. *J. Phys. Chem. B* **1998**, *102*, 5228.

(49)   Goodman, M. F. *Nature* **1995**, *378*, 237.

(50)   Müller, J.; Zangrando, E.; Pahlke, N.; Freisinger, E.; Randaccio, L.; Lippert, B. *Chem. Eur. J.* **1998**, *4*, 397.

(51)   Brüning, W.; Sigel, R. K. O.; Freisinger, E.; Lippert, B. *Angew. Chem. Int. Ed. Engl.* **2001**, *40*, 3397.

(52)   Vasquez, K. M.; Wilson, J. H. *Trends Biochem. Sci.* **1998**, *23*, 4.

(53)   Thuong, N. T.; Hélène, C. *Angew. Chem. Int. Ed. Engl.* **1993**, *32*, 666.

(54) Stephenson, M. L.; Zamecnik, P. C. *Proc. Natl. Acad. Sci. U. S. A* **1978**, *75*, 285.

(55) Stephenson, M. L.; Zamecnik, P. C. *Proc. Natl. Acad. Sci. U. S. A* **1978**, *75*, 280.

(56) Nielsen, P.; Egholm, M.; Berg, R. H.; Buchardt, O. *Science* **1991**, *254*, 1497.

(57) Nielsen, P. E. *Biophys. Chem.* **1997**, *68*, 103.

(58) Letsinger, R. L.; Singman, C. N.; Histand, G.; Salunkhe, M. *J. Am. Chem. Soc.* **1988**, *110*, 4470.

(59) Browne, K. A.; Dempcy, R. O.; Bruice, T. C. *Proc. Natl. Acad. Sci. U. S. A.* **1995**, *92*, 7051.

(60) Dempcy, R. O.; Browne, K.; Bruice, T. C. *Proc. Natl. Acad. Sci. U. S. A.* **1994**, *91*, 7864.

(61) Dempcy, R. O.; Browne, K.; Bruice, T. C. *J. Am. Chem. Soc.* **1995**, *117*, 6140.

(62) Dempcy, R. O.; Browne, K.; Bruice, T. C. *Proc. Natl. Acad. Sci. U. S. A.* **1995**, 92.

(63) Nowak, R. Dissertation, Universität Dortmund, 2002.

(64) Sigel, R. K. O. Dissertation, Universität Dortmund, 1999.

(65) Burchenal, J. H.; Ciovacco, K.; Kalaher, K.; O'Toole, T.; Dowling, M. H.; Chu, C. K.; Watanabe, K. A.; Fox, J. *J. Cancer Res.* **1976**, *36*, 1520.

(66) Beauchamp, L. M.; Serling, B. L.; Kelsey, J. E.; Biron, K. K.; Collins, P.; Selway, J.; Lin, J. C.; Schaeffer, H. J. *J. Med. Chem* **1988**, *31*, 144.

(67) Ono, A.; Ts'o, P. O. P.; Kan, L.-s. *J. Am. Chem. Soc.* **1991**, *113*, 4032.

(68) Oyelere, A. K.; Kardon, J. R.; Strobel Scott, A. *Biochemistry* **2002**, *41*, 3667.

(69) Roberts, C.; Bandaru, R.; Switzer, C. *J. Am. Chem. Soc.* **1997**, *119*, 4640.

(70) Switzer, C.; Moroney, S. E.; Benner, S. A. *J. Am. Chem. Soc.* **1989**, *111*, 8322.

(71) Switzer, C.; Moroney, S. E.; Benner, S. A. *Biochemistry* **1993**, *32*, 10489.

(72)   Bain, J. D.; Switzer, C.; Chamberlin, A. R.; Benner, S. A. *Nature* **1992**, *356*, 537.

(73)   Roberts, C.; Bandaru, R.; Switzer, C. *Tetrahedron Lett.* **1995**, *36*, 3601.

(74)   Tor, Y.; Dervan, P. B. *J. Am. Chem. Soc.* **1993**, *115*, 4461.

(75)   Strobel, S. A.; Cech, T. R.; Usman, N.; Beigelman, L. *Biochemistry* **1994**, *33*, 13824.

(76)   Musier-Forsyth, K.; Shi, J.-P.; Henderson, B.; Bald, R.; Fürste, J. P.; Erdmann, V. A.; Schimmel, P. *J. Am. Chem. Soc.* **1995**, *117*, 7253.

(77)   Brüning, W.; Freisinger, E.; Sabat, M.; Sigel, R. K. O.; Lippert, B. *Chem. Eur. J.* **2002**, *8*, 4681.

(78)   Brüning, W.; Ascaso, I.; Freisinger, E.; Sabat, M.; Lippert, B. *Inorg. Chim. Acta* **2002**, *339*, 400.

(79)   Müller, J.; Sigel, R. K. O.; Lippert, B. *J. Inorg. Biochem.* **2000**, *79*, 261.

(80)   Lippert, B. *Inorg. Chem.* **1981**, *20*, 4326.

(81)   Faggiani, R.; Lippert, B.; Lock, C. J. L. *Inorg. Chem.* **1980**, *19*, 295.

(82)   Rodriguez-Bailey, V. M.; Clarke, M. *J. Inorg. Chem.* **1997**, *36*, 1611.

(83)   LaChance-Galang, K. J.; Maldonado, I.; Gallagher, M. L.; Jian, W.; Prock, A.; Chacklos, J.; Galang, R. D.; Clarke, M. *J. Inorg. Chem.* **2001**, *40*, 485.

(84)   Fiol, J. J.; Garcia-Raso, A.; Mata, T., A.; Molins, E. *Inorg. Chim. Acta* **1997**, *262*, 85.

(85)   Garcia-Raso, A.; Fiol, J. J.; Adrover, B.; Moreno, V.; Molins, E.; Mata, I. *J. Chem. Soc. Dalton Trans.* **1998**, 1031.

(86)   Price, C.; Rees, N. H.; Elsegood, M. R. J.; Clegg, W.; Houlton, A. *J. Am. Chem. Soc., Dalton Trans.* **1998**, 2001.

(87)   Gehring, K.; Leroy, J.-L.; Guernon, M. *Nature* **1993** *363*, 561.

(88)   Sigel, R. K. O.; Freisinger, E.; Lippert, B. *J. Inorg. Biochem.* **1999**, *74*, 296.

(89)   Sharma, B. D.; McConnell, J. F. *Acta Crystallogr.* **1965**, *19*, 797.

(90)   McConnell, J. F.; Sharma, B. D.; Marsh, R. E. *Nature* **1964**, *203*, 399.

(91)   Watson, J. D.; Crick, F. H. C. *Nature* **1953**, *171*, 964.

(92)   Stimson, M. M.; O'Donnell, M. J. *J. Am. Chem. Soc.* **1952**, *74*, 1805.

(93)   Morita, H.; Nagakura, S. *Theor. Chim. Acta* **1968**, *11*, 279.

(94)   Hélène, C.; Douzou, P. *C. R. Hebd. Seances Acad. Sci.* **1964**, *259*, 4853.

(95)   Kwiatkowski, J. S.; Leszczynski, J. *Int. J. Quant. Chem* **1997**, *61*, 453.

(96)   Brown, D. J.; Teitei, T. *Aust. J. Chem.* **1965**, 559.

(97)   Hélène, C.; Douzou, P. *C. R. Hebd. Seances Acad. Sci.* **1964**, *259*, 4387.

(98)   Vranken, H.; Smets, J.; Maes, G.; Lapinski, L.; Nowak, M. J.; Adamowicz, L. *Spectrochim. Acta* **1994**, *50A*, 875.

(99)   Zhanpeisov, N. U.; Leszczynski, J. *Int. J. Quant. Chem.* **1998**, *69*, 37.

(100)   Ha, T.-K.; Keller, H. J.; Gunde, R.; Gunthard, H. H. *J. Mol. Struct.* **1996**, *376*, 375.

(101)   Becke, A. D. *J. Chem. Phys.* **1993**, *98*, 5648.

(102)   Lee, C.; Yang, W.; Parr, R. G. *Phys. Rev.* **1998**, 785.

(103)   Miehlich, B.; Savin, A.; Stoll, H.; Preuss, H. *Chem. Phys. Lett.* **1989**, *157*, 200.

(104)   Lippert, B. *J. Raman Spectrosc.* **1979**, *8*, 274.

(105)   Baddley, W. H.; Basolo, F. *J. Am. Chem. Soc.* **1966**, *88*, 2944.

(106)   Britten, J. F.; Lock, C. J. L.; Pratt, W. M. C. *Acta Crystallogr.* **1982**, *B38*, 2148.

(107)   Schöllhorn, H.; Thewalt, U.; Lippert, B. *Inorg. Chim. Acta* **1985**, *108*, 77.

(108)   Schöllhorn, H.; Thewalt, U.; Lippert, B. *J. Am. Chem. Soc.* **1989**, *111*, 7213.

(109)   Lippert, B. *Inorg. Chim. Acta* **1981**, *55*, 5.

(110)   Hobza, P.; Šponer, J. *Chem. Rev.* **1999**, *99*, 3247.

(111)   Luisi, B.; Orozco, M.; Šponer, J.; Luque, F. J.; Shakked, Z. *J. Mol. Biol.* **1998**, *279*, 1123.

(112)   Burda, J. V.; Šponer, J.; Hobza, P. *J. Phys.Chem.* **1996**, *100*, 7250.

(113) Burda, J. V.; Šponer, J.; Leszczynski, J.; Hobza, P. *J. Phys.Chem. B* **1997**, *101*, 9670.

(114) Reed, A. E.; Curtiss, A. E.; Weinhold, F. *Chem. Rev.* **1988**, *88*, 899.

(115) King, B. F.; Weinhold, F. *J. Chem. Phys.* **1995**, *103*, 333.

(116) NBO "5.0 Program Manual, Technical Report," Theoretical Chemistry Institute, University of Wisconsin, 1996-2001.

(117) Lippert, B.; Schöllhorn, H.; Thewalt, U. *J. Am. Chem. Soc.* **1986**, *108*, 525.

(118) Sanz Miguel, P. J.; Lax, P.; Willermann, M.; Lippert, B. *Inorg. Chim. Acta* **2004**, *357*, 4552.

(119) Frommer, G.; Mutikainen, I.; Pesch, F. J.; Hillgeris, E. C.; Preut, H.; Lippert, B. *Inorg. Chem.* **1992**, *31*, 2429.

(120) Arpalahti, J.; Klika, K. D. *Eur. J. Inorg. Chem.* **1999**, 1199.

(121) Viljanen, J.; Klika, K. D.; Sillanpaa, R.; Arpalahti, J. *Inorg. Chem.* **1999**, *38*, 4924.

(122) Garijo Añorbe, M.; Luth, M. S.; Roitzsch, M.; Morell Cerdà, M.; Lax, P.; Kampf, G.; Sigel, H.; Lippert, B. *Chem. Eur. J.* **2004**, *10*, 1046.

(123) Vrkic, A. K.; Taverner, T.; James, P. F.; O'Hair, R. A. J. *Dalton Trans.* **2004**, 197.

(124) Pedersen, D. B.; Simard, B.; Martinez, A.; Moussatova, A. *J. Chem. Phy. A* **2003**, *107*, 6464.

(125) Burda, J. V.; Šponer, J.; Leszczynski, J. *J. Biol. Inorg. Chem.* **2000**, *5*, 178.

(126) Gupta, D.; Huelsekopf, M.; Morell Cerdà, M.; Ludwig, R.; Lippert, B. *Inorg. Chem.* **2004**, *43*, 3386.

(127) Chatake, T.; Ono, A.; Ueno, Y.; Matsuda, A.; Takénaka, A. *J. Mol. Biol.* **1999**, *294*, 1215.

(128) Chatake, T.; Hikima, T.; Ono, A.; Ueno, Y.; Matsuda, A.; Takénaka, A. *J. Mol. Biol.* **1999**, *294*, 1223.

(129) Bell, T. W.; Hou, Z.; Luo, Y.; Drew, M. G. B.; Chapoteau, E.; Czech, B. P.; Kumar, A. *Science* **1995**, *269*, 671.

(130) Dabkowska, I.; Gutowski, M.; Ratz, J. *J. Am. Chem. Soc.* **2005**, *127*, 2238.

(131) Rossi, M.; Kistenmacher, T. J. *Acta Crystallogr.* **1977**, *B33*, 3962.

(132) Faggiani, R.; Lippert, B.; Lock, C. J. L. *Inorg. Chem.* **1982**, *21*, 3210.

(133) Newmark, R. A.; Cantor, C. R. *J. Am. Chem. Soc.* **1968**, *18*, 5010.

(134) Fujinami, F.; Ogawa, K.; Arakawa, Y.; Shirotake, S.; Fujii, S.; Tomita, K.-I. *Acta Crystallogr.* **1979**, *B35*, 968.

(135) Kistenmacher, T. J.; Rossi, M.; Chiang, C. C.; Caradonna, J. P.; Marzilli, L. G. *Adv. Mol. Relax Interact. Processes* **1980**, *17*, 113.

(136) Müller, J.; Freisinger, E. *Acta Crystallogr.* **2005**, *E6*, o320.

(137) Schimanski, A.; Freisinger, E.; Erxleben, A.; Lippert, B. *Inorg. Chim. Acta* **1998**, *283*, 223.

(138) Wahl, M. C.; Rao, S. T.; Sundaralingam, M. *Nature Struct. Biol.* **1996**, *3*, 24.

(139) Auffinger, P.; Louise-May, S.; Westhof, E. *J. Am. Chem. Soc.* **1996**, *118*, 1181.

(140) Desiraju, G. R.; Steiner, T. *The Weak Hydrogen Bond*; Oxford Univ. Press: Oxford, 1999.

(141) Les, A.; Adamowicz, L. *J. Phys. Chem.* **1990**, *94*, 7021.

(142) Matsukawa, T.; Ban, S.; Shirakawa, K.; Yoneda, M. *Yakugaku Zasshi* **1953**, *73*, 159.

(143) Lever, O. W., Jr.; Bell, L. N.; Hyman, C.; McGuire, H. M.; Ferone, R. *J. Med. Chem* **1986**, *29*, 665.

(144) Biswas, G.; Iitaka, I.; Shugar, D.; Banerjee, A. *Nucleosides and Nucleotides* **1989**, *8*.

(145) Cooper, D. G.; Durant, G. J.; Ganellin, C. R.; Ife, R. J.; Meeson, M. L.; Sach, G. S. *Il Farmaco* **1991**, *46*, 3.

(146) Taylor, E. C.; Young, W. B. *J. Org. Chem.* **1995**, *60*, 747.

(147) Taylor, E. C.; Zhou, P. *Tetrahedron Lett.* **1997**, *38*, 4339.

(148) Yakovlev, K. I.; Stetsenko, A. I.; Alekseyeva, G. M.; Tulub, A. A.; Mamelkina, I. Yu in Nicolini, M. (*Ed.*) *5th Int. Symp. on Platinum and Other Coordination Compounds in Cancer Chemotherapy; Padua* **1987**, *Nijhoff Publishing*, 763.

(149) Šponer, J. E.; Sanz Miguel, P. J.; Rodríguez-Santiago, L.; Erxleben, A.; Krumm, M.; Sodupe, M.; Šponer, J.; Lippert, B. *Angew. Chem. Int. Ed. Engl.* **2004**, *43*, 5396.

(150) Kistenmacher, T. J.; Rossi, M.; Caradonna, J. P.; Marzilli, L. G. *Adv. Mol. Relax Interact. Processes* **1979**, *15*, 119.

(151) Brown, D. J.; Jacobsen, N. W. *J. Chem. Soc.* **1962**, 3172.

(152) Angier, R. B.; Curran, W. V. *J. Org. Chem.* **1961**, *26*, 1891.

(153) Szczesniak, M.; Leszczynski, J.; Person, W. B. *J. Am. Chem. Soc.* **1992**, *114*, 2731.

(154) Szczesniak, M.; Nowak, M. J.; SzczepaniaK, K. *J. Mol. Struct.* **1984**, *115*.

(155) Martin, R. B. *Acc. Chem. Res.* **1985**, 32.

(156) Martin, R. B.; in *B. Lippert (Ed.), Cisplatin - Chemistry and Biochemistry of a Leading Anticancer Drug* **1999**, *Wiley,VCH, Weinheim*, 183.

(157) Sanz Miguel, P. J. Dissertation, Universität Dortmund, 2005.

(158) Ménard, R.; Phan Viet, M. T.; Zardor, M. *Inorg. Chim. Acta* **1987**, *136*, 25.

(159) Frommer, G.; Schöllhorn, H.; Thewalt, U.; Lippert, B. *Inorg. Chem.* **1990**, *29*, 1417.

(160) Melanson, R.; Rochon, F. D. *Can. J. Chem.* **1979**, *57*, 57.

(161) Unger, B. *Ann. Chem.* **1846**, *59*, 58.

(162) Unger, B. *Ann. Chem.* **1846**, *58*, 18.

(163) Shapiro, R. *Prog. Nucl. Acid Res. Mol. Biol* **1968**, *8*, 73.

(164) Szczepaniak, K.; Szczepaniak, M.; Szaida, W.; Person, W. B.; Leszczynski, J. *Can. J. Chem.* **1991**, *69*, 1718.

(165) Leszczynski, J. *Encyclopedia of Computational Chemistry; von Schleyer, P. R., Ed.*; John Wiley, Chichester, 1998.

(166) Leszczynski, J. *J. Phys. Chem. A* **1998**, *102*, 2357.

(167) Colominas, C.; Luque, F. J.; Orozco, M. *J. Am. Chem. Soc.* **1996**, *118*, 6811.

(168) Dolgounitcheva, O.; Zakrzewski, V. G.; Ortiz, J. V. *J. Am. Chem. Soc.* **2000**, *122*, 12 304.

(169) Sabio, M.; Topiol, S.; Lumma, W. C. *J. Phys. Chem.* **1990**, *94*, 1366.

(170) Mons, M.; Dimicoli, I.; Piuzzi, F.; Tardivel, B.; Elhamine, M. *J. Phys. Chem. A* **2002**, *106*, 5088.

(171) Piuzzi, F.; Mons, M.; Dimicoli, I.; Tardivel, B.; Zhao, Q. *Chem. Phys. Lett.* **2001**, *270*, 205.

(172) Thewalt, U.; Bugg, C. E.; Marsh, R. E. *Acta Crystallogr. Sect. B* **1971**, *27*, 2358.

(173) Pfleiderer, W. *Ann. Chem.* **1961**, *647*, 167.

(174) Frederick, W.; Bernhauer, K. *Z. Physiol. Chem.* **1959**, *317*, 116.

(175) Clarke, M. J.; Taube, H. *J. Am. Chem. Soc.* **1974**, *96*, 5413.

(176) Kong, P. C.; Theophanides, T. *Inorg. Chem.* **1974**, *13*, 1981.

(177) Kistenmacher, T. J.; Szalda, P. J.; Marzilli, L. G. *Inorg. Chem.* **1975**, *14*, 2623.

(178) Mikulski, C. M.; Mattucci, L.; Weiss, L.; Karayannis, N. M. *Inorg. Chim. Acta* **1985**, *107*, 147.

(179) Tu, A. T.; Reinosa, J. A. *Biochemistry* **1966**, *5*, 3375.

(180) Tu, A. T.; Friederich, C. G. *Biochemistry* **1968**, *7*, 4367.

(181) Cramageclunescu, D.; Fruma, A. *Inorg. Chim. Acta* **1970**, *4*, 287.

(182) Srinivasan, L.; Taylor, M. R. *J. Chem. Soc. Chem. Commun.* **1970**, 1668.

(183) Carrabine, J. A.; Sundaralingam, M. *J. Am. Chem. Soc.* **1970**, *92*, 369.

(184) Frommer, G. Dissertation, Universität Dortmund, 1991.

(185) Wagner, R.; Phillipsborn, W. *Helv. Chim. Acta* **1971**, *54*, 1543.

(186) Hegmans, A.; Sabat, M.; Baxter, I.; Freisinger, E.; Lippert, B. *Inorg. Chem.* **1998**, *37*, 4921.

(187) Raudaschl, G.; Lippert, B. *Inorg. Chim. Acta* **1983**, *80*, L49.

(188) Albinati, A.; Isaia, F.; Kaufmann, W.; Sorato, C.; Venanzi, L. M. *Inorg. Chem.* **1989**, *28*, 1112.

(189) Stang, P. J.; Cao, D. H.; Saito, S.; Arif, A. M. *J. Am. Chem. Soc.* **1995**, *117*, 6273.

(190) Gellert, R. W.; Bau, R. *J. Am. Chem. Soc.* **1975**, *97*, 7379.

(191) Bau, R.; Gellert, R. W. *Biochimie* **1978**, *60*, 1040.

(192) Cramer, R. E.; Dahlstrom, P. L.; Seu, M. J. T.; Norton, T.; Kashiwagi, M. *Inorg. Chem.* **1980**, *19*, 148.

(193) Marzilli, L. G.; Chalilpoyil, P.; Chiang, C. C.; Kistenmacher, T. J. *J. Am. Chem. Soc.* **1980**, *102*, 2480.

(194) Lippert, B.; Raudaschl, G.; Lock, C. J. L.; Pilon, P. *Inorg. Chim. Acta* **1984**, *93*, 43.

(195) Schöllhorn, H.; Raudaschl-Sieber, G.; Müller, G.; Thewalt, U.; Lippert, B. *J. Am. Chem. Soc.* **1985**, *107*, 5932.

(196) Qu, Y.; Farrell, N. *J. Am. Chem. Soc.* **1991**, *113*, 4851.

(197) Stang, P. J.; Cao, D. H. *J. Am. Chem. Soc.* **1994**, *116*, 4981.

(198) Siedle, A. R.; Mann, K. R.; Bohling, D. A.; Filipovich, G.; Toren, P. E.; Palensky, F. J.; Newmark, R. A.; Duerst, R. W.; Stebbings, W. L.; Mishmash, H. E.; Melancon, K. *Inorg. Chem.* **1985**, *24*, 2216.

(199) Wheatley, P. J. *Acta Cryst.* **1957**, *10*, 182.

(200) Singer, B. *Prog. Nucl. Acid Res. Mol. Biol.* **1975**, *15*, 219.

(201) Lawley, P. D. *I.A.R.C.*; Scientific Publications, 1976.

(202) Lawley, P. D.; Orr, D. J. *Chem. Biol. Int.* **1970**, *2*, 154.

(203) Dunn, D. B. *Biochim. Biophys. Acta* **1961**, *46*, 198.

(204) Dunn, D. B. *Biochem. J.* **1963**, *86*, 14P.

(205) Zueva, V. S.; Mankin, A. S.; Bogdanov, A.; Thurlow, D. L.; Zimmermann, R. A. *FEBS Lett.* **1985**, *188*, 233.

(206) Sigel, R. K. O.; Freisinger, E.; Abbate, M.; Lippert, B. *Inorg. Chim. Acta* **2002**, *339*, 355.

(207) Sorrell, T.; Epps, L. A.; Kistenmacher, T. J.; Marzilli, L. G. *J. Am. Chem. Soc.* **1978**, *100*, 5756.

(208) Sorrell, T.; Epps, L. A.; Kistenmacher, T. J.; Marzilli, L. G. *J. Am. Chem. Soc.* **1977**, *99*, 2173.

(209) Sheldrick, W. S.; Gross, P. *Inorg. Chim. Acta* **1988**, *153*, 247.

(210) Woollins, A.; Rosenberg, B. *J. Inorg. Biochem.* **1984**, *20*, 23.

(211) Matsuoka, Y.; Norden, B.; Kurucsev, T. *J. Phys. Chem.* **1984**, *88*, 971.

(212) Boiteux, S.; Belleney, J.; Roques, B. P.; Laval, J. *Nucl. Acids Res.* **1984**, *12*, 5429.

(213) Rodriguez-Bailey, V. M.; LaChance-Galang, K. J.; Doan, P. E.; Clarke, M. *Inorg. Chem.* **1997**, *36*, 1873.

(214) Zobi, F.; Blacque, O.; Schmalle, H. W.; Spingler, B.; Alberto, R. *Inorg. Chem.* **2004**, *43*, 2987.

(215) Schöllhorn, H.; Thewalt, U.; Lippert, B. *Inorg. Chim. Acta* **1985**, *106*, 177.

(216) Sigel, H.; Lippert, B. *Pure & Appl. Chem.* **1998**, *70*, 845.

(217) Cude, W. A.; Watt, G. W. *Inorg. Chem.* **1968**, 335.

(218) Kauffman, G. B.; Cowan, D. O. *Inorg. Synth.* **1963**, 239.

(219) Chow, Y. M.; Britton, B. *Acta Crystallogr. Sect. B* **1975**, *31*, 1934.

(220) Aletras, V.; Hadjiliadis, N.; Lippert, B. *Polyhedron* **1992**, *11*, 1359.

(221) Erxleben, A.; Metzger, S.; Britten, J. F.; Lock, C. J. L.; Albinati, A.; Lippert, B. *Inorg. Chim. Acta* **2002**, *339*, 461.

(222) Jaworski, S.; Schöllhorn, H.; Eisenmann, P.; Thewalt, U.; Lippert, B. *Inorg. Chim. Acta* **1998**, *153*, 31.

(223) Krizanovic, O.; Sabat, M.; Beyerle-Pfnur, R.; Lippert, B. *J. Am. Chem. Soc.* **1993**, *115*, 5538.

(224) Tribolet, R.; Sigel, H. *Eur. J. Biochem.* **1987**, *163*, 353.

(225) Martin, R. B. *Science* **1963**, 1198.

(226) Frisch, M. J.; Trucks, G. W.; Schlegel, H. B.; Scuseria, G. E.; Robb, M. A.; Cheeseman, J. R.; Zakrzewski, V. G.; Montgomery, J., J. A.; Stratmann, R. E.; Burant, J. C.; Dapprich, S.; Millam, J. M.; Daniels, A. D.; Kudin, K. N.; Strain, M. C.; Farkas, O.; Tomasi, J.; Barone, V.; Cossi, M.; Cammi, R.; Mennucci, B.; Pomelli, C.; Adamo, C.; Clifford, S.; Ochterski, J.; Petersson, G. A.; Ayala, P. Y.; Cui, Q.; Morokuma, K.; Malick, D. K.; Rabuck, A. D.; Raghavachari, K.; Foresman, J. B.; Cioslowski, J.; Ortiz, J. V.; Baboul, A. G.; Stefanov, B. B.; Liu, G.; Liashenko, A.; Piskorz, P.; Komaromi, I.; Gomperts, R.; Martin, R. L.; Fox, D. J.; Keith, T.; Al-Laham, M. A.; Peng, C. Y.; Nanayakkara, A.; Gonzalez, C.; Challacombe, M.; Gill, P. M. W.; Johnson, B.; Chen, W.; Wong, M. W.; Andres, J. L.; Gonzalez,

C.; HeadGordon, M.; Replogle, E. S.; Pople, J. A. In *Gaussian 98 (Revision A.7)* Pittsburgh, 1998.

(227) Nonius In *KappaCCD package* The Netherlands, 1997.

(228) Otwinowsky, Z.; Minor, W. *Methods Enzymol.* **1997**, *276*, 307.

(229) G. M. Sheldrick In *programs for crystal structure refinement*; University of Göttingen: Göttingen, Germany, 1997.

(230) Foresman, J. B.; Frisch, A. *Exploring Chemistry with Electronic Structure Methods*; Second ed.; Gaussian, Inc., 1993.